Doctoral Dissertation

Lanthanum-modified Boehmite-derivatives as Solid Acid-Base Catalyst for Highly Efficient Aldol Condensation

Ling Zijian

Supervisor : Shun Nishimura

Japan Advanced Institute of Science and Technology
Kanazawa University
Division of Transdisciplinary Sciences
[Doctor of Philosophy in Engineering]
March 2026

Lanthanum-modified Boehmite-derivatives as Solid Acid-Base Catalyst for Highly Efficient Aldol Condensation

Ling, Zijian
Nishimura Laboratory, Division of Transdisciplinary Sciences, JAIST

To address the demands for sustainable development and a low-carbon economy, the catalytic conversion of biomass resources has been extensively investigated in recent decades. 3-Methyl-2-cyclopentenone (MCP), derived from biomass, has been recognized as a key intermediate in the synthesis of various natural products and gasoline additives. This study explores the selective synthesis of MCP from 2,5-hexanedione (HD) using La-modified boehmite catalysts by two different preparation methods of impregnation and co-precipitation with/without calcination.

In the case of La-supported boehmite catalysts prepared by an impregnation method (*imp*-La/AlOOH), it gave no activity without calcination. It was very attractive that the highest MCP yield of 60% at 84% conversion could be obtained when it was calcined at 500℃. On the other hand, La-Al mixed catalyst obtained by a co-precipitation method (*cp*-La-Al-(OH)) exhibited good performance without calcination; it served 55% yield of MCP and 65% conversion. While such nice performance was decreased after calcination as 40% yield of MCP at 50% conversion. XRD showed the main phases of both *cp*-La-Al-(OH) and *imp*-La/AlOOH without calcination were identified as boehmite (AlOOH) crystalline. While, after calcinations at 500 ℃, γ-Al_2O_3 was retained as the dominant crystalline phase in both catalysts. The N_2 adsorption–desorption isotherms revealed the non-calcined *cp*-La-Al-(OH) catalyst displays less defined mesoporosity and more macroporous features whereas the non-calcined imp-La/AlOOH exhibited a clear Type

IV isotherm with distinct mesoporosity. These pore structures of both catalysts became were not significantly affected by the thermal treatment. Accordingly, it was very interesting that both *cp*-La-Al-(OH) and *imp*-La/AlOOH catalysts exhibited similar XRD crystalline structures with/without calcination, however their catalytic activities differed markedly.

Poisoning experiments confirmed that the reaction over the non-calcined *cp*-La-Al-(OH) catalyst proceeds via a base-catalyzed mechanism. The co-precipitation method generated unique basic surface sites without calcination, and then most of which disappeared or were weakened after calcination. In contrast, the reaction over the calcined *imp*-La/AlOOH catalyst proceeded through an acid–base cooperative mechanism, where calcination led to the formation of Lewis acid sites in addition to basic sites. These findings underscore the potential of non-calcined *cp*-La-Al-(OH) catalysts as effective solid base systems and highlight the importance of preserving surface basicity during catalyst design.

Keywords: Lanthanum-modified alumina; Co-precipitation; Impregnation; Aldol condensation; Acid–base catalysis

Preface

Catalysis plays a central role in modern chemical science and continues to support numerous industrial processes essential to society. In recent years, the increasing demand for sustainable chemical transformations has prompted significant efforts toward developing environmentally benign catalytic systems. Within this context, alumina-based catalysts modified with mentals have attracted considerable interest due to their tunable acid–base properties and potential applications in biomass-derived chemical upgrading. This dissertation focuses on lanthanum-modified boehmite-derived alumina catalysts prepared through impregnation and co-precipitation methods, with particular emphasis on how synthesis route and thermal treatment govern the formation of active acid–base sites and their roles in the intramolecular aldol condensation of 2,5-hexanedione.

The research presented in this thesis was conducted at the School of Materials Science, Japan Advanced Institute of Science and Technology, under the guidance of Associate Professor Dr. Shun Nishimura. Throughout the course of my doctoral studies, he provided continuous guidance, insightful discussions, and patient supervision that shaped both my scientific approach and the completion of this work. His encouragement allowed me the freedom to explore ideas independently while offering timely advice whenever needed.

I am also deeply grateful to my co-supervisors, Professor Dr. Noriyoshi Matsumi and Professor Dr. Kazuaki Ninomiya, whose valuable feedback, constructive comments, and warm support greatly contributed to the progress of my research. Their expertise and perspectives significantly enriched my academic development.

The collaborative environment in Nishimura Laboratory made daily research both

productive and enjoyable. I sincerely appreciate all laboratory members for their technical assistance, helpful discussions, and the supportive atmosphere that accompanied our work together. I would also like to acknowledge JAIST for providing excellent research facilities and the administrative staff for their kind assistance throughout my studies.

My gratitude extends to my friends, whose encouragement helped me navigate challenges during these years. Finally, I wish to express my heartfelt appreciation to my family for their unwavering support, understanding, and constant belief in my efforts. Their support has been the foundation that enabled me to pursue and complete this doctoral research.

Ling, Zijian

November 2025

Contents

Chapter 1 General Introduction

1.1 Background

In recent decades, biomass resources have attracted significant attention across multiple research fields—including sustainable aviation fuels (SAFs), fine chemical production, and polymer industries—owing to their carbon-neutral and renewable characteristics as shown in **Fig.1.1** [1–3]. For the realization of a next-generation, environmentally responsible society, it is essential to establish biorefinery methodologies capable of systematically converting lignocellulosic feedstocks into value-added fuels and chemicals.

Such methodologies typically combine several catalytic transformations—depolymerization, isomerization, dehydration, hydrogenolysis, hydrogenation, oxidation, and esterification—to design efficient and integrated chemical supply chains based on bio-renewable carbon [4, 5]. Among the many possible upgrading routes, the intramolecular aldol condensation of 2,5-hexanedione (HD) to 3-methyl-2-cyclopentenone (MCP) represents an attractive and versatile process for transforming a biomass-derived linear diketone into a cyclic enone with broad synthetic utility [6, 7]. MCP can serve as a valuable platform molecule for the production of fine chemicals, fragrance intermediates, and potential fuel components owing to its suitable volatility and energy density [8]. The precursor molecule, HD, can be obtained from a multistep route proceeding via 5-hydroxymethyl-2-furaldehyde (HMF) and 2,5-dimethylfuran (DMF) as shown in **Scheme 1** [9–12]. HMF, derived from glucose or fructose through catalytic dehydration, can be further hydrogenated and hydrolyzed to yield DMF, a well-known biofuel additive with high energy density. However, DMF suffers from significant drawbacks, such as high toxicity and instability, which limit its large-scale utilization [6, 13]. In contrast, the hydrolysis of DMF to HD, followed by intramolecular aldol condensation to MCP, offers a safer and more flexible route for biomass valorization.

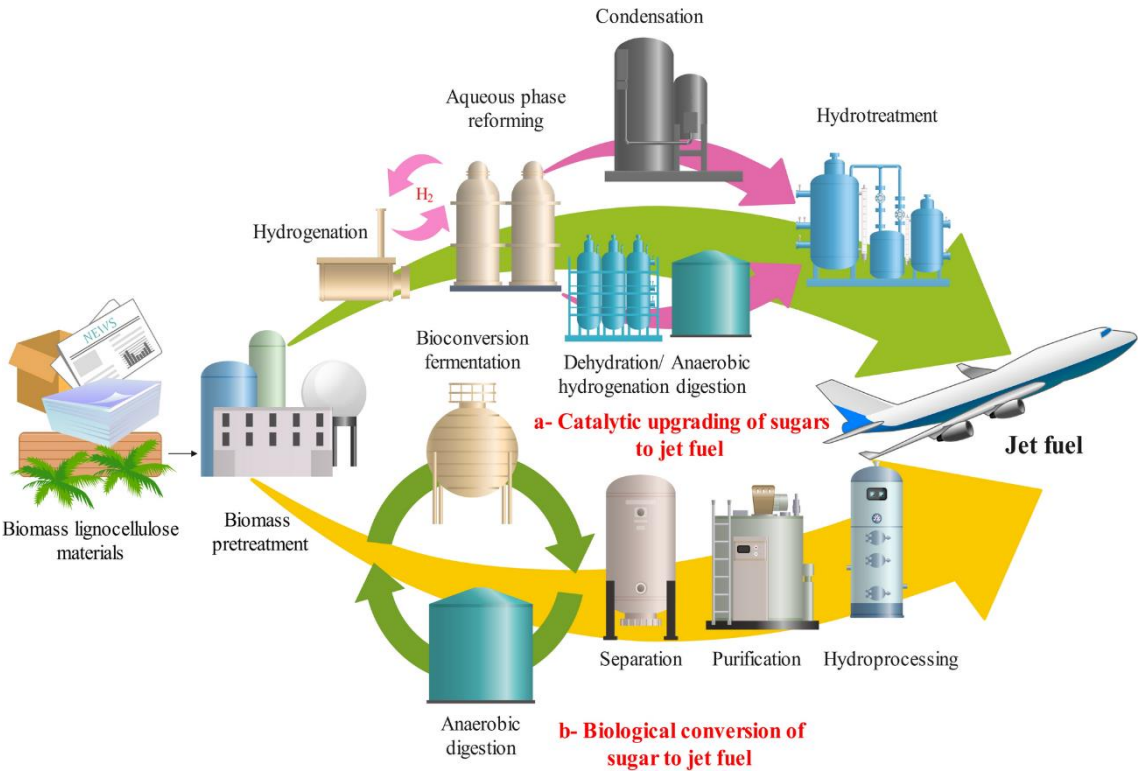

Fig.1.1 Catalytic production of aviation jet biofuels from biomass [14]

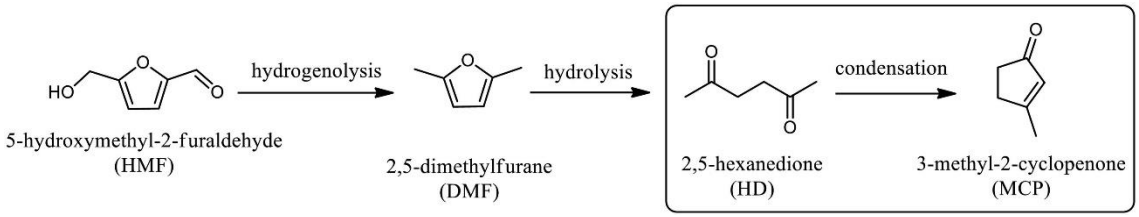

Scheme 1 Possible reaction pathway to the target reaction from HMF.

Historically, the intramolecular aldol condensation of HD to MCP has been carried out using homogeneous basic catalysts such as NaOH [15], KOH [16], or aqueous Na_2CO_3 [17]. Although these systems exhibit high catalytic activity, their recyclability, separation, and environmental compatibility remain major limitations. Consequently, considerable research effort has focused on developing heterogeneous catalytic systems that provide comparable activity while enabling solid–liquid separation and catalyst reuse. Various solid base catalysts have been examined for this transformation, including Li_2O/ZrO_2 [18], Ag/Ca-hydroxyapatite [19], yttrium zirconate (YZrO) [7], calcined Mg–Al hydrotalcite [8], and Ce- or Zr-incorporated mesoporous SBA-15 materials [20]. These heterogeneous

catalysts not only improve process sustainability but also serve as excellent model systems for investigating the relationship between surface acid–base properties and catalytic selectivity. Notably, the HD transformation provides a useful typical reaction to distinguish the nature and function of different catalytic sites. It has been reported that Brønsted acidic centers promote the formation of DMF via intramolecular etherification, whereas Brønsted basic centers favor the formation of MCP through condensation and dehydration pathways [20–22]. Therefore, the intramolecular aldol condensation of HD to MCP not only represents a promising route for bio-based chemical and fuel production but also serves as a model reaction for elucidating the cooperative roles of acidic and basic sites in bifunctional heterogeneous catalysis. Designing bifunctional solid catalysts with controllable acid–base properties is crucial for achieving both high MCP selectivity and catalyst stability, which forms the central focus of the present study.

1.2. Effective use of biomass

The energy and chemical products necessary for modern industry and human life are heavily dependent on petroleum due to the continuous supply of cheap and abundant petroleum resources. A large and cheap supply of energy promotes the development of industry, and at the same time, the relationship between energy and chemical raw materials is so close that the quality and structure of industry is affected by what energy resources are used. Although synthetic chemistry using coal as a raw material has existed for a long time, the use of petroleum as a chemical raw material did not reach its zenith until coal was consumed cheaply and in large quantities as an energy source, including in the case of thermal power generation. [23,24]

In recent years, renewable resources, including solar energy, tidal energy, wind energy, geothermal energy, and biomass energy, have been widely promoted as new energy sources that can replace exhaustible resources such as petroleum. [25]

Biomass refers to the general term for the accumulation of a certain amount of animal and plant resources and the resulting waste, such as wood, sugar cane, sludge, municipal waste, organic industrial waste as shown in **Fig. 1.2**. Unlike chemical resources such as petroleum and natural gas, biomass has the great feature of being non-exhaustive (renewable) and is considered to play a role as a complementary or local alternative carbon resource. And biomass, as the only renewable carbon resource, can be used not only as an energy source, but also as a material resource that can replace petroleum, such as raw materials for chemical products. [26,27]

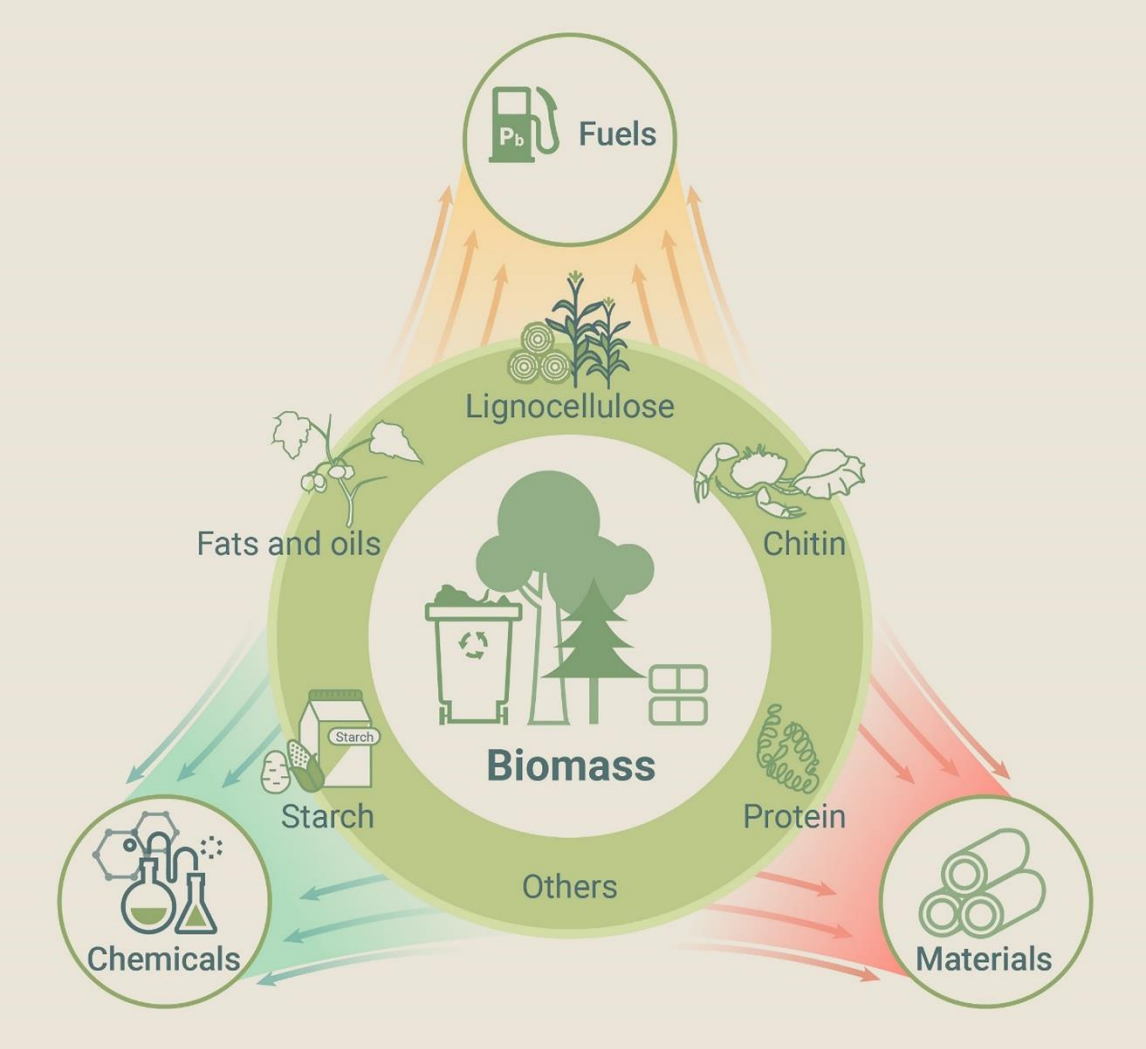

Figure 1.2 Opportunities for switching from fossil fuel to renewable resources for chemicals, fuels, and materials [28]

The process for producing these versatile fine chemicals from biomass will reduce the supply and cost constraints of these compounds, which are currently produced from petroleum resources or extracted from rare natural materials, and will dramatically improve the competitiveness of the products, enabling them to be used in a wider range of applications, such as agricultural materials. The new products are expected to be used in a wider range of applications, such as agricultural materials. [18,29]

1.3 Solid base and acid–base bifunctional catalysts

Catalysis plays a decisive role in the selective transformation of biomass-derived oxygenates into value-added chemicals and fuels, and among various catalytic reaction types, aldol condensation is particularly sensitive to the acid–base characteristics of the catalyst surface, since both carbonyl activation and enolate formation are involved in the rate-determining steps [30–32]. Solid base catalysts form one of the most important families of heterogeneous catalysts used for C–C bond–forming reactions, including aldol condensation, Knoevenagel condensation, and transesterification. Their catalytic performance is strongly governed by the nature, strength, and accessibility of surface basic sites, which generally arise from lattice oxygen anions, surface hydroxyl groups, or oxygen vacancies acting as proton acceptors [33–35]. In contrast to homogeneous bases, solid bases offer superior stability, straightforward separation from liquid products, and easier regeneration, aligning well with green-chemistry principles.

From a mechanistic perspective, basic sites on oxide surfaces abstract α-hydrogens from carbonyl compounds to form reactive enolate intermediates, which subsequently attack another carbonyl species to form C–C bonds. The resulting β-hydroxy intermediates then undergo dehydration to yield unsaturated carbonyl products [36]. The general concept of acid–base bifunctional catalysis is illustrated in **Figure 1.3**.

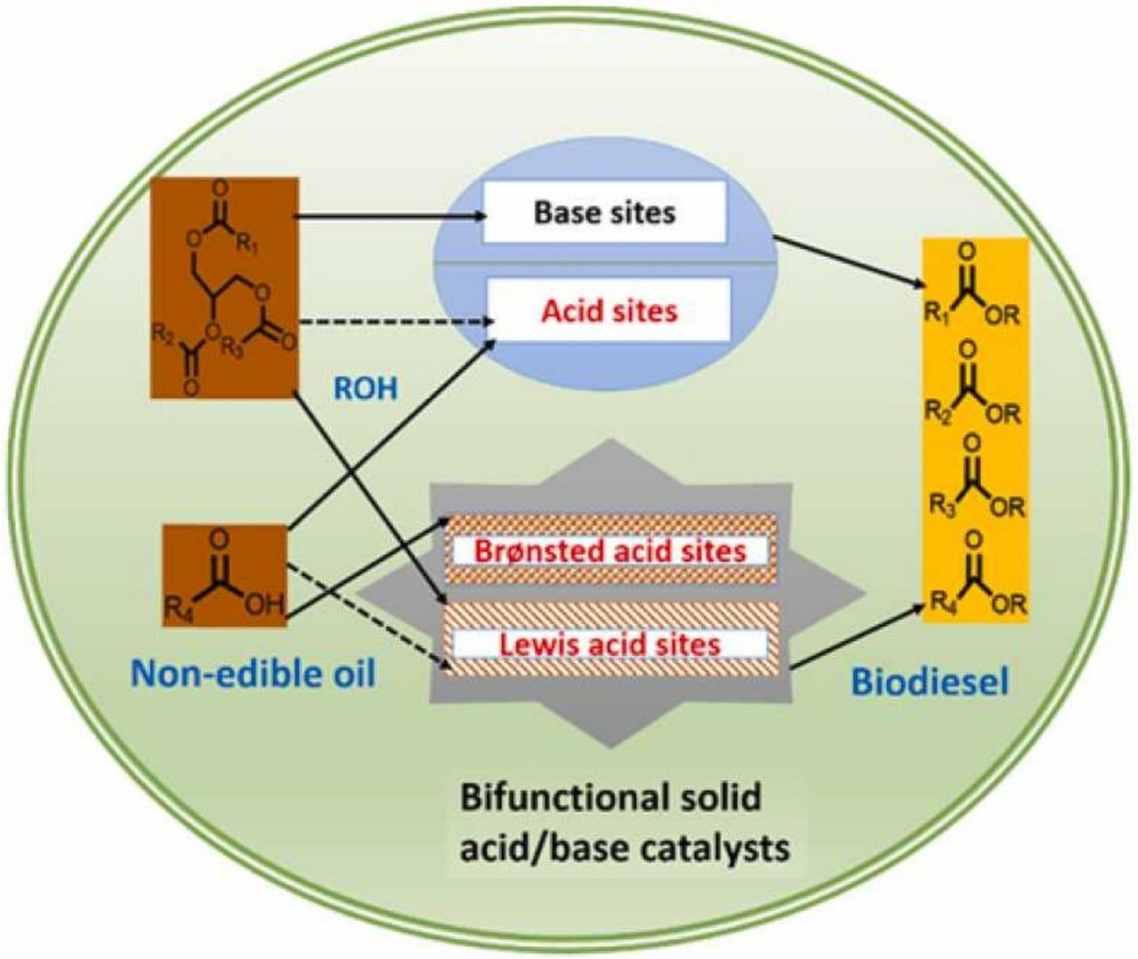

Figure 1.3 Illustration of acid–base cooperative catalysis relevant to C–C coupling reactions such as aldol condensation. [37]

The overall catalytic efficiency therefore depends not only on the number of active basic sites but also on their strength distribution. Weak basic sites such as surface –OH groups can activate moderately acidic substrates, whereas strong O^{2-} centers are capable of deprotonating less acidic molecules but may also induce side reactions such as over-condensation or carbon deposition [37,38]. When catalysts contain only strong basic sites, side reactions such as polymerization and excessive dehydration of intermediates tend to occur, ultimately leading to coke deposition and deactivation [39,40]. Therefore, the development of acid–base bifunctional catalysts has gained increasing attention as a means to achieve high activity without sacrificing selectivity.

In such catalysts, basic sites facilitate α-hydrogen abstraction (enolate formation), while adjacent acidic or Lewis-acid sites activate the carbonyl group and assist in the dehydration of β-hydroxy intermediates [41–43]. The cooperation between these two types of sites allows more efficient C–C coupling under milder conditions and with better selectivity toward unsaturated carbonyl products [44]. Typical mechanisms of base- and acid-catalyzed aldol reactions are illustrated in **Figure 1.4** A variety of bifunctional materials have been reported, including Mg–Al layered double oxides, ZrO_2- and CeO_2-based oxides, mesoporous silicas modified with alkali or rare-earth elements, and mixed oxides derived from hydrotalcites [45–48]. Among them, Mg–Al mixed oxides are widely studied because their composition and calcination conditions allow precise control of both site density and strength. Incorporation of transition or rare-earth elements into zirconia or ceria matrices also creates oxygen vacancies that act as moderate basic sites, while the metal cations serve as Lewis acid centers [49].

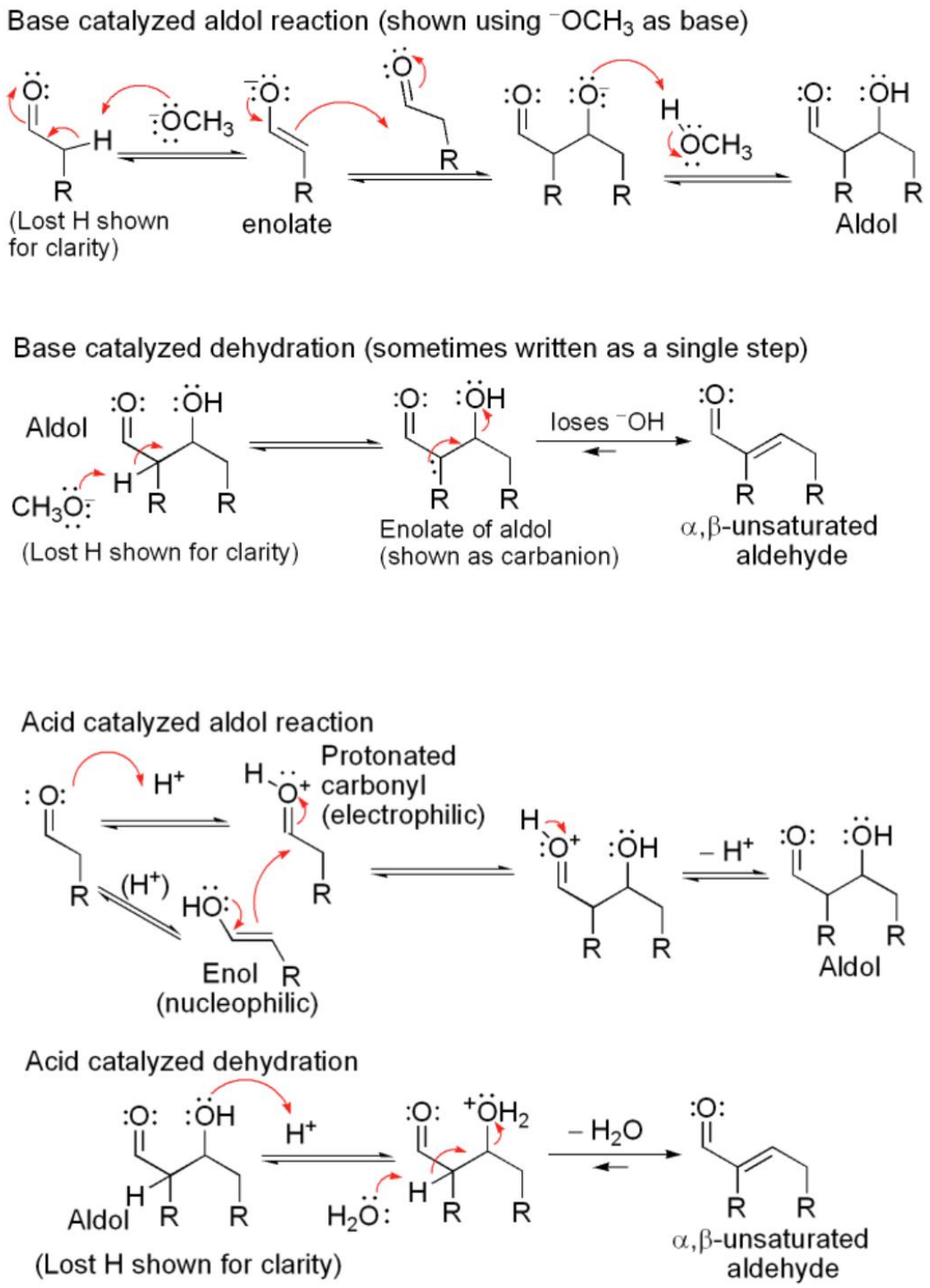

Figure 1.4 Acid- and base-catalyzed mechanisms of aldol condensation, illustrating enolate and enol pathways. [50]

In this context, alumina (Al_2O_3) is an intriguing support because it inherently possesses both acidic and basic surface sites. The acid sites originate mainly from coordinatively unsaturated Al^{3+} cations and bridging hydroxyl groups, whereas basic sites are associated with surface O^{2-} or terminal hydroxyls [51]. The relative abundance and strength of these sites depend strongly on synthesis method, precursor phase (boehmite, pseudo-boehmite, or aluminum hydroxide), and calcination temperature, which together determine the specific surface area and defect density [52]. Furthermore, alumina can be effectively modified by incorporating rare-earth elements, particularly lanthanum, which stabilizes high-surface-area γ-Al_2O_3 phases, suppresses phase transformation to α-Al_2O_3, and simultaneously introduces new La–O–Al linkages that function as basic centers [53–55]. The modification neutralizes excessively strong acid sites and improves the acid–base balance, resulting in higher selectivity and resistance to deactivation.

In the intramolecular aldol condensation of HD, such acid–base cooperation is particularly important. Basic sites drive enolate formation, while Lewis acid sites facilitate intramolecular attack and dehydration, yielding the cyclic enone MCP. A controlled balance between the two types of sites minimizes side reactions and maximizes MCP selectivity [56–58]. Consequently, La-modified alumina catalysts serve not only as efficient bifunctional systems for the condensation of biomass-derived oxygenates but also as model materials for elucidating the relationship between synthesis, structure, and catalytic performance in heterogeneous acid–base catalysis.

1.4 Influence of preparation methods on catalyst structure

The preparation method exerts a decisive influence on the textural, structural, and acid–base characteristics of oxide catalysts. Even when the chemical composition is identical, different synthesis routes can lead to distinct distributions of active species, surface morphologies, and defect structures that ultimately determine catalytic behavior [33, 57]. Among the various approaches, the

impregnation and co-precipitation methods are the most commonly employed for fabricating metal-modified alumina catalysts, as their procedures strongly affect metal dispersion, phase composition, and the chemical environment of surface active sites.

In the impregnation method, metal precursors are deposited onto a pre-formed alumina support through wet impregnation or incipient wetness techniques, followed by drying and calcination. This process typically produces catalysts with metal species concentrated near the outer surface, existing as isolated oxides, surface clusters, or weakly interacting cations [42, 51]. The degree of metal dispersion is governed by the pore structure of the support, the precursor concentration, and the drying rate. High local concentrations of nitrate or hydroxide species during solvent evaporation can cause uneven deposition and local aggregation of the active phase. Upon calcination, these surface-enriched species may crystallize or sinter, generating strong local basicity but often reducing the effective surface area. Consequently, impregnated catalysts tend to exhibit surface heterogeneity, with regions of strong basic or acidic activity coexisting with less active areas.

In contrast, the co-precipitation method allows the metal cations and aluminum species to precipitate simultaneously from a homogeneous solution, typically in the presence of urea, ammonia, or carbonate as a precipitating agent. This approach promotes atomic-scale mixing of metal and support components, yielding precursors such as metal–aluminum hydroxides or layered double hydroxides [53, 54]. During subsequent drying and calcination, the modifying cations can be partially incorporated into the alumina lattice, forming La–O–Al linkages or substituted spinel-type structures. As a result, co-precipitated catalysts usually display higher specific surface areas, uniform pore distributions, and better metal–support interactions than impregnated counterparts [55, 59]. Such structural homogeneity often translates into more uniform acid–base site distributions and enhanced resistance to phase segregation during thermal treatment.

Thermal treatment further governs the structural evolution of these materials. When boehmite (AlOOH) or amorphous hydroxides are calcined, dehydration occurs between 350–600 °C, leading

to the formation of γ-Al_2O_3. This transition is accompanied by the loss of surface hydroxyl groups and the generation of coordinatively unsaturated Al^{3+} cations, which act as Lewis acid sites [60, 61]. The presence of dopant cations such as La^{3+}, Ce^{4+}, or Y^{3+} stabilizes the high-surface-area γ-phase by anchoring at defect sites or forming strong La–O–Al bonds that prevent lattice collapse [62]. These dopants inhibit the migration and growth of alumina crystallites, suppressing transformation into α-Al_2O_3—a dense and catalytically less active phase. Thus, the calcination temperature, together with the synthesis route, dictates the final pore structure, crystallinity, and surface site distribution.

Another critical factor is the interaction between dopant and support, which differs greatly between impregnation and co-precipitation. In impregnated La/AlOOH systems, La species mainly reside on the surface as La_2O_3 clusters or amorphous La–O–Al phases, whereas in co-precipitated samples, La is more likely to occupy subsurface or lattice positions within the alumina matrix [63]. This difference in distribution has a direct impact on acid–base bifunctionality. Surface La_2O_3 domains in impregnated catalysts contribute to strong basic sites associated with O^{2-} anions, while La incorporation within the alumina lattice in co-precipitated samples yields more balanced acid–base properties and enhanced stability. The degree of La dispersion also affects the availability of surface hydroxyl groups; highly dispersed La species can promote the formation of weak to medium-strength basic sites, beneficial for selective C–C coupling reactions such as intramolecular aldol condensation [30,45].

Porosity and morphology are likewise dependent on the synthesis method. Impregnation often retains the textural features of the parent alumina, with mesopores formed by interparticle voids, whereas co-precipitation tends to generate hierarchical pore structures containing both mesopores and macropores [64, 65]. The higher porosity and larger pore volume of co-precipitated catalysts facilitate reactant diffusion and improve accessibility of active sites. Furthermore, residual hydroxyl groups and defect-rich surfaces in co-precipitated samples enhance their hydrophilicity and adsorption capacity toward polar molecules such as diketones or alcohols, which are common intermediates in

biomass conversion.

Taken together, the preparation route controls not only the physical texture of the catalyst but also the chemical nature of the surface—that is, the type, strength, and proximity of acidic and basic sites. Impregnation generally favors the formation of strong, localized surface sites, whereas co-precipitation promotes uniform, cooperative acid–base distributions. Both factors critically influence catalytic performance. In the case of the intramolecular aldol condensation of 2,5-hexanedione, the impregnation-derived La/Al_2O_3 catalyst exhibits high activity due to strong surface basicity, while the co-precipitated La–Al–(OH) precursor shows higher selectivity and stability due to well-dispersed and moderate acid–base sites. Therefore, systematic comparison of these two preparation methods provides fundamental insight into how synthesis parameters govern structure–property–performance relationships in La–modified alumina catalysts.

1.5 Role of acid–base sites in the intramolecular aldol condensation

The intramolecular aldol condensation of 2,5-hexanedione (HD) into 3-methyl-2-cyclopentenone (MCP) provides a representative model reaction for understanding the cooperative functions of acid and base sites on heterogeneous catalysts. The transformation involves three key steps: (i) enolate formation through α-hydrogen abstraction from one carbonyl group, (ii) intramolecular nucleophilic addition of the enolate to another carbonyl group forming a cyclic β-hydroxyketone, and (iii) subsequent dehydration to yield the conjugated enone MCP [66–68]. Because each elementary step is promoted by distinct catalytic centers, the spatial proximity and balance of acid–base sites play a decisive role in controlling both activity and selectivity.

Basic sites are indispensable for the initiation of the reaction. Lattice oxygen anions and surface hydroxyl groups act as proton acceptors to generate the enolate intermediate [69]. Catalysts rich in strong basic sites typically exhibit high initial activity, as they facilitate rapid α-hydrogen abstraction

and C–C bond formation. However, excessively strong basicity often induces undesired parallel reactions such as polymerization, resinification, or over-dehydration of intermediates, leading to carbon deposition and catalyst deactivation [70,71]. In contrast, weak or medium-strength basic sites tend to stabilize the enolate species and enable selective formation of MCP under moderate conditions. Therefore, controlling the strength distribution of basic sites is a key parameter for ensuring reaction selectivity and catalyst longevity.

Acidic sites complement this function by activating carbonyl groups and facilitating dehydration. Coordinatively unsaturated metal cations—such as Al^{3+}, La^{3+}, or Zr^{4+}—act as Lewis acids that polarize the C=O bond, enhancing its electrophilicity and enabling intramolecular attack by the enolate [72]. During the final dehydration stage, these Lewis acid centers also assist the elimination of water molecules from β-hydroxy intermediates, producing the conjugated enone structure of MCP. A small number of Brønsted acid sites, derived from surface hydroxyl groups, can participate in proton transfer during this step. However, excessive Brønsted acidity may shift the reaction toward etherification, forming 2,5-dimethylfuran (DMF) instead of MCP [7].

The most efficient catalysts are those exhibiting acid–base bifunctionality, where both site types coexist in appropriate strength and proximity. In such systems, the base site initiates α-hydrogen abstraction, while an adjacent Lewis acid site simultaneously activates the carbonyl group, creating a cooperative catalytic domain [46,73,74]. This proximity-driven mechanism enables the enolate and carbonyl species to interact within a confined environment, lowering activation barriers and minimizing intermediate diffusion. As a result, the condensation proceeds under milder conditions with higher MCP selectivity. The synergistic operation of these complementary sites represents the essential mechanistic feature distinguishing bifunctional solid catalysts from purely basic or purely acidic ones.

In La-modified alumina catalysts, the acid–base balance can be finely adjusted through compositional and structural control. The incorporation of La^{3+} ions into the alumina framework is

known to generate La–O–Al linkages, which are expected to introduce moderate basic centers while simultaneously neutralizing excessively strong acid sites associated with unsaturated Al^{3+} species [63–65]. In addition, the presence of La can stabilize the γ-Al_2O_3 phase during calcination, preserving surface area and preventing structural collapse. Through these effects, La modification is anticipated to create a more balanced surface environment comprising both Lewis acid sites and medium-strength basic oxygen species. Such an environment is considered favorable for the intramolecular aldol condensation of 2,5-hexanedione, as it may promote the sequential steps of enolate formation, intramolecular carbonyl activation, and dehydration in a cooperative manner. Compared with unmodified γ-Al_2O_3, the La-modified catalyst is expected to exhibit improved selectivity toward MCP by suppressing side reactions that typically occur on catalysts dominated by either strong bases or strong acids. Therefore, the transformation of HD to MCP serves not only as a model reaction to assess the distribution and strength of acid–base sites, but also as a valuable system for understanding how surface modification and compositional tuning can optimize bifunctional catalytic performance.

1.6 Research motivation and objectives

Previous studies have shown that the intramolecular aldol condensation of 2,5-hexanedione (HD) to 3-methyl-2-cyclopentenone (MCP) can be catalyzed by conventional homogeneous bases such as NaOH and KOH, typically affording MCP yields in the range of 50–70%[15,16]; however, these homogeneous systems suffer from inherent drawbacks associated with catalyst separation and recyclability. In contrast, heterogeneous catalytic systems have been demonstrated to effectively overcome these limitations. Bell et al. reported that a Mg–Al–Ox mixed oxide catalyst derived from the calcination of Mg–Al hydrotalcite at 700 °C achieved an outstanding MCP yield and selectivity of up to 98% in a toluene/water biphasic system [8]. In addition, Huo and co-workers investigated a Zn-based catalytic system for the direct production of HD and MCP from biomass-derived HMF,

obtaining an MCP yield of 30.5% at 250 °C, although the overall efficiency remained relatively limited [75]. More recently, Sato et al. developed a vapor-phase catalytic process using Li_2O/ZrO_2 as the catalyst, which enabled 99% HD conversion with 96% MCP selectivity at 250 °C, highlighting the considerable potential of solid catalysts for this transformation under gas-phase conditions [18].

On the other hand, aldol condensation reactions are known to proceed not only over Brønsted basic sites but also over Lewis acidic sites and acid–base bifunctional catalysts [74, 76,77]. Owing to its intrinsic acid–base properties, alumina-based catalysts have therefore been reported to catalyze the intramolecular aldol condensation of HD to MCP [6]. Nevertheless, the catalytic activity and selectivity of pristine alumina are often limited by an imbalance in surface acid–base properties: strong acidic sites tend to promote etherification side reactions leading to the formation of 2,5-dimethylfuran (DMF), whereas insufficient basicity suppresses enolate formation, resulting in reduced HD conversion. To address these limitations, the introduction of metal species into alumina has been widely recognized as an effective strategy for tuning acid–base balance and enhancing catalytic performance.

Among various modifiers, lanthanum (La) has attracted particular attention for its pronounced effects on the structural and catalytic properties of alumina-based materials. Yamamoto et al. provided fundamental microstructural insights into La-modified Al_2O_3, demonstrating that La can exist either as highly dispersed LaO_x species anchored on the alumina surface or as $LaAlO_3$-like domains embedded within the Al_2O_3 matrix, depending on La loading and calcination temperature; these distinct La species were shown to play a critical role in governing surface basicity, thermal stability, and resistance to sintering [78]. Furthermore, Garbarino et al. demonstrated that the incorporation of lanthana into Al_2O_3 significantly improved Ni dispersion and enhanced catalytic activity in CO_2 conversion reactions over $Ni/La–Al_2O_3$ catalysts, an effect attributed to La-induced enhancement of surface basicity and strengthened metal–support interactions [55]. However, the catalytic performance of La-modified alumina is highly dependent on preparation methods and thermal

treatment conditions, which ultimately determine the dispersion state of La species, their interaction with the alumina matrix, and the resulting distribution of surface acid–base sites.

Despite these advantages, systematic investigations of La–Al catalysts in the intramolecular aldol condensation of HD remain scarce. Most prior studies on La-incorporated alumina have focused on reactions such as alcohol dehydration, transesterification, and furan condensation, while only limited information is available on how La loading, preparation method, and calcination temperature influence the conversion of diketone substrates. Moreover, the correlation between textural evolution, acid–base site characteristics, and catalytic selectivity has not been comprehensively established. Addressing this knowledge gap is crucial for understanding the mechanistic basis of La modification and optimizing catalyst design for biomass-derived condensation reactions. Therefore, this study aims to elucidate how lanthanum modification influences the catalytic performance of alumina in the intramolecular aldol condensation of 2,5-hexanedione. First, the effect of La loading amount is investigated to determine the optimal promoter content that enhances both conversion and selectivity. Subsequently, attention is directed toward understanding how lanthanum incorporation modifies the structure, surface chemistry, and acid–base properties of alumina. In parallel, the influence of preparation methods—impregnation and co-precipitation—and calcination temperature is systematically examined to clarify how these parameters affect the dispersion of La species, textural evolution, and overall catalytic activity. Through these investigations, this work seeks to establish clear correlations between structural characteristics, acid–base site distribution, and catalytic behavior, thereby providing fundamental insight into the design of efficient La–Al-based solid acid–base bifunctional catalysts for biomass-derived condensation reactions.

1.7 Thesis Outline

Chapter 1 presents an overview of the research background and motivation, emphasizing the development of biomass-derived chemical production as a sustainable strategy to reduce reliance on

fossil fuels. It introduces the significance of catalyst design—particularly the influence of preparation methods—in controlling the structure and acid–base properties of metal-loaded alumina catalysts. This study specifically focuses on rare-earth-metal-modified alumina catalysts, aiming to optimize catalytic performance through rational material design for enhanced conversion efficiency of biomass-derived intermediates.

Chapter 2 describes the experimental methodologies, including catalyst synthesis via impregnation and co-precipitation routes, followed by detailed physicochemical characterization and catalytic activity testing. The techniques employed provide a comprehensive understanding of the structure–property relationships of the prepared materials.

Chapter 3 presents the screening results of various metal-modified boehmite-derived alumina catalysts, identifying lanthanum as the most effective promoter. It further discusses the effects of calcination temperature, lanthanum loading, and other preparation parameters on textural characteristics, surface properties, and catalytic activity.

Chapter 4 provides a comparative analysis of the catalysts synthesized by impregnation and co-precipitation methods, highlighting differences in crystal structure, surface acidity and basicity, and catalytic performance in the intramolecular aldol condensation of 2,5-hexanedione. This chapter elucidates how synthesis strategy governs the physicochemical properties and reaction behavior of La–Al catalysts.

Chapter 5 summarizes the key findings and conclusions of this work and proposes future research directions toward the rational design of lanthanum-based solid base catalysts for efficient and sustainable biomass valorization.

References

[1] A. J. Ragauskas, C. K. Williams, B. H. Davison *et al.*, *Science*, 2006, 311, 484–489.

[2] F. H. Isikgor, C. R. Becer, *Polym. Chem.*, 2015, 6, 4497–4559.

[3] L. Tao, W.-C. Wang, *Renew. Sustain. Energy Rev.*, 2016, 53, 801–822.

[4] Y. Liu, G. Li, Y. Hu, A. Wang, F. Lu, J. Zou, Y. Cong, N. Li, T. Zhang, *Joule*, 2019, 3, 1028.

[5] Y. Liang, H. Wang, H. Xin, X. Hu, L. Yan, Q.i Zhang, C. Wang, Q. Liu, L. Ma, *ACS Sustainable Chem. Eng.*, 2021, 9, 15394.

[6] S. Nishimura, S. Ohmatsu, K. Ebitani, *Fuel Process. Technol.* 2019, 196, 106185.

[7] T. Adachi, E. Kurniawan, T. Hara, S. Sato, *Appl. Catal. A: Gen.* 2024, 685, 119887

[8] E. R. Sacia, M. H. Deaner, Y. L. Louie and A. T. Bell, *Green Chem.*, 2015, 17, 2393–2397.

[9] R. Wang, Y. Liu, G. Li, A. Wang, X. Wang, Y. Cong, T. Zhang and N. Li, *ACS Catal.*, 2021, 11, 4810–4820.

[10] Y. Liu, R. Wang, H. Qi, X. Y. Liu, G. Li, A. Wang, X. Wang, Y. Cong, T. Zhang and N. Li, *Nat. Commun.*, 2021, 12, 7.

[11] Y. Zhang, G. Zhang, Q. Hou, S. Zhao, S. Wang, E. Xu, L. Wang, X. Zhang, F. Li, Y. Yang and M. Wei, *ACS Catal.*, 2025, 15, 1206–1216.

[12] Y. Li, L. Lu, X. Jiang, D. Yang, J.-L. Chen, A. D. Chowdhury, W. Li, X. Pei and A. Lei, *Nat. Commun.*, 2025, 16, 2296.

[13] S. Nishimura, S. D. Le, Y. Asai, N. Takahashi, M. Endo and S. Ohmatsu, *Chem. Lett.*, 2022, 51, 131–134.

[14] A. E. Mansy *et al.*, *Environ. Chem. Lett.* 2025, 23, 419-461.

[15] M. L. Karpinski, D. Nicholas, J. C. Gilbert, *Org. Prep. Proced. Int.*, 1995, 27, 569.

[16] L. Bagnell, M. Bliese, T. Cablewski, C. R. Strauss, J. Tsanaktsidis, *Aust. J. Chem.*, 1997, 50,921.

[17] C. Liu, Y. Hu, Z. Yu, G. Li, A. Wang, Y. Cong, X. Wang, N. Li, *ACS Sustainable Chem. Eng.*, 2022, 10, 17221.

[18] D. Sun, S. Chiba, Y. Yamada, S. Sato, *Catal. Commun.*, 2017, 92, 105.

[19] E. Kurniawan, T. Yoshinari, Y. Yamada, S. Sato, *Appl. Catal. A: Gen.*, 2022, 644, 118812.

[20] P. Kaminski, M. Ziolek, *J. Catal.*, 2014, 312, 249.

[21] G. V. Shanbhag, M. Choi, J. Kim, R. Ryoo, *J. Catal.*, 2009, 264, 88.

[22] J. Alcaraz, *Catal. Today.*, 1998, 43,89.

[23] R. Chandra, H. Takeuchi, T. Hasegawa, *Renew Sust Energy Rev.*, 2012, 16, 1462-1476.

[24] Agency of Industrial Science and Technology, "Forefront of global environment and energy", Morikita Publishing Co., Ltd, 1997.

[25] A. Demirbas. *Energy Covers. Manag.*, 2001, 42, 1357-1378.

[26] A. Demirbas. *Energy Sources. Part A,* 2008, 30, 788-796.

[27] T. Werpy, G. Petersen, "Top Value-Added Chemicals From Biomass", National Renewable Energy Laboratory, 2004.

[28] Y. Queneau, B. Han, *The Innovation.*, 2022, 3(1), 100184.

[29] F. A. Kucherov, L. V. Romashov, K. I. Galkin, V. P. Ananikov, ACS *Sustainable Chem. Eng*, 2018, 6(7), 8064–8092.

[30] P. Sudarsanam, S. Vijayaraghavan, P. Saha, A. K. Bhattacharyya, *Chem. Soc. Rev.*, 2019, 48, 2366–2421.

[31] F. Chambon, F. Rataboul, C. Pinel, A. Cabiac, E. Guillon, N. Essayem, *Appl. Catal. A: Gen.*, 2015, 504, 664–671.

[32] K. Shimizu, *Catal. Sci. Technol.*, 2015, 5, 1412–1427.

[33] Y. Ono, *J. Catal.*, 2003, 216, 406–415

[34] Z. Zuo, Y. Sha, P. Wang, Z. Da, *RSC Adv.*, 2024, 14, 7468–7489.

[35] M. E. Borges, L. Díaz, *Renew. Sustain. Energy Rev.*, 2012, 16, 2839–2849.

[36] D. K. Jambhulkar, R. P. Ugwekar, B. A. Bhanvase, D. P. Barai, *Chem. Eng. Commun.*, 2020, 207, 433–484.

[37] A. Munyentwali, H. Li, Q. H. Yang, *Appl. Catal. A: Gen.*, 2022, 633, 118525.

[38] X. Zhang, Y. Li, C. Qian, L. An, W. Wang, X. Li, X. Zhao, Z. Li, *RSC Adv.*, 2023, 13, 9466–9478.

[39] A. Primo, H. Garcia, *Chem. Soc. Rev.*, 2014, 43, 7548–7561.

[40] Q. Zhang, Y. Hu, S. Li, M. Zhang, Y. Wang, Z. Wang, Y. Peng, M. Wang, X. Li and H. Pan, *Front. Chem.*, 2022, 10, 999607.

[41] D. Zhao, J. Sun, Q. Li, G. D. Stucky, *Chem. Mater.*, 2000, 12, 275–279.

[42] F. Cavani, F. Trifirò, A. Vaccari, *Catal. Today.*, 1991, 11, 173–301.

[43] C. J. Li, *Chem. Rev.*, 2005, 105, 3095–3165.

[44] S. Abelló, F. Medina, *ChemSusChem.*, 2011, 4, 1538–1556.

[45] A. M. Hengne, S. N. Biradar, C. V. Rode, *Green Chem.*, 2012, 14, 1064–1072.

[46] X. You, L. Chen, S. He, G. Zhang, *Catalysts.*, 2024, 14, 28.

[47] Y. Liu, Z. Chen, *Front. Chem.*, 2021, 9, 812331.

[48] X. J. Hu, Y. Li, Q. Wang, *Chin. Chem. Soc. Rev.*, 2020, 1, 40–55.

[49] Z. Helwani, M. Othman, N. Aziz, N. A. A. Aziz, M. R. Safuan, *Catal. Today.*, 2009, 363, 1–10.

[50] J. Ashenhurst, *Master Organic Chemistry,* The Aldol Condensation, 2017.

[51] C. Morterra, G. Magnacca, *Catal. Today.*, 1996, 27, 497–532.

[52] H. Hattori, *J. Jpn. Petrol. Inst.*, 2004, 47(2), 67–81.

[53] V. V. Danilevich, K. A. Nadeina, E. Gerasimov, K. I. Shefer, *Microporous and Mesoporous Materials,* 2022*,* 335*,* 111800*.*

[54] Ketan Patel, Victoria Blair, Justin Douglas, Qilin Dai, Yaohua Liu, Shenqiang Ren and Raymond Brennan, *Sci. Rep.*, 2017, 7, 39946.

[55] G. Garbarino, C. Wang, I. Valsamakis, S. Chitsazan, P. Riani, E. Finocchio, M. Flytzani-Stephanopoulos and G. Busca, *Appl. Catal. B: Environ.*, 2017, 200, 458–468.

[56] D. Salinas, N. Escalona, G. Pecchi and J. L. G. Fierro, *Fuel.*, 2019, 253, 400–408.

[57] H. Hattori, *Chem. Rev.*, 1995, 95(3), 537–558.

[58] Q. Bao, W. Zhu, J. Yan, C. Zhang, C. Ning, Y. Zhang, M. Hao and Z. Wang, *RSC Adv.*, 2017, 7, 52304–52311.

[59] M. Mosińska, D. Rutkowska, A. Machocki, M. Rutkowska, P. Nowak and M. Ziolek, *Catalysts*, 2021, 11(10), 1174.

[60] T. Ren, L.-N. N. Nforbi, R. Kanakala and O. A. Graeve, *Inorg. Chem.,* 2018*,* 57(6)*,* 3035–3041.

[61] E. Weidner, R. Dubadi, B. Samojeden, A. Piasecki, T. Jesionowski and M. Jaroniec, *Sci. Rep.*, 2022, 12, 21294.

[62] G. Garbarino, P. Riani, A. Comite, E. Finocchio and G. Busca, *J. Chem. Technol. Biotechnol.*, 2024, 99, 727–736.

[63] S. Wang, A. Y. Borisevich, S. N. Rashkeev, M. V. Glazoff, K. Sohlberg, S. J. Pennycook, S. T. Pantelides, *Nat. Mater.,* 2004, 3, 143–146.

[64] S. Nishimura, Z. Ling, *ChemistrySelect*, 2025, 10(6), e202404244.

[65] Z. Ling, S. Nishimura, *React. Chem. Eng.*, 2025, 10(12), 2895-2901.

[66] T. J. Schwartz, B. J. O'Neill, B. H. Shanks, J. A. Dumesic, *ACS Catal.*, 2014, 4, 2060–2069.

[67] A. M. Hengne, A. V. Biradar, C. V. Rode, *Catal. Lett.*, 2012, 142, 779–787.

[68] K. Tanabe, W. F. Hölderich, *Appl. Catal. A: Gen.*, 1999, 181, 399–434.

[69] T. Okuhara, *Chem. Rev.*, 2002, 102, 3641–3666.

[70] F. Lin, Z. Liu, J. E. Johnson, A. Bhan, C. T. Maravelias, P. J. Dauenhauer, *JACS Au*, 2021, 1, 710–722.

[71] Q. Bao, Y. Hu, X. Liu, G. Wu, P. Sun, J. Ge, M. Xu, *Energy & Fuels*, 2022, 36, 978–990.

[72] T. Miyazawa, Y. Kusunoki, K. Kunimori, K. Tomishige, *J. Catal.*, 2006, 240, 213–221.

[73] L. Liu, A. Corma, *Chem. Rev.*, 2018, 118, 4981–5079.

[74] V.E. Collier, N.C. Ellebracht, G.I. Lindy, E.G. Moschetta, C.W. Jones, *ACS Catal.*, 2016, 6, 460–468.

[75] D. Ren, Z. Song, L. Li, Y. Liu, F. Jin, Z. Huo, *Green Chem*., 2016, 18, 3075–3081.

[76] R. Mahrwald, in *Aldol Reactions*; R. Mahrwald, Ed.; Springer: Dordrecht, 2009, 73–82.

[77] J. D. Lewis, S. V. de Vyver, Y. Roman-Leshkov, *Angew. Chem. Int. Ed.*, 2015, 54, 9835–9838.

[78] T. Yamamoto, T. Hatsui, T. Matsuyama, T. Tanaka, and T. Funabiki, *Chem. Mater*, 2003, 15, 25, 4830–4840.

Chapter 2 Experimental Section

2.1 Materials

All the chemicals and their details are listed in Table 2.1 below

Table 2-1 Reagents information.

Materials	Chemical formula	Supplier	purity
2,5-Hexanedione (HD)	$C_6H_{10}O_2$	FUJIFILM Wako Pure Chem Corp.	97.0%
3-Methyl-2-cyclopentenone (MCP)	C_6H_8O	Sigma-Aldrich Corp.	97.0%
1,4-Dioxane (super dehydrated)	$C_4H_8O_2$	FUJIFILM Wako Pure Chem Corp.	99.5%
Dodecane	$C_{12}H_{26}$	Wako Pure Chem. Inds. Ltd.	99.0%
Aluminium Nitrate Nonahydrate	$Al(NO_3)_3 \cdot 9H_2O$	FUJIFILM Wako Pure Chem Corp.	98.0%
Lanthanum(III) Nitrate Hexahydrate	$La(NO_3)_3 \cdot 6H_2O$	FUJIFILM Wako Pure Chem Corp	99.9%
Urea	CH_4N_2O	Junsei Chemical Co., Ltd.	99.0%
Benzoic acid	$C_7H_6O_2$	FUJIFILM Wako Pure Chem Corp.	99.5%
2,6-Dmiethylpyridine	C_7H_9N	FUJIFILM Wako Pure Chem Corp.	97.5%
3,5-Dimethypyridine	C_7H_9N	FUJIFILM Wako Pure Chem Corp	98.0%
Phenolphthalein	$C_{20}H_{14}O_{10}$	Kanto Chemical Co. Inc.	98.0%
Toluene	$C_6H_5CH_3$	Kanto Chemical Co. Inc.	99.5%
Pyridine (dehydrated)	C_5H_5N	Wako Pure Chem. Inds. Ltd.	99.5%
2-Furaldehyde	C_5H_4O	Kanto Chemical Co. Inc.	97%
Furfuryl alcohol	$C_5H_6O_2$	Sigma-Aldrich Corp.	98%
Naphthalene	$C_{10}H_8$	Tokyo Chemical Industry Co., Ltd	98%
2-Propanol	C_3H_8O	Kanto Chemical Co. Inc.	99.7%

As solid acid catalysts, AlOOH (SASOL Germany GmbH), hydrotalcite (HT; Mg/A1 = 2.93, Tomita-AD 500NS, Lot No. S30878, Tomita Seiyaku Co.), and Nb_2O_5 (Wako Pure Chemicals Co., Ltd.) were used. SiO_2 (silica Gel 60N, spherical, neutral), TiO_2 (Anatase form) were from Kanto Chemical Co. Inc. Zeolite (ZSM-5 type, SiO_2/Al_2O_3 = 100) was from Toso Nikkemi Co., Ltd.

2.2. Synthesis of catalyst

2.2.1 Co-precipitated method

Co-precipitated La^{3+}/AlOOH catalysts were prepared by a urea homogeneous co-precipitation (*cp*-) method in a mixed aqueous solution of Al $(NO_3)_3 \cdot 9H_2O$ and La^{3+} $(NO_3)_3 \cdot 6H_2O$, , where the total amount of metal ions (La^{3+} + Al^{3+}) was fixed at 12.5 mmol. Urea (3.0 g, corresponding to a urea/(La + Al) molar ratio of 4) was dissolved together with the metal nitrates in 500 mL of distilled water (Auto Still WG203; Yamato Scientific Co., Ltd.). After stirring at 95 ° C for 24 h, the precipitates were filtered, washed thoroughly with 2 L of distilled water, and dried (**Figure 2.1(A)**). The as-prepared sample was described as cp-La-Al-(OH).

2.2.2 Impregnation method

A series of 1-5wt% La^{3+}-modified γ-Al_2O_3 were prepared by an evaporation to dryness method using an aqueous solution of La $(NO_3)_3 \cdot 6H_2O$ (6.0 ml) and AlOOH (1.0 g). The metal nitrate was dissolved in 6 ml of ultra-pure water (Smart 2 pure, Nikko Hansen Co. Ltd; 18.2 MΩ · cm). First stirring at room temperature for 24 h, then centrifuge under vacuum at 80 ℃ for 6 h and dried at 110 ℃ overnight. Finally calcined at 500 ℃ for 5 h (10 ℃/min) and got the catalysts for the study after grinding (**Figure 2.1(B)**). All samples were ground before use. These are described as imp- samples.

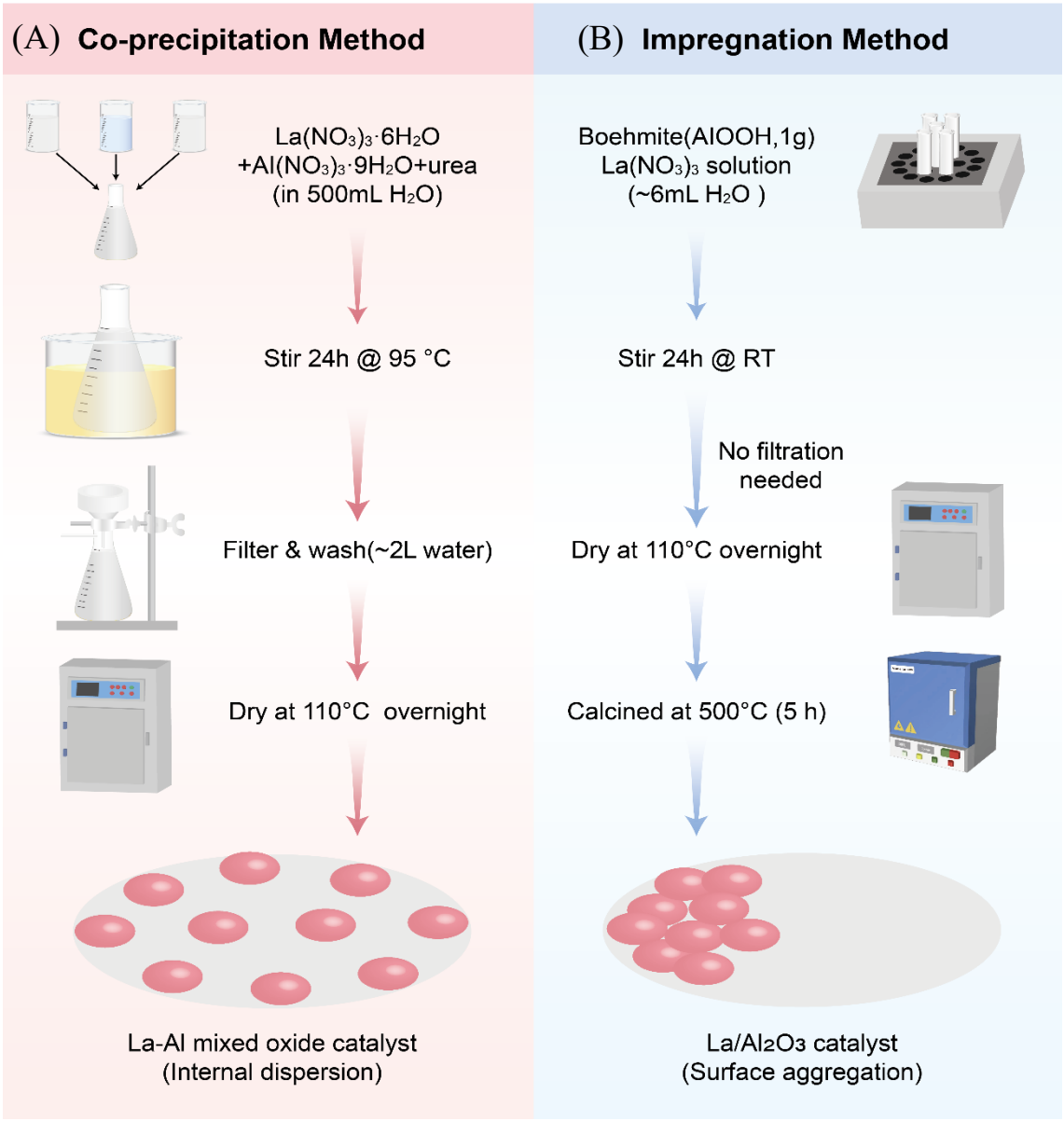

Figure 2.1. Schematic illustration of La–Al catalyst preparation by co-precipitation(A) and impregnation methods(B).

2.3. Catalyst Evaluation

2.3.1 Batch Reactor

Solid catalysts were screened for the intramolecular aldol reaction of HD. An 18 ml pressure-resistant tube (manufactured by ACE GLASS) was used as the reaction vessel. The reaction procedure was as follows: 5 ml of solvent (1,4-dioxane), 3 mmol of HD, and 50 mg of catalyst were added to the ACE closed reactor tube, stirred for 3 h in an oil bath heated to 140 °C, and then naturally cooled to room temperature without stirring. Next, 1.5 mmol of dodecane was added as an internal standard, and the catalyst was removed from the reaction solution with a filter (PTFE membrane: Milex, 0.20 μm)

2.3.2 Flow Reactor

Prior to reaction testing, the calcined catalyst powder was compressed under a pressure of 15–20 MPa, subsequently crushed, and sieved to obtain particles in the 18–26 mesh range. A total of 500 mg of the resulting catalyst was then loaded into a stainless-steel tubular reactor (inner diameter = 5 mm, length = 10.4 cm). A mixed feed solution of 2,5-hexanedione (HD) and 1,4-dioxane (0.03 mmol mL^{-1}) was introduced through the catalyst bed at 140 °C using an EYELA MCR-1000 flow reactor system. The reaction was operated in an up-flow configuration, meaning that the reactant solution passed upward through the catalyst bed. The feed rate was adjusted to 0.60 mL min^{-1} with an EYELA EUI-23 flow pump. The output solution is collected for each 1 h. All the samples were analyzed by using a GC-FID (Shimadzu GC-2014) equipped with a capillary column (Agilent DB-1, 50 m × 0.320 mm × 0.25 μm) under operation in the temperature program shown in **Fig. 2.2**.

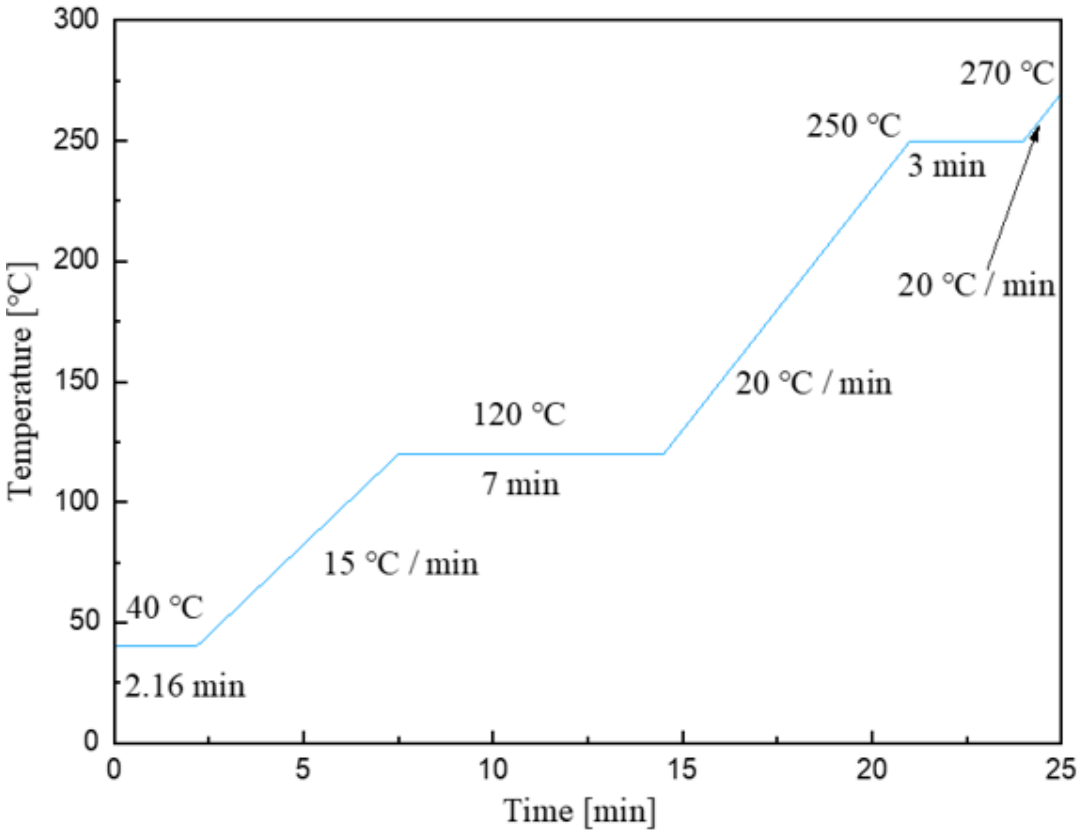

Fig. 2.2 Temperature program for the GC measurement

A substrate of HD and a product of MCP are detected at 7.87 min and 8.39 min in a GC-chart, respectively, as shown in **Fig. 2.3**. The activity of the catalysts was evaluated by the conversion of HD and yield and selectivity of MCP based on the following formulas

$$\text{Conversion} = \frac{HD_{in} - HD_{GC}}{HD_{in}} \times 100\ (\%) \quad (1)$$

$$\text{Yield} = \frac{MCP_{GC}}{HD_{in}} \times 100\ (\%) \quad (2)$$

$$\text{Selectivity} = \frac{Yield_{MCP}}{Conversion_{HD}} \times 100\ (\%) \quad (3)$$

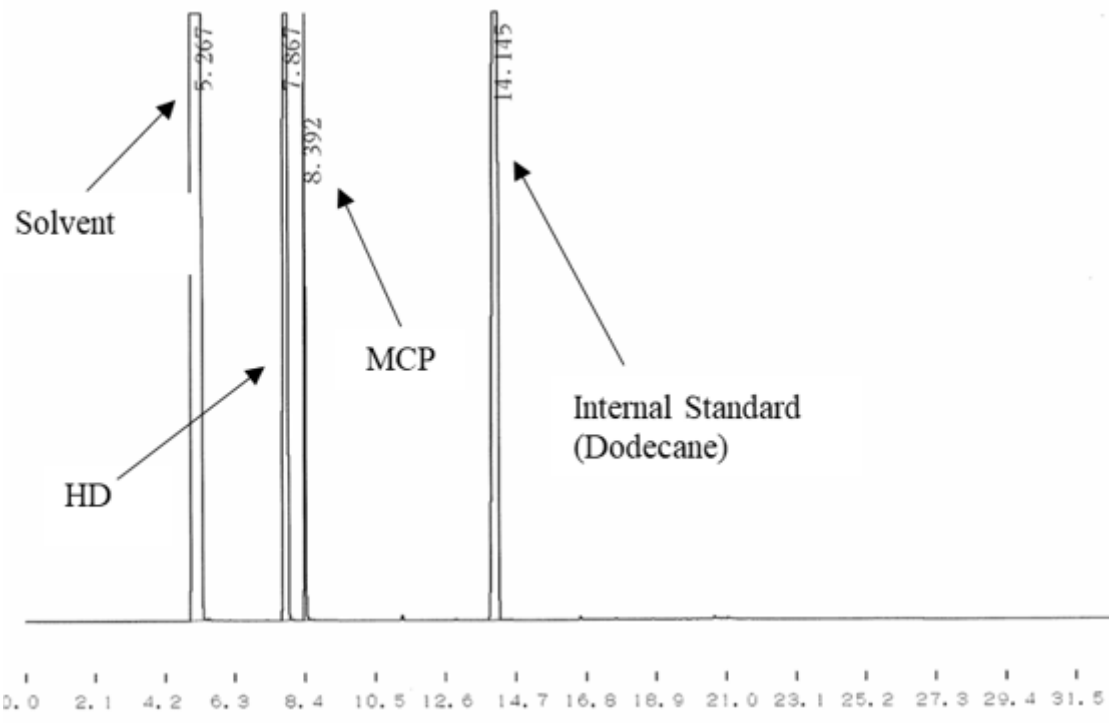

Fig. 2.3 An example of GC chart.

2.4 Catalyst Characterization

The crystal structure was obtained by the powder X-ray diffraction (XRD) method using a Rigaku MiniFlex X-ray diffractometer (Rigaku Co.) with a Cu K_α radiation (= 0.154 nm) at 40 kV and 15 mA. The data were collected at a scanning speed of 4.0 degrees per minute with a step size of 0.01 degrees, over a 2θ range of 5-80 degrees. The diffraction patterns were analyzed using the database of the Joint Committee of Powder Diffraction Standard. For the measurements, all samples were stabilized on a glass holder. Adsorption and desorption N_2 isotherms were recorded at liquid nitrogen temperature (77 K) using a Belsorp-mini (MicrotracBEL, Japan). The samples were evacuated for 3 h at 423 K as a pretreatment before measurement, and the specific surface area was calculated based on N_2 physisorption analysis with the Brunauer Emmett Teller (BET) method.

Chapter 3 Enhancement of Boehmite-derived Aluminum Oxide Catalysis for Intramolecular Aldol Condensation of 2,5-hexanedione to 3-methyl-2-cyclopentenone by Lanthanum Loading and Thermal Treatment

3.1 Abstract

La-modified alumina catalysts prepared by the impregnation method(*imp*-) were systematically investigated for the aldol condensation reaction of 2,5-hexanedione (HD) to 3-methyl-2-cyclopentenone (MCP). Although changes in La loading and calcination temperature resulted in only minor variations in crystalline phase, surface area and pore structure, these textural parameters showed no clear correlation with catalytic performance. In contrast, selective poisoning experiments provided direct insight into the active-site environment. Incorporating La generated catalytically active basic oxygen species while suppressing strong acidity and introducing moderate Lewis acid sites, creating an acid–base cooperative environment favorable for HD deprotonation, cyclization and dehydration. Owing to this synergy, the 5wt% *imp*-La/AlOOH catalyst calcined at 500 °C achieved an MCP yield of 60% with 71% selectivity in batch reactions, representing the highest activity among all samples. Moreover, this catalyst displayed outstanding durability under continuous-flow conditions, maintaining 87–96% MCP yield for more than 20 h, whereas the 0wt% *imp*-La/AlOOH catalyst (none catalyst) calcined at 500 °C rapidly deactivated. These findings demonstrate that La incorporation combined with appropriate thermal treatment significantly enhances both catalytic efficiency and long-term stability, offering a robust strategy for developing rare-earth-modified alumina catalysts for biomass-derived aldol-condensation reactions.

3.2 Introduction

Previous studies have demonstrated that γ-Al_2O_3, which possesses Lewis acidic surface sites, can selectively convert HD into MCP with a yield of 64.0% and a selectivity of 71.1% [1]. In addition, simple thermal treatment of boehmite (AlOOH) produces various Al_2O_3 phases, leading to notable changes in catalytic activity and structural stability [2]. It has also been reported that γ-Al_2O_3 is an excellent catalyst support; depositing metal species onto its surface can enhance Lewis acidity and introduce additional acid–base sites, thereby improving catalytic performance [3–5]. Furthermore, the synthesis method strongly influences both the physical structure and chemical properties of the resulting catalysts [6,7].

Building upon these findings, a series of metal-modified alumina catalysts were prepared by impregnation method first in this study. Specifically, different metal species were deposited at 3wt% onto boehmite-derived alumina and calcined at 600 °C to evaluate the influence of metal type on catalytic performance. The results revealed that among all tested catalysts, La-modified Al_2O_3 exhibited the best performance, achieving an MCP yield of 49.9% and a selectivity of 76.8% [8], which were significantly higher than those of other metal-modified samples. This suggests that the incorporation of La effectively modulates the acid–base properties and structural features of alumina, creating a more favorable environment for the key steps of HD deprotonation, cyclization, and dehydration. Based on this superior performance, La–Al_2O_3 was selected as the primary research target. Subsequent investigations focused on elucidating how La loading and calcination temperature influence the crystalline structure, textural properties, Lewis and Brønsted acidity, and surface basicity of the catalyst, and how these factors correlate with catalytic performance.

Further studies have shown that controlled thermal treatment of AlOOH allows transformation into various alumina phases with distinct catalytic behaviors. Under continuous-flow reaction conditions, MCP could be produced steadily at a HD feed concentration of 0.03 mmol mL^{-1}, achieving approximately 70% yield and 80% selectivity [2]. However, catalytic activity and long-term

durability remain major challenges for industrial applications, particularly in flow-type reactors. In this context, the present study explores the effects of additive elements on AlOOH-derived alumina catalysts over a wider range of thermal treatment conditions. Notably, the incorporation of the inexpensive La species significantly enhanced the catalytic activity toward MCP production. In a continuous-flow system, the La-modified catalyst exhibited excellent durability, maintaining high MCP yields of 87–96% over more than 20 hours of operation without noticeable deactivation.

3.3 Result and discussion

In my previous study, various $M^{2+}/\gamma\text{-}Al_2O_3$ catalysts were examined for the intramolecular aldol condensation of HD, and the catalytic results are summarized in **Table 3-1**. Among all the tested metals, $La/\gamma\text{-}Al_2O_3$ showed the highest MCP yield (49.0%) and HD conversion (63.9%). This trend suggests that La introduces a more favorable surface environment for the reaction compared with the other examined metals, making it a particularly promising candidate for further investigation. And as shown in **Fig. 3-1**, all 3 wt% M-modified AlOOH catalysts calcined at 600 °C exhibit $\gamma\text{-}Al_2O_3$ as the dominant crystalline phase, indicating that the transformation from AlOOH to aluminum oxide was completed irrespective of the additive element. Notably, no diffraction peaks attributable to La-containing crystalline phases were detected for the La-modified catalyst, suggesting that La species are highly dispersed or XRD-amorphous on the alumina surface. In contrast, several other metal-modified samples exhibit additional diffraction features, implying the formation of segregated metal oxide or aluminate phases. These results indicate that La uniquely interacts with alumina without disrupting its crystalline framework, providing a structural basis for its superior catalytic performance compared with other metal additives. Therefore, the subsequent experiments focused on the $La/\gamma\text{-}Al_2O_3$ catalysts for further investigation.

Table 3-1 Result for HD transformation towards MCP over various M-supported AlOOH catalysts.[a]

Entry	Supported-metal (M)	MCP yield (%)	HD conversion (%)	MCP selectivity (%)
1	none	39.9	51.5	77.6
2	La	49.0	63.9	76.8
3	Ni	37.9	51.3	74.0
4	Cu	34.5	45.7	75.5
5	Fe	33.2	43.6	76.1
6	Mn	30.3	40.3	75.2
7	Zn	30.0	42.3	71.0
8	Sr	28.2	36.2	77.9
9	Gd	27.6	36.0	76.6
10	Ca	23.8	33.0	71.9
11	Ga	23.6	36.1	65.4
12	In	23.6	33.4	70.6
13	Co	14.1	24.9	56.7
14	Ce	12.9	20.3	63.7
15	Cr	11.1	16.7	66.8

Reaction condition: HD (3.0 mmol), dehydrated 1,4-dioxane (5 ml), catalyst (50 mg), Temp. (140 ℃), Time (3 h), stirring (500 rpm).

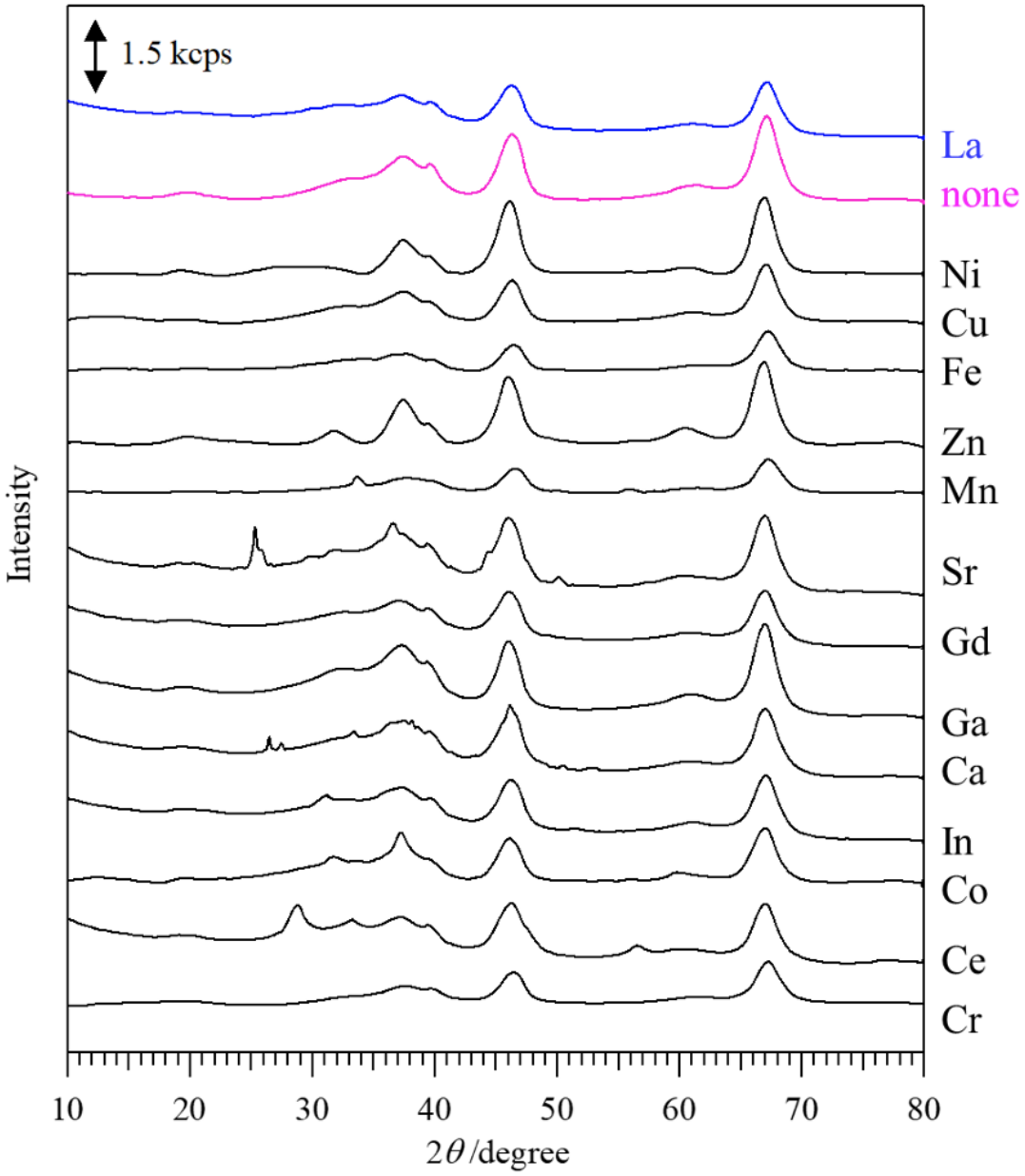

Fig. 3.1 XRD patterns of 3wt% M-modified AlOOH catalyst calcined at 600℃

To identify the optimal catalyst formulation, a series of La/AlOOH samples with La loadings of 1–5wt% were prepared by the impregnation method and subsequently calcined at temperatures between 300 and 900 °C. As summarized in **Table 3-2**, the catalytic performance was strongly influenced by both La loading and calcination temperature. For each calcination temperature, the activity generally increased with increasing La content, and the 5wt% La samples consistently

showed higher MCP yields and HD conversions than the lower-loading counterparts. In addition to La loading, calcination temperature also played a decisive role. Catalysts calcined at 300–400°C exhibited only moderate activity, whereas a clear enhancement was observed at 500°C. The 5wt% La catalyst calcined at 500°C demonstrated the highest performance among all tested samples, achieving an MCP yield of 60.0% and a conversion of 84.3%. Further increasing the calcination temperature above 600°C led to a gradual decline in activity, indicating that excessively high temperatures may diminish the number or accessibility of catalytically active sites. These results highlight that both the amount of La introduced and the thermal treatment conditions significantly influence the catalytic behavior of La-modified alumina. Based on this combined trend, the 5wt% La catalyst calcined at 500°C was identified as the most active formulation and was therefore selected for further investigation in the subsequent chapters. Several additional GC peaks can be reasonably attributed to intermolecular self-condensation of HD forming C12 aldol dimers (β-hydroxy diketones) and their dehydrated enone derivatives, as well as subsequent Michael-type additions and oligomerization leading to higher-molecular-weight species [9].

Table 3-2 Results for HD transformation towards MCP over La/AlOOH catalysts prepared with various La loading amounts and calcination temperatures.[a]

Entry	Catalyst	MCP yield (%)	HD conversion (%)	MCP selectivity (%)
1	1wt% La[b]	20.8	26.8	77.6
2	2wt% La[b]	14.3	19.7	72.7
3	3wt% La[b]	3.9	7.9	49.5
4	4wt% La[b]	5.1	9.7	53.0
5	5wt% La[b]	1.1	4.4	25.2
6	None[b]	34.6	42.0	82.4
7	1wt% La[c]	44.1	54.4	81.2
8	2wt% La[c]	45.9	57.4	80.0
9	3wt% La[c]	44.8	55.6	80.5
10	4wt% La[c]	44.9	55.4	81.1
11	5wt% La[c]	53.5	65.1	82.1
12	None[c]	43.4	56.4	76.9
13	1wt% La[d]	40.5	53.6	75.5
14	2wt% La[d]	47.5	63.6	74.6
15	3wt% La[d]	54.7	69.4	78.9
16	4wt% La[d]	49.5	73.8	67.1
17	5wt% La[d]	60.0	84.3	71.2
18	None[d]	41.7	53.8	77.4
19	1wt% La[e]	42.5	54.9	77.3
20	2wt% La[e]	45.4	58.9	77.1
21	3wt% La[e]	49.0	63.9	76.8
22	4wt% La[e]	45.1	58.3	77.4
23	5wt% La[e]	46.5	58.7	79.2
24	None[e]	39.9	51.5	77.6
25	1wt% La[f]	43.6	55.9	78.1
26	2wt% La[f]	42.3	54.8	77.1
27	3wt% La[f]	41.6	52.4	79.4
28	4wt% La[f]	48.1	63.3	76.0
29	5wt% La[f]	45.5	58.4	78.0
30	None[f]	39.4	51.7	76.2

31	1wt% La[g]	40.3	52.4	77.0
32	2wt% La[g]	46.1	60.0	76.9
33	3wt% La[g]	43.1	56.5	76.3
34	4wt% La[g]	40.2	52.2	76.9
35	5wt% La[g]	45.3	58.3	77.6
36	None[g]	31.4	39.1	80.4
37	1wt% La[h]	41.0	51.9	79.1
38	2wt% La[h]	44.6	56.3	79.1
39	3wt% La[h]	43.0	53.6	80.2
40	4wt% La[h]	45.0	55.2	81.6
41	5wt% La[h]	51.7	65.1	79.4
42	None[h]	19.7	27.1	72.5

[a]Reaction condition: HD (3.0 mmol), dehydrated 1,4-dioxane (5 ml), catalyst (50 mg), Temp. (140 °C), Time (3 h), stirring (500 rpm). Calcined at [b]300 °C, [c]400 °C, [d]500 °C, [e]600 °C, [f]700 °C, [g]800 °C, and [h]900 °C for 5 h before use.

To further investigate the effects of La loading and calcination temperature on the structural properties, a series of *imp*-La/AlOOH catalysts were analyzed by XRD. As shown in **Fig. 3.2**, when the calcination temperature did not exceed 300 °C, all samples retained the boehmite (AlOOH) phase without transformation to γ-Al_2O_3, which accounts for the relatively low catalytic activity observed at low temperatures. Upon increasing the calcination temperature to the range of 400–700 °C, all samples exhibited the characteristic diffraction peaks of γ-Al_2O_3 (**Fig. 3.3**), and the peak positions, shapes, and full widths at half maximum were barely affected by the La loading, indicating that La incorporation does not significantly modify the crystalline framework of γ-Al_2O_3. According to literature reports, La-related crystalline phases can only be detected by XRD when the La loading exceeds approximately 33wt% [10]. Notably, distinct diffraction peaks attributable to $LaAlO_3$ appeared only when the calcination temperature was raised above 800 °C (**Fig. 3.4**), which is consistent with the observations reported by Yamamoto et al. [10]. However, recycling experiments revealed that the formation of $LaAlO_3$ mainly improved the thermal stability rather than the catalytic

performance, indicating that this crystalline phase is not the decisive factor responsible for the enhanced activity.

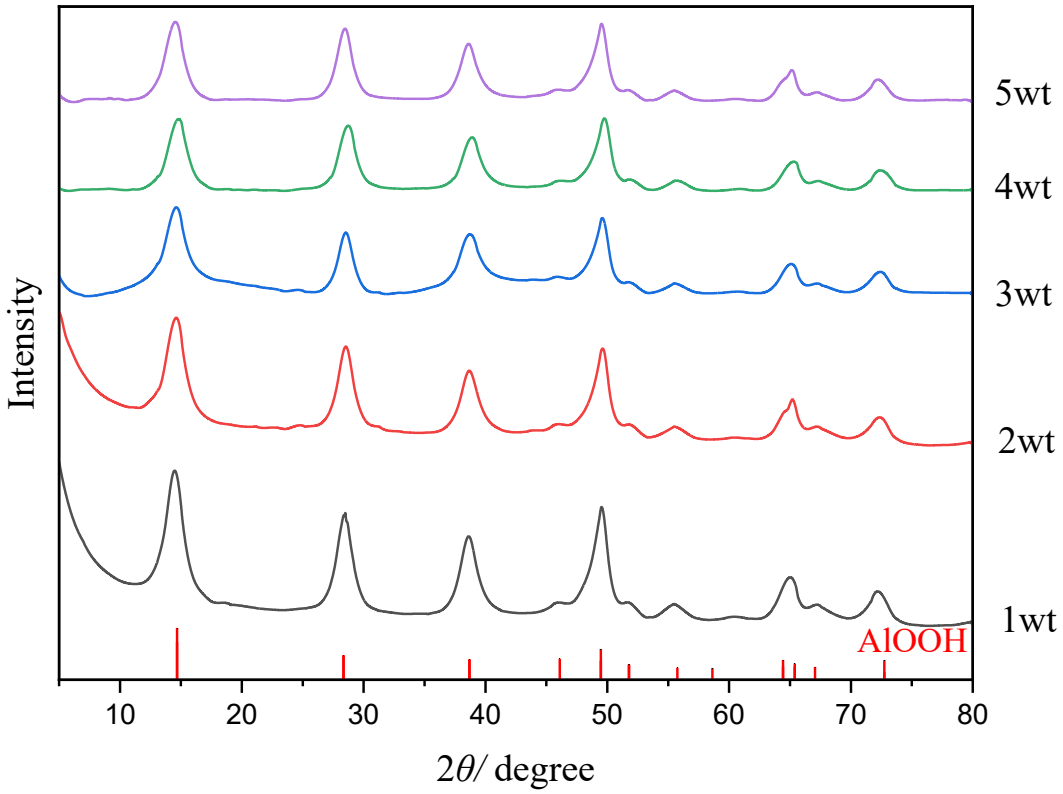

Figure 3.2 XRD patterns of La/AlOOH catalysts prepared with various La loading amounts and calcined at 300℃.

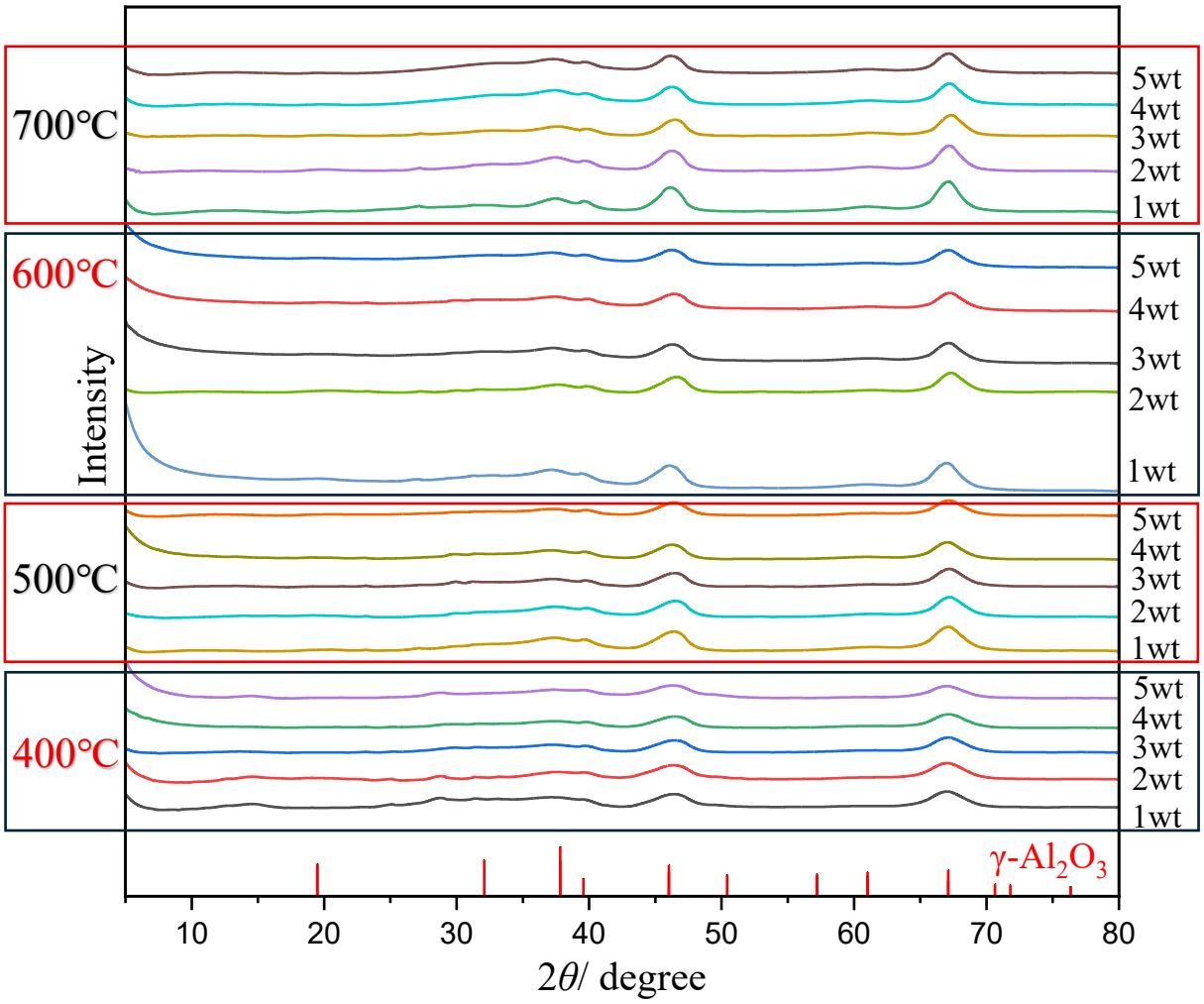

Figure 3.3 XRD patterns of La/AlOOH catalysts prepared with various La loading amounts and calcined at 400°C, 500°C, 600°C, and 700°C.

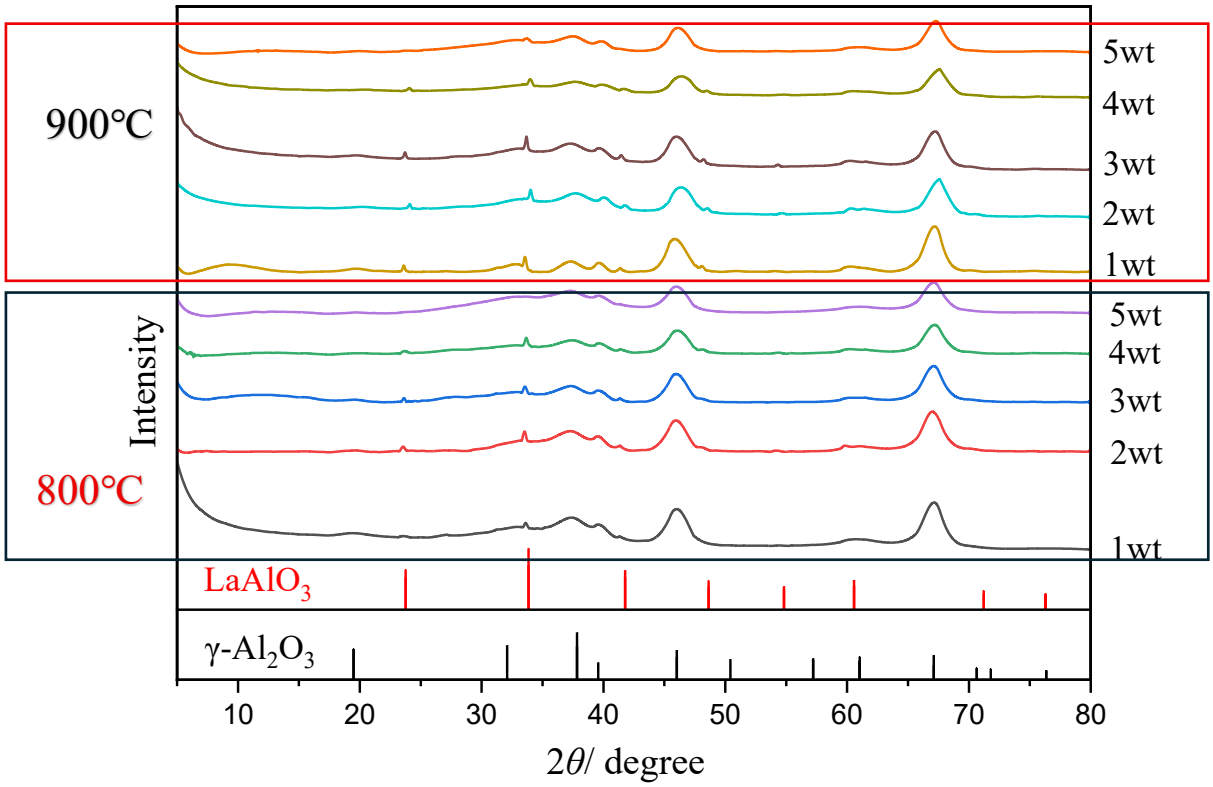

Figure 3.4 XRD patterns of La/AlOOH catalysts prepared with various La loading amounts and calcined at 800℃ and 900℃.

Nitrogen adsorption–desorption measurements were conducted to examine the textural properties of the La/AlOOH catalysts after calcination. As summarized in **Table 3-3**, both the specific surface area and pore diameter decreased gradually with increasing calcination temperature, which is consistent with the phase transformation of boehmite into γ-Al_2O_3 and the progressive sintering of the material at higher temperatures. However, these textural changes were relatively moderate compared with the large variations observed in catalytic performance. For example, the catalyst calcined at 500°C showed the highest MCP yield but did not exhibit the maximum surface area; several samples calcined at lower or higher temperatures displayed comparable or even larger BET surface areas but significantly lower catalytic activity. These results indicate that the catalytic performance cannot be directly explained by simple textural metrics such as surface area or pore

diameter. Instead, the activity is more strongly influenced by the chemical nature of the La–Al surface species generated during calcination, rather than by the physical textural properties of the support. Therefore, the BET results suggest that textural factors play a secondary role, and the observed reactivity trends must originate from differences in surface active-site formation rather than from differences in surface area or porosity.

Table 3-3 N_2 adsorption-desorption analysis results of La/AlOOH catalysts.

Entry	Catalyst	$V_m\,[cm^3\,(STP)\,g^{-1}]$	$a_{S,\,BET}\,[m^2\,g^{-1}]$	P[nm]
1	1wt% La[a]	57.3	249.3	5.62
2	2wt% La[a]	56.3	245.1	5.65
3	3wt% La[a]	55.2	240.1	5.44
4	4wt% La[a]	52.8	229.8	5.40
5	5wt% La[a]	50.8	221.0	5.57
6	None[a]	55.2	240.3	6.48
7	1wt% La[b]	56.8	247.2	6.00
8	2wt% La[b]	58.6	254.9	6.10
9	3wt% La[b]	59.8	260.3	6.06
10	4wt% La[b]	61.7	268.4	6.00
11	5wt% La[b]	62.5	272.1	5.88
12	None[b]	58.8	256.1	7.17
13	1wt% La[c]	55.9	243.5	7.20
14	2wt% La[c]	55.7	242.2	6.87
15	3wt% La[c]	53.2	231.5	6.97
16	4wt% La[c]	51.6	224.6	7.00
17	5wt% La[c]	51.0	222.0	6.88
18	None[c]	54.9	238.9	7.78
19	1wt% La[d]	49.8	216.8	8.37
20	2wt% La[d]	50.5	220.0	7.61
21	3wt% La[d]	47.7	207.7	7.70
22	4wt% La[d]	45.4	197.6	7.53
23	5wt% La[d]	46.5	202.6	7.38
24	None[d]	49.5	215.6	8.57

25	1wt% La[e]	41.5	180.6	9.51
26	2wt% La[e]	41.7	181.6	8.97
27	3wt% La[e]	40.4	175.8	8.95
28	4wt% La[e]	39.1	170.4	8.91
29	5wt% La[e]	39.2	174.2	8.76
30	None[e]	45.4	197.7	9.38
31	1wt% La[f]	29.5	128.5	9.98
32	2wt% La[f]	39.3	171.1	9.70
33	3wt% La[f]	37.0	160.9	9.84
34	4wt% La[f]	36.1	157.2	9.81
35	5wt% La[f]	36.2	157.7	9.80
36	None[f]	39.0	169.7	10.62
37	1wt% La[g]	33.6	146.0	11.01
38	2wt% La[g]	35.0	152.2	10.43
39	3wt% La[g]	33.9	147.4	10.33
40	4wt% La[g]	34.1	148.5	10.25
41	5wt% La[g]	31.6	137.6	10.32
42	None[g]	32.6	142.1	12.06

Calcined at [a]300 °C, [b]400 °C, [c]500 °C, [d]600 °C, [e]700 °C, [f]800 °C, and [g]900 °C, for 5 h before use. Note that Vm: monomolecular layer adsorption, $a_{s,\,BET}$: surface area calculated by BET method, and p: pore diameter

Further characterization of the surface acid–base properties was conducted using CO_2-TPD analyses. As shown in **Fig. 3.5**, although slight variations in peak areas and desorption temperatures were observed among the samples, the overall profiles did not exhibit significant differences, nor did they show systematic trends corresponding to La loading or calcination temperature. Similarly, FT-IR pyridine adsorption results indicated that the amounts and strengths of Lewis and Brønsted acid sites remained largely comparable across the catalysts (**Fig. 3-6** and **Fig. 3.7**). These observations suggest that neither the total acidity/basicity nor the distribution of acid site types could satisfactorily account for the variations in catalytic activity observed in this catalyst series.

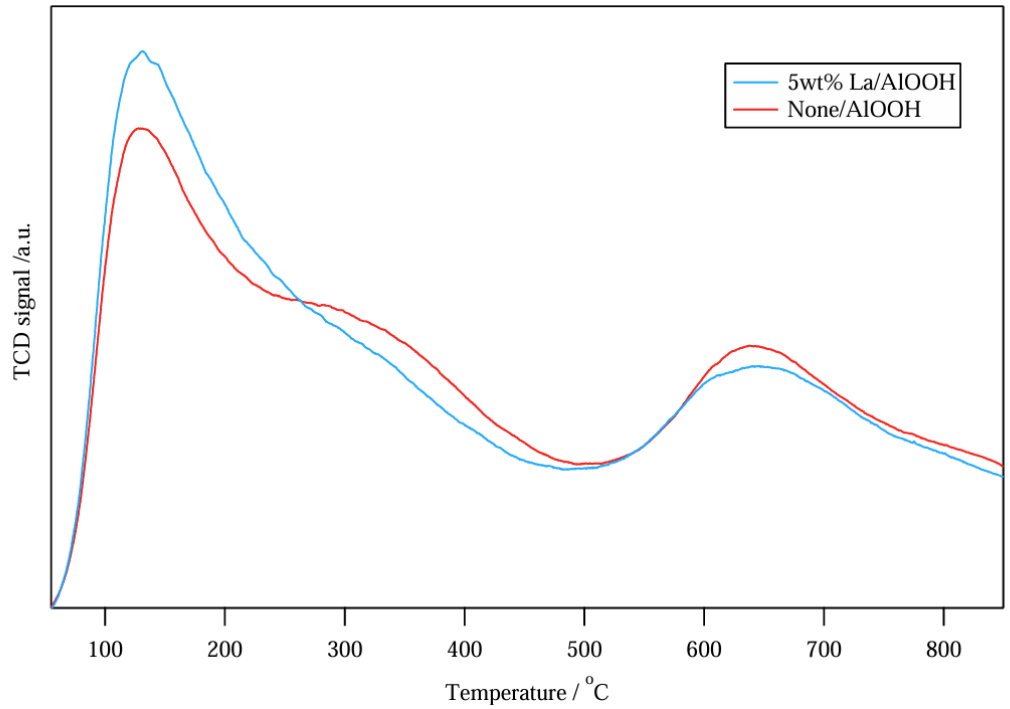

Figure 3.5 CO_2-TPD profile of 5wt% La-impregnated AlOOH catalyst calcined at 500°C together with none.

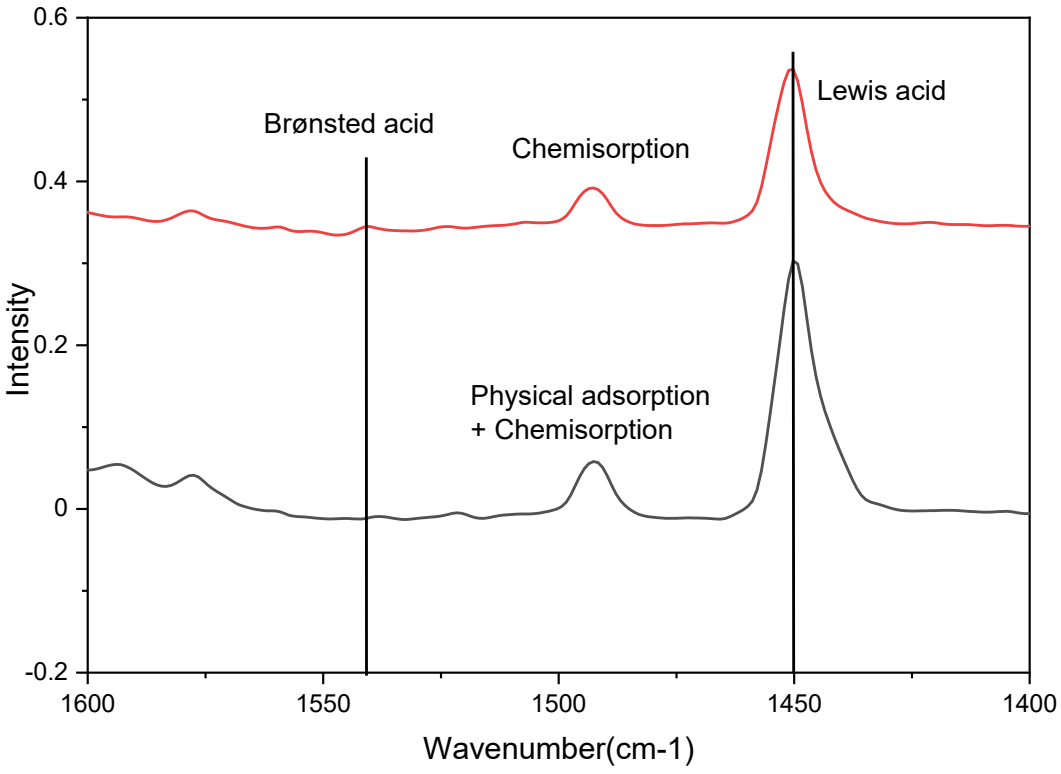

Figure 3.6 FT-IR of pyridine adsorption of none catalyst

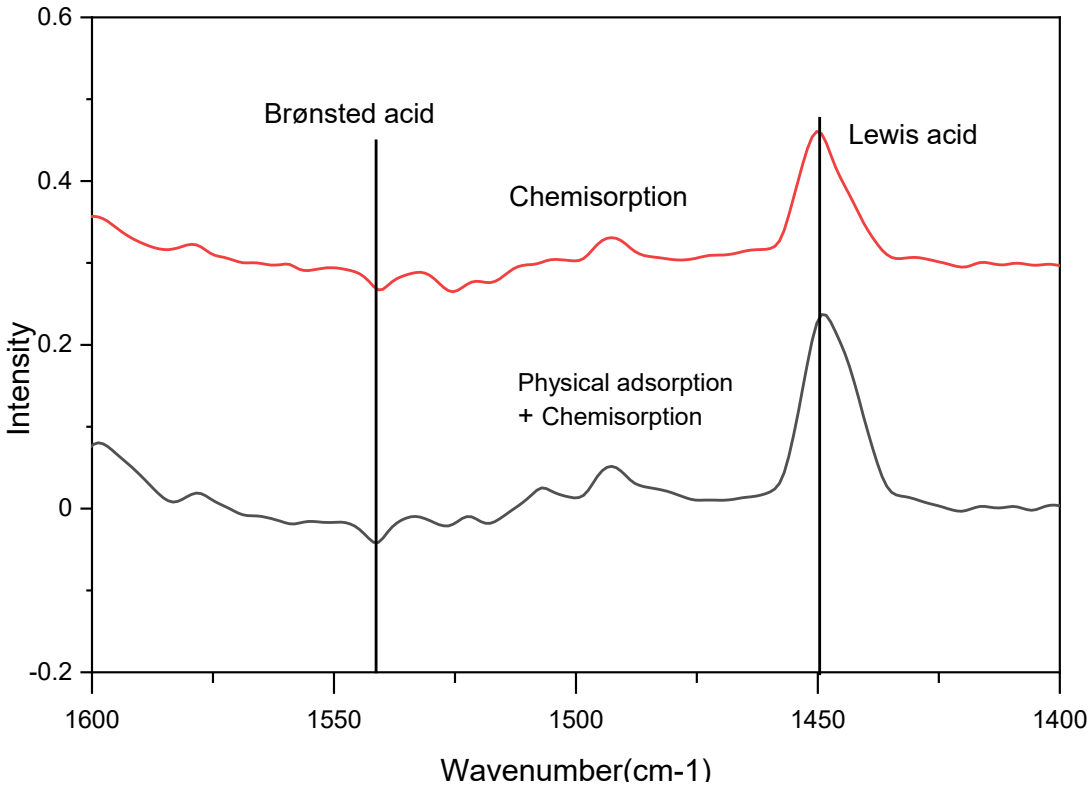

Figure 3.7 FT-IR of pyridine adsorption of 5wt% La/AlOOH catalyst

In summary, the conventional characterization techniques (XRD, BET, CO_2-TPD, and FT-IR/pyridine) did not reveal any systematic differences in structure or acid–base properties among the samples that could be directly correlated with their catalytic performances. Therefore, in order to further clarify the nature and role of surface acid–base sites, selective poisoning experiments were introduced. By examining how acidic or basic probe molecules suppress the catalytic activity, these poisoning tests allow a more reliable evaluation of the strength and amount of the surface active sites involved in the reaction.

Poisoning experiments using probe molecules are widely employed to distinguish the nature, amount, and accessibility of acid–base sites on heterogeneous catalysts. Typical acidic or basic probes—such as pyridine, 2,6-dimethylpyridine, and benzoic acid—can selectively neutralize specific active sites, enabling indirect quantification of the functional groups responsible for catalytic activity. Although such probe-based methods have been extensively applied in acid-catalyzed and

oxidation reactions, their use in aldol-condensation systems over metal-modified alumina remains limited. Among the various potential probes, benzoic acid has attracted interest due to its moderate acidity, strong hydrogen-bonding ability, and well-defined interactions with basic oxygen sites on metal oxides [11]. For La-modified alumina catalysts, where conventional characterization techniques fail to reveal clear differences in acid–base properties among samples, benzoic-acid poisoning provides a more sensitive and discriminating approach. As shown in **Fig. 3.8**, by selectively interacting with basic oxygen anions or surface hydroxyl groups, benzoic acid can inhibit reaction pathways involving base-catalyzed enolate formation. Importantly, owing to its moderate acidity, benzoic acid does not completely neutralize all basic sites but instead induces partial catalyst deactivation, the extent of catalytic activity loss upon benzoic-acid addition offers a more direct measure of the effective amount and strength of basic sites participating in the intramolecular aldol condensation. For this reason, benzoic acid was selected in this study as an acidic probe to evaluate the contribution of surface basicity to the transformation of HD to MCP and to clarify the influence of La incorporation on the active-site environment.

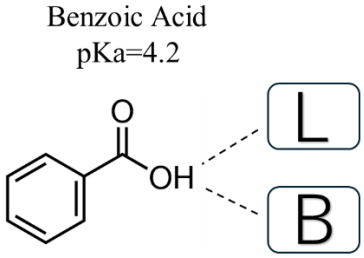

Figure 3.8 Illustration of the poisoning effect of benzoic acid on Lewis and Brønsted base site of a catalyst.

The results of the benzoic-acid poisoning experiments showed that both the conversion and yield decreased progressively with increasing amounts of co-fed BA, as illustrated in **Fig. 3.9, Fig. 3.10** and **Table 3.4, Table 3.5**. These trends clearly indicate a significant difference between the La-loaded

and the none catalyst. For the none catalyst, the reaction activity was almost completely suppressed when 5mg of BA was added. In contrast, the 5wt% *imp*-La/AlOOH catalyst retained noticeable activity even in the presence of 5mg of BA, affording a yield of 6.9%. This observation suggests that La loading generates new basic sites, enabling the *imp*-La/AlOOH catalyst to maintain high activity and stability in both batch and continuous-flow transformations of the intramolecular aldol condensation of HD. Typically, the base-catalyzed transformation of HD proceeds through α-proton abstraction by basic sites, nucleophilic attack on the carbonyl group, and subsequent dehydration to form MCP [12,13].

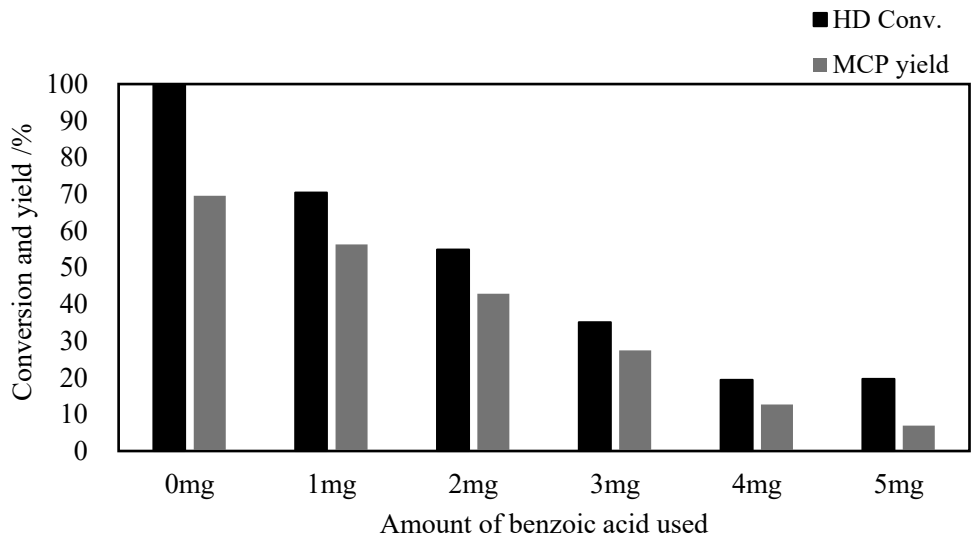

Figure 3.9 Poisoning test results by benzoic acid obtained with 5wt% *imp*-La/AlOOH catalyst calcined at 500 °C

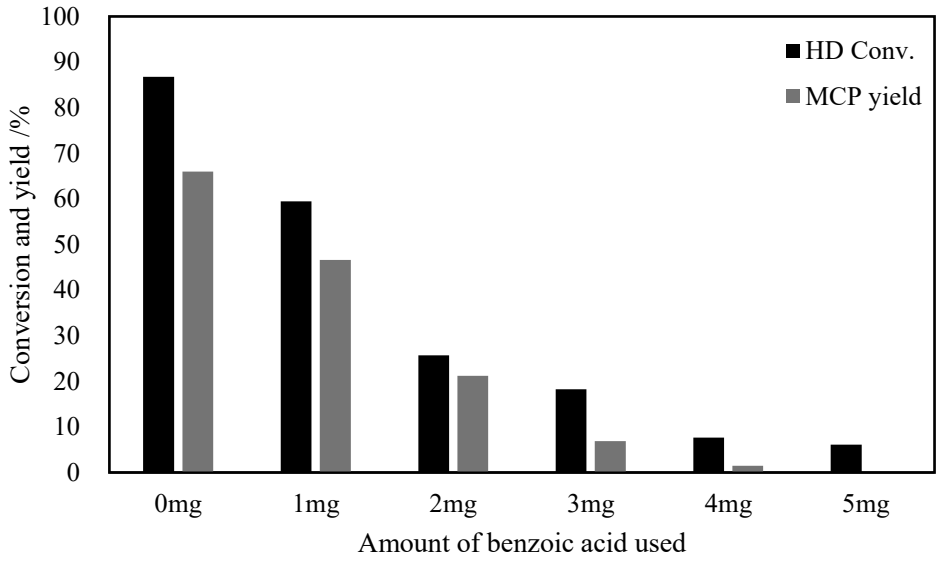

Figure 3.10 Poisoning test results by benzoic acid obtained with 0wt% *imp*-La/AlOOH(none) catalyst calcined at 500 °C

Table 3.4 Poisoning test by benzoic acid over 5wt% *imp*-La/AlOOH

Catalyst	Benzoic acid /mg	Conv. /%	Yield /%	Sel. /%
5wt *imp*-La/AlOOH calcined at 500 °C	0	100	69.6	69.6
	1	70.5	56.3	79.9
	2	54.9	42.8	78.0
	3	35.1	27.4	78.2
	4	19.4	12.7	65.2
	5	19.7	6.9	35.1

Reaction conditions: HD (1.0 mmol), catalyst (50 mg), 1,4-dioxane (5 mL), 3 h, 140 °C, 500 rpm, and benzoic acid (1-5 mg).

Table 3.5 Poisoning test by benzoic acid over 0wt% none/AlOOH

Catalyst	Benzoic acid /mg	Conv. /%	Yield /%	Sel. /%
0wt% none/AlOOH calcined at 500 °C	0	86.7	66.0	76.1
	1	59.5	46.3	78.4
	2	25.7	21.2	82.6
	3	18.3	6.9	37.5
	4	7.7	1.5	19.2
	5	6.1	0	0

Reaction conditions: HD (1.0 mmol), catalyst (50 mg), 1,4-dioxane (5 mL), 3 h, 140 °C, 500 rpm, and benzoic acid (1-5 mg).

On the other hand, Al_2O_3 inherently possesses a certain amount of acidic sites. To examine whether acidic sites remain on the catalyst surface after La loading and to evaluate their potential influence on catalytic performance, 2,6-dimethylpyridine (2,6-DMP) and 3,5-dimethylpyridine (3,5-DMP) were employed to selectively suppress the adsorption of HD on acidic sites. Specifically, previous studies have reported that 2,6-DMP selectively poisons Brønsted acid sites (BAS), as the two methyl groups adjacent to the nitrogen atom hinder its coordination to Lewis acid sites (LAS). In contrast, the methyl groups in 3,5-DMP are located away from the nitrogen atom, allowing this molecule to interact with both BAS and LAS [14,15] (**Fig. 3.11**). The use of such pyridine derivatives for probing and interpreting surface acidity has been well established in the literature [16–18]. Therefore, I anticipated that poisoning studies using 2,6-DMP and 3,5-DMP would provide a reliable basis for understanding the catalytic behavior observed in our experiments.

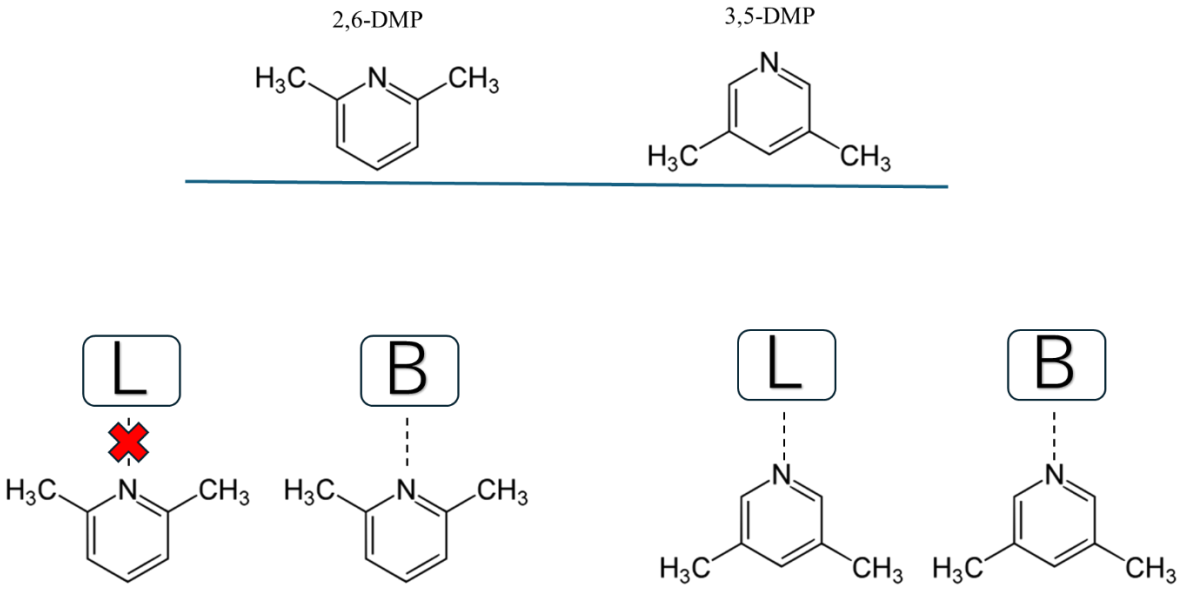

Figure 3.11 Illustration of the poisoning effect of 2,5- and 3,5-DMP on Lewis and Brønsted acid site of a catalyst. [15]

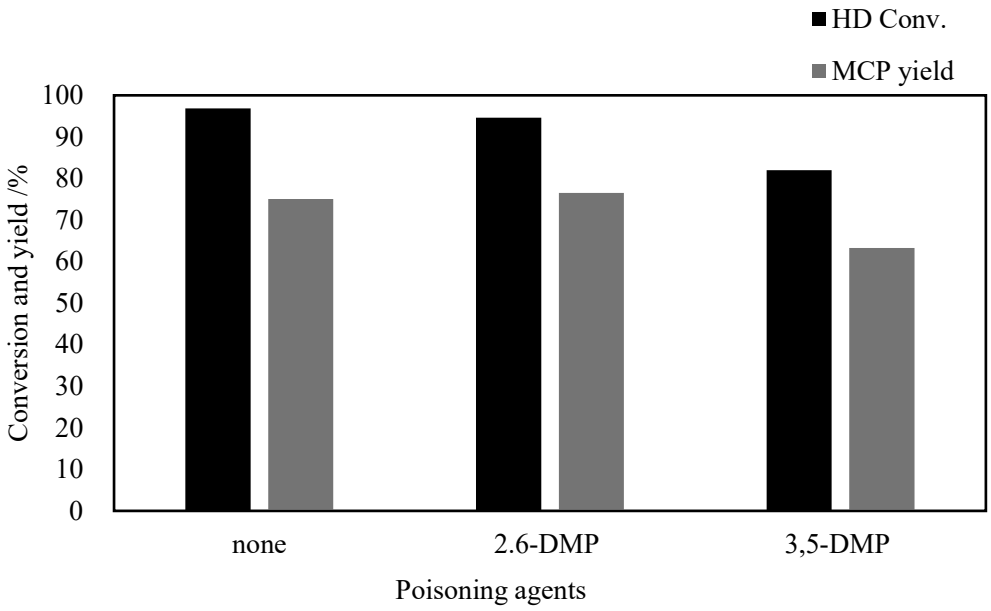

Figure 3.12 Poisoning test results obtained with 5wt% *imp*-La/AlOOH catalyst calcined at 500 °C

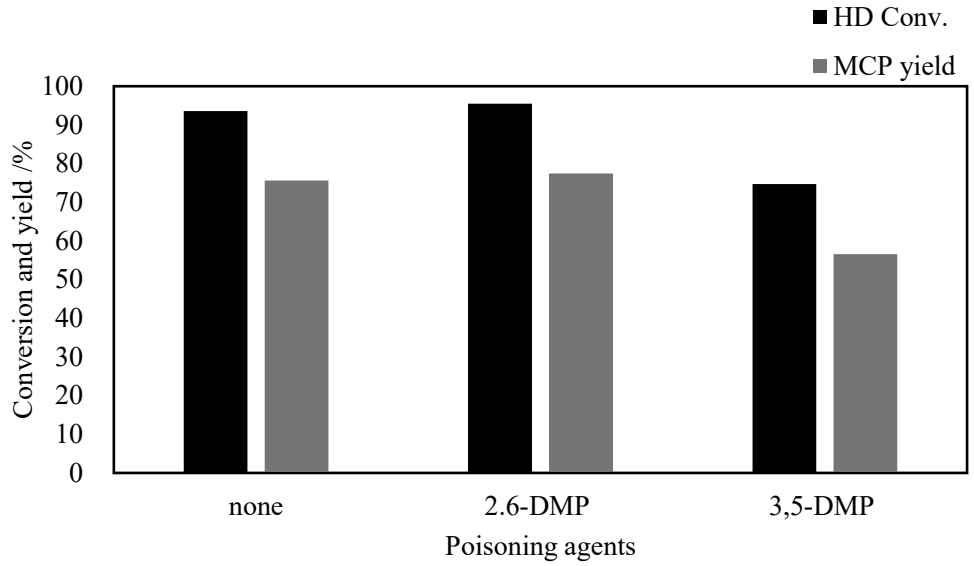

Figure 3.13 Poisoning test results obtained with 0wt% *imp*-La/AlOOH catalyst calcined at 500 °C.

Table 3.6 Poisoning test with 2,6-DMP, or 3,5-DMP over *imp*-La/AlOOH catalysts.

Catalyst	Poisoning agent	Conv. /%	Yield /%	Sel. /%
5wt% *imp*-La/AlOOH	none	93.6	75.6	80.7
calcined at 500 °C	2,6-DMP	95.5	77.4	81.1
	3,5-DMP	81.5	67.0	82.2

Reaction conditions: HD (1.0 mmol), catalyst (50 mg), 1,4-dioxane (5 mL), 3 h, 140 °C, 500 rpm, 2,6-DMP (10 mg), or 3,5-DMP (10 mg).

Table 3.7 Poisoning test with 2,6-DMP, or 3,5-DMP over *imp*-none/AlOOH catalysts.

Catalyst	Poisoning agent	Conv. /%	Yield /%	Sel. /%
0wt% *imp*-none/AlOOH	none	96.9	75.1	77.5
calcined at 500 °C	2,6-DMP	94.6	76.5	80.9
	3,5-DMP	74.7	56.6	75.8

Reaction conditions: HD (1.0 mmol), catalyst (50 mg), 1,4-dioxane (5 mL), 3 h, 140 °C, 500 rpm, 2,6-DMP (10 mg), or 3,5-DMP (10 mg).

Fig. 3.12 and **Fig. 3.13** shows the effects of 2,6-DMP and 3,5-DMP poisoning on the catalytic performance of the 5wt% *imp*-La/AlOOH catalyst and the 0wt% *imp*-La/AlOOH. While 2,6-DMP had almost no influence on the activity of the 500 °C calcined *imp*-La/AlOOH catalyst, giving nearly identical yields (76–77%) and conversions (94–96%), the addition of 3,5-DMP led to a slight decrease in activity, with the yield and conversion dropping to 67% and 81.5%, respectively. These results suggest that the 500 °C calcined *imp*-La/AlOOH catalyst contains Lewis acid sites (LAS), whereas the amount of Brønsted acid sites (BAS) is very limited, indicating that LAS play a crucial role in the aldol condensation of HD to form MCP.

A similar poisoning trend was observed for the none catalyst, 2,6-DMP caused almost no change in catalytic activity, whereas 3,5-DMP induced a pronounced decrease. However, the extent of deactivation by 3,5-DMP was significantly larger for the none catalyst compared with the La-loaded catalyst. This indicates that the surface of the none catalyst possesses weaker basic sites and relatively stronger acidic sites. Due to insufficient basicity, the enolization step is less favorable, resulting in

intrinsically lower catalytic activity. At the same time, the comparatively stronger acidity makes the catalyst more susceptible to poisoning by 3,5-DMP, further diminishing its activity. These observations imply that the none catalyst lacks the moderate basicity and moderate acidity balance created by La modification, making it difficult to establish an effective acid–base cooperative environment. This also explains the lower overall catalytic performance of the none catalyst relative to La/AlOOH. These findings help rationalize why the calcined *imp*-La/AlOOH catalyst exhibits the highest catalytic activity. The results demonstrate that the catalysts prepared by the impregnation method promote the transformation of HD to MCP through an acid–base cooperative catalytic mechanism. The reaction is initiated by α-proton abstraction at basic sites to form an enolate intermediate, which subsequently undergoes intramolecular nucleophilic attack on the second carbonyl group, yielding a cyclic β-hydroxyketone. Finally, dehydration affords the product MCP. Although strong basic sites are essential for enolate formation and C–C bond formation, our results show that the coexistence of acidic and basic sites enhances catalytic activity. Acidic sites may facilitate the dehydration of the β-hydroxyketone intermediate or stabilize key transition states through acid–base interactions, thereby improving overall reaction efficiency. This acid–base synergy explains why catalysts prepared by the impregnation method, which possess both acidic and basic sites, outperform those dominated solely by basic sites. These results highlight the importance of balancing acidity and basicity in designing optimized catalysts for aldol condensation.

Compared with conventional batch reactors, continuous flow liquid reactors have attracted increasing attention in the upgrading of biomass derived platform molecules because they offer higher heat and mass transfer efficiency, more stable reaction environments and better suitability for industrial scale up [19]. Batch reactions are often limited by reactor volume, heat accumulation and the increased likelihood of side reactions as products build up over time, which makes long term stable operation difficult. In contrast, continuous flow reactors allow the substrate to enter the catalytic bed at a constant concentration and undergo selective conversion within short residence

times. This greatly improves reaction controllability and process reproducibility. As a result, continuous flow technology is well suited for upgrading biomass derived oxygenates that are thermally sensitive, proceed through multiple steps or tend to undergo excessive condensation. However, continuous flow operation places more stringent requirements on the physical and chemical stability of catalysts. The catalyst must withstand prolonged liquid flow, temperature fluctuations and coke formation otherwise its activity and selectivity cannot be maintained. Previous studies have reported that AlOOH derived alumina catalysts can retain reasonable MCP selectivity under certain continuous flow conditions [2], although their long-term stability is still limited.

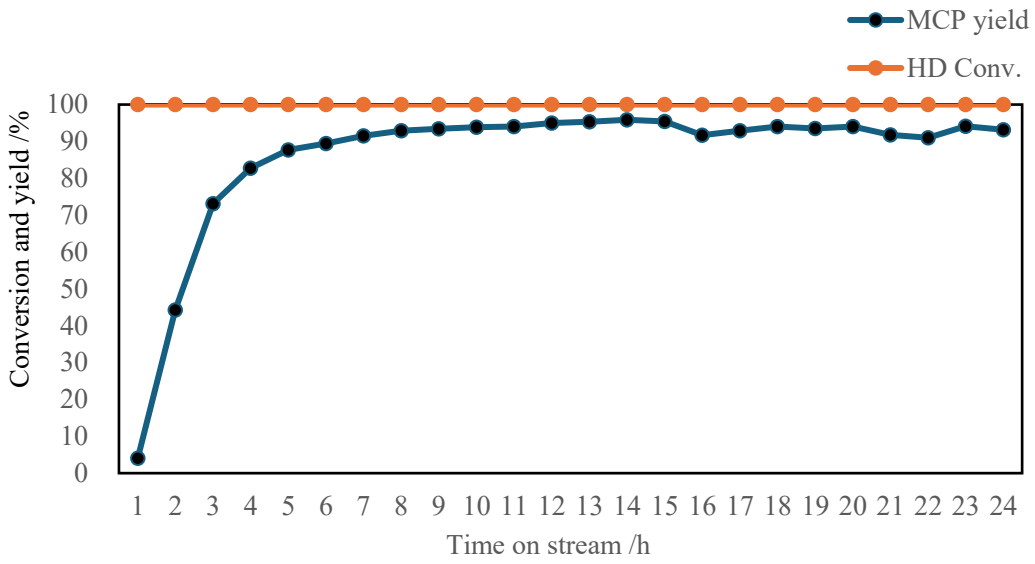

Figure 3.14 Continuous transformation of HD to MCP with a liquid-flow reactor with 5wt% *imp*-La/AlOOH catalyst calcined at 500 ℃.

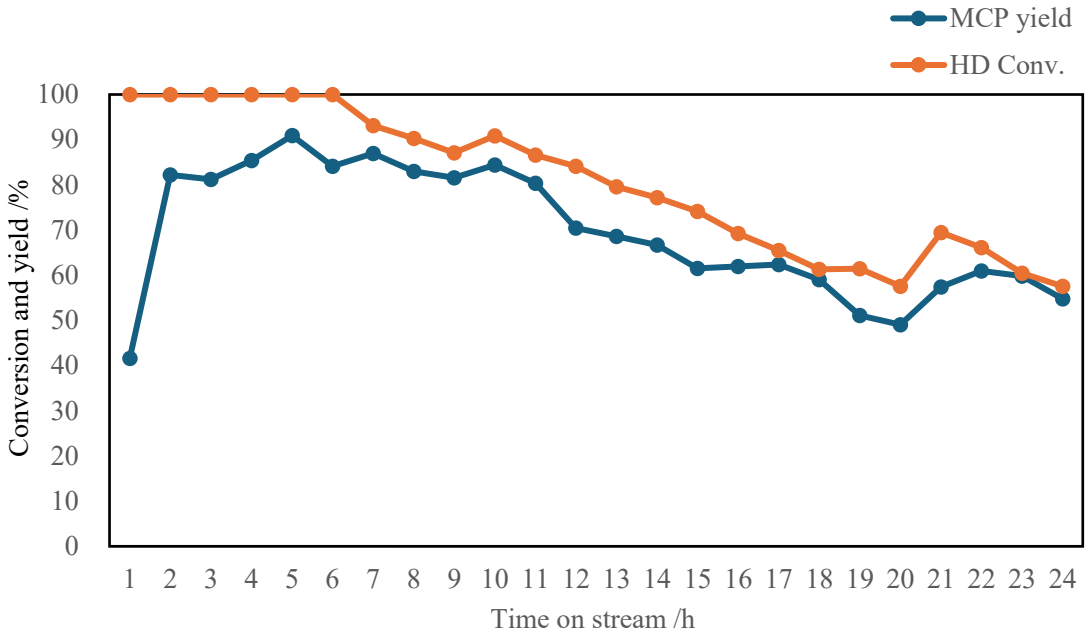

Figure 3.15 Continuous transformation of HD to MCP with a liquid-flow reactor with 0wt% *imp*-La/AlOOH catalyst calcined at 500 ℃.

Reaction conditions: HD concentration in 1,4-dioxane (0.03 mmol mL^{-1}), catalyst bed (500 mg), temperature (140 ℃), flow pump 0.3 ml/min.

As shown in **Fig. 3.14** and **Fig. 3.15**, the results indicate that the AlOOH catalyst loaded with 5 wt percent La was able to operate stably for more than 20 hours after reaching steady state, while consistently maintaining an MCP yield of 87 to 96 percent. This demonstrates its excellent stability under continuous flow conditions. In contrast, the unmodified sample initially reached steady state, but its activity began to decline after approximately 9 hours, indicating catalyst deactivation. Compared with the unmodified sample, the La modified catalyst exhibited significantly higher stability and durability during continuous flow operation. In addition, its stability was clearly superior to that of conventional unmodified Al_2O_3 catalysts reported in the literature [2]. These results show that introducing La together with appropriate thermal treatment not only enhances the catalytic activity of Al_2O_3 in the intramolecular aldol condensation of HD to form MCP but also greatly improves its structural stability and resistance to deactivation in continuous flow systems.

3.4 Conclusion

In summary, the systematic investigation of La–Al_2O_3 catalysts prepared via the impregnation method shows that although variations in La loading and calcination temperature introduce slight changes in physical properties—such as crystalline phase, surface area, and pore structure—these changes do not exhibit any clear correlation with catalytic performance and therefore cannot account for the observed differences in activity. In contrast, selective poisoning experiments reveal critical distinctions that conventional characterization fails to capture: the incorporation of La generates more catalytically active basic oxygen sites on the γ-Al_2O_3 surface while suppressing strong acid sites and forming a moderate population of Lewis acid sites. This modification results in a more favorable acid–base cooperative environment for the transformation of HD to MCP transformation. Benefiting from this synergy, the impregnated–calcined catalyst with 5 wt% La treated at 500 °C exhibits the highest activity in batch reactions and demonstrates exceptional stability under continuous-flow operation, maintaining MCP yields of 87–96% for more than 20 h, whereas the none catalyst undergoes noticeable deactivation after approximately 4 h. These findings indicate that the impregnation method, combined with appropriate thermal treatment, effectively tunes the acid–base properties of alumina and enhances both its structural and operational stability. This strategy represents a crucial approach for achieving highly efficient and long-term stable catalysis in the intramolecular aldol condensation of HD and provides a solid foundation for the further development of rare-earth-modified alumina catalysts for upgrading biomass-derived platform molecules.

References

[1] S. Nishimura, S. Ohmatsu and K. Ebitani, *Fuel Process. Technol*., 2019, 196, 106185.

[2] S. Nishimura, S.D. Le, Y. Asai, N. Takahashi, M. Endo and S. Ohmatsu, *Chem. Lett*., 2022, 51, 131–134.

[3] R. Mahrwald (Ed.), Aldol Reactions, Springer, Dordrecht, 2009, pp. 73–82.

[4] V. E. Colier, N. C. Ellebracht, G. I. Lindy, E. G. Moschetta and C. W. Jones, *ACS Catal*., 2016, 6, 460–468.

[5] J. D. Lewis, S. V. de Vyver and Y. Roman-Leshkov, *Angew. Chem. Int. Ed.,* 2015, 54, 9835–9838.

[6] G. Li, L. Hu and J. M. Hill, *Appl. Catal. A-Gen.*, 2006, 301, 16–24.

[7] M. A. Goula, N. D. Charisiou, K. N. Papageridis, A. Delimitis, E. Pachatouridou and E. F. Iliopoulou, *Int. J. Hydrogen Energy*, 2015, 40, 9183–9200.

[8] Z. J. Ling, Master's Thesis, Japan Advanced Institute of Science and Technology (JAIST), 2023.

[9] E. R. Sacia, M. H. Deaner, Y. L. Louie and A. T. Bell, *Green Chem.*, 2015, 17, 2393–2397.

[10] T. Yamamoto, T. Hatsui, T. Matsuyama, T. Tanaka, and T. Funabiki, *Chem. Mater,* 2003, 15, 25, 4830–4840.

[11] Q. Bao, W. Zhu, J. Yan, C. Zhang, C. Ning, Y. Zhang, M. Hao and Z. Wang, *RSC Adv.*, 2017, *7*, 52304–52311.

[12] H. Hunsdiecker, *Chem. Ber*. 1942, 75, 455.

[13] A. Guida, M. H. Lhouty, D. Tichit, F. Figueras, P. Geneste, *Appl. Catal. A: Gen.* 1997, 164, 215.

[14] S. Sato, M. Tokumitsu, T. Sodesawa and F. Nozaki, *Bull. Chem. Soc. Jpn.*, 1991, 64, 1005–1007.

[15] L. Yu, E. Kurniawan, T. Ozawa, H. Kobayashi, Y. Yamada and S. Sato, *Mol. Catal.*, 2023, 537, 112939.

[16] T. Adachi, E. Kurniawan, T. Hara, R. Takahashi, Y. Yamada, S. Sato, *Appl. Catal. A Gen*., 2024, 685, 119887.

[17] A. Borgna, J. Sepulveda, S. I. Magni, C. R. Apesteguia, *Appl. Catal. A: Gen*., 2024, 276, 207.

[18] A. Corma, C. Rodellas, V. Fornes, *J. Catal.* 1984, 88, 374–381.

[19] R. Gérardy, D. P. Debecker, J. Estager, P. Luis, J.-C. M. Monbaliu, *Chem. Rev*. 2020, 120, 7219.

Chapter 4 Co-precipitated La-modified Boehmite-derivatives as Solid Base Catalyst for the Intramolecular Aldol Condensation of 2,5-Hexanedione

4.1 Abstract

This study focuses on the design and evaluation of lanthanum (La)-modified boehmite (AlOOH)-derived catalysts synthesized by a urea homogeneous precipitation (*cp*-) method, with performance compared to that of catalysts prepared by conventional impregnation (*imp*-) method. These catalysts were applied in the intramolecular aldol condensation of 2,5-hexanedione (HD) to produce 3-methyl-2-cyclopentenone (MCP). A range of La loadings and calcination temperatures were investigated. Structural characterization by XRD and N_2 physisorption were conducted to correlate physical properties with catalytic performance. The *cp*-La-Al-(OH) catalyst exhibited high activity even without calcination as 54% yield with 82% selectivity, which was comparable to the imp-La/AlOOH catalyst required thermal treatment to become active as 60% yield with 71% selectivity, in 3.0 mmol scale of the reaction. These differences were attributed to distinct surface characteristics and active site distributions arising from the preparation method. Poisoning experiments using benzoic acid, 2,6-dimethylpyridine and 3,5-dimethylpyridine indicated that the reaction proceeds via an acid–base cooperative mechanism.

4.2 Introduction

In my previous studies, I demonstrated that La-loaded alumina catalysts (La/AlOOH) prepared via the impregnation method exhibit remarkable catalytic advantages, particularly when basic La-derived active sites are introduced onto the alumina surface. These catalysts showed exceptionally high activity toward the intramolecular aldol condensation of HD to MCP, and it was found that the amount and strength of these basic sites played a decisive role in determining catalytic performance, being strongly influenced by La loading, calcination temperature, reaction temperature, and contact time [1, 2]. In contrast, the co-precipitation method offers an efficient synthetic route capable of achieving homogeneous metal incorporation at the molecular level while simultaneously forming nanocrystalline precursor phases [3, 4]. Although both impregnation and co-precipitation are widely employed for the preparation of metal-loaded catalysts, they typically generate fundamentally different surface structures, metal dispersion states, and acid–base characteristics. Thus, even when the overall chemical composition is identical, the catalytic behaviors of the resulting materials may differ substantially [5]. However, to date, few studies have systematically compared lanthanum-based catalysts prepared by these two methods for the intramolecular aldol condensation of HD to MCP.

Our investigations further revealed that thermal treatment induces significant changes in the structural features and acid–base properties of La–Al catalysts derived from the co-precipitation method. Moreover, selective poisoning experiments highlighted the cooperative roles of acidic and basic sites in the transformation of HD to MCP, demonstrating that differences in the type, strength, and accessibility of these sites can profoundly affect catalytic performance. Against this backdrop, the present work provides the first systematic comparison of La/AlOOH derived catalysts prepared by co-precipitation and impregnation, evaluated both with and without thermal treatment, focusing on their structural characteristics, acid–base properties, and catalytic behaviors in the intramolecular aldol condensation of HD.

The results show that the non-calcined La/AlOOH catalyst prepared via the simple co-precipitation

method exhibits excellent catalytic activity owing to its unique and well-balanced acid–base surface properties. These findings reveal that an efficient bifunctional catalytic environment can be constructed solely by optimizing the preparation strategy—without the need for high-temperature calcination—thus providing a new direction for the design of green, highly active La-based catalysts for biomass-derived molecular upgrading.

4.3 Result and discussion

Fig. 4.1 shows the MCP yield and HD conversion over non-calcined *cp*-La–Al–(OH) catalysts with various La:Al ratios. The detailed values, together with the specific surface area (S_{BET}), are summarized in **Table 4.1**. In all cases, the total amount of La + Al was fixed at 12. 5 mmol and the urea/metal ratio was kept at 4.0. The La:Al ratio markedly influenced the activity toward the intramolecular aldol condensation of HD to MCP. As the La/Al ratio increased from 1:0 to 1:50, both MCP yield and HD conversion increased steadily. Further increase of Al content resulted in a gradual decline in reactivity. The highest activity was observed at La:Al = 1:50, affording an MCP yield of 54% and an HD conversion of 66% (82% selectivity). The S_{BET} values exhibited a similar trend, although the maximum surface area of 204 $m^2 g^{-1}$ was obtained at La:Al = 1:80.

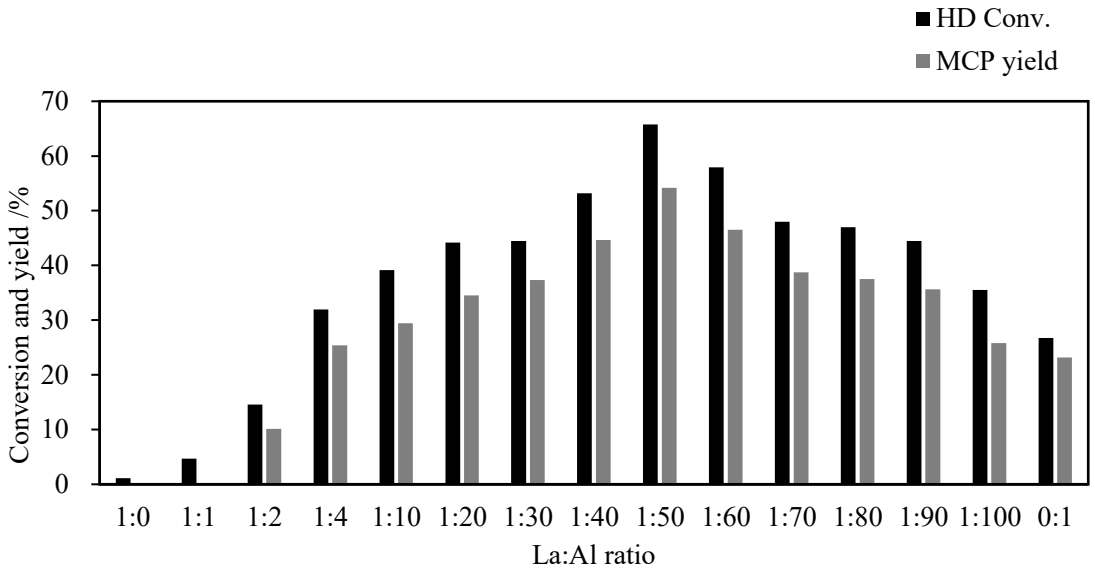

Figure 4.1 Reactivity over non-calcined *cp*-La-Al-(OH) catalysts with different La:Al ratios.

Table 4.1 Reactivity over non-calcined *cp*-La-Al-(OH) catalysts with different ratio.

Entry	Molecular ratio of La: Al*	Conv. /%	Yield /%	Sel. /%	Specific surface area /m^2 g^{-1}
1	1:0	1.1	0	0	0.7
2	1:1	4.7	0	0	56.4
3	1:2	14.6	10.1	69.4	80.1
4	1:4	32.0	25.4	79.4	129.8
5	1:10	39.2	29.4	75.1	171.4
6	1:20	44.2	34.5	78.2	168.0
7	1:30	44.5	37.3	84.0	173.5
8	1:40	53.2	44.6	83.9	158.2
9	1:50	65.8	54.2	82.4	141.9
10	1:60	57.9	46.5	80.3	161.7
11	1:70	48.0	38.7	80.7	198.9
12	1:80	47.0	37.5	79.8	204.2
13	1:90	44.5	35.6	80.1	196.7
14	1:100	35.5	25.8	72.6	129.5
15	0:1	26.7	23.1	86.6	140.8

Reaction conditions: HD (3.0 mmol), Catalyst (50 mg), 1,4-dioxane (5.0 mL), Time (3 h), Temp. (140°C), and 500 rpm. *La + Al = 0.0125 mmol (*const.*)

For comparison, non-calcined *imp*-La/AlOOH catalysts with La loadings of 1.0–5.0 wt% exhibited almost no catalytic activity under the same reaction conditions (**Fig. 4.2** and **Table 4.2**). The MCP yield decreased progressively with increasing La loading, from 13% at 1.0 wt%, and eventually approached 0% at 4.0–5.0 wt%. Meanwhile, the SBET value decreased from 256 $m^2 g^{-1}$ (1.0 wt% La) to 139 $m^2 g^{-1}$ (5.0 wt% La). These striking contrasts underline the importance of the preparation method in generating catalytically active La–Al–(OH) derivatives without thermal treatment. In particular, non-calcined *cp*-derived samples clearly outperform their *imp*-derived counterparts in the direct La-loading methodology for AlOOH-based catalysts. Notably, my previous studies attributed the enhanced activity of calcined *imp*-La/AlOOH to strong interactions between La and alumina formed during thermal treatment. In contrast, the present results reveal that, without calcination, the hp route provides a fundamentally different and more effective pathway for producing catalytically functional materials, offering new insights into La–Al catalyst design.

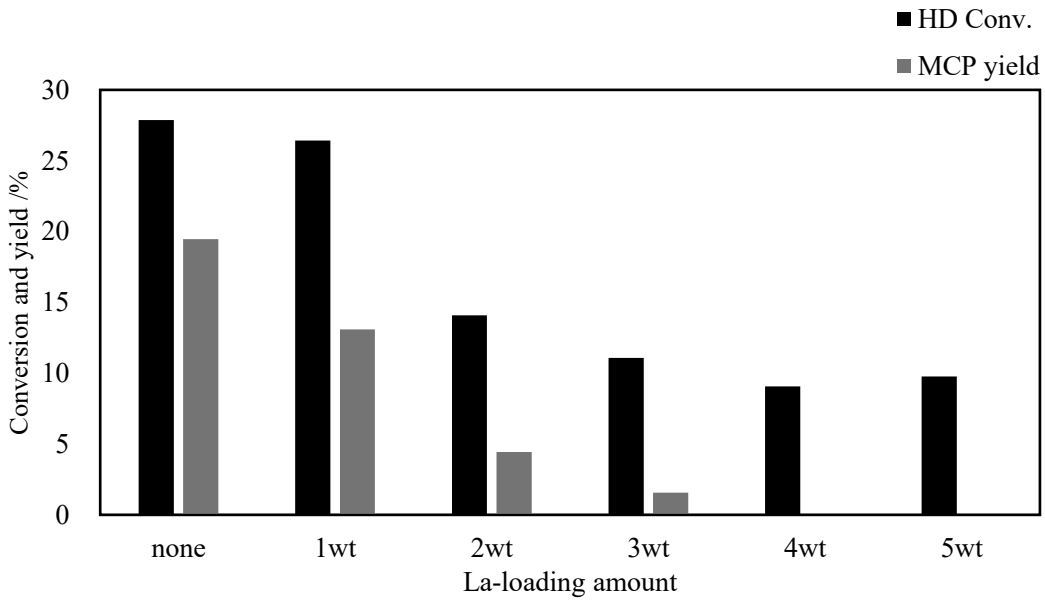

Figure 4.2 Reactivity over non-calcined *imp*-La/AlOOH catalysts with different different La loadings.

Table 4.2 Reactivity and S_{BET} over non-calcined *imp*-La/AlOOH catalysts with different La loadings.

Loading amount /wt%	Conversion /%	Yield /%	Sel. /%	Specific surface area /m^2 g^{-1}
0	27.9	19.5	69.8	222.2
1.0	26.4	13.1	49.6	256.4
2.0	14.1	4.4	31.5	257.5
3.0	11.1	1.6	14.0	245.6
4.0	9.8	0	0	172.3
5.0	9.1	0	0	139.3

Reaction conditions: HD (3.0 mmol), Catalyst (50 mg), 1,4-dioxane (5.0 mL), Time (3 h), Temp. (140°C), and 500 rpm.

The most critical point to address is that the catalysts were used without calcination. In this state, the presence of residual impurities is unavoidable, and such species may potentially influence the acid–base properties of the materials. Therefore, it is essential to verify experimentally that the observed catalytic activity does not originate from impurity-derived effects but from the intrinsic properties of the La–Al-based solids. Without such confirmation, the discussion regarding the relationship between acid–base characteristics and catalytic performance would remain inconclusive. To clarify this point, a hot filtration test was conducted to verify whether the catalytic activity originated from the solid catalyst rather than dissolved species. The hot filtration method is a commonly employed protocol for distinguishing truly heterogeneous catalysis from homogeneous or leached-species catalysis. In this method, the reaction is first allowed to proceed in the presence of the solid catalyst until measurable conversion is obtained. The solid catalyst is then removed from the reaction mixture at the reaction temperature, typically by rapid filtration or decantation under hot conditions to avoid the re-adsorption of dissolved species. If the reaction continues after catalyst removal, the active species are considered to be homogeneous or leached into the solution. Conversely, if no further conversion occurs, the active sites are confirmed to reside on the solid catalyst surface rather than in the liquid phase. This methodology has been widely adopted in heterogeneous catalysis studies to validate catalyst heterogeneity and exclude the contribution of dissolved metal species [6,7].

In this study, the reaction was conducted for 1 h in the presence of the catalyst. The solid catalyst was then removed under reaction conditions, and the reaction was allowed to proceed until 3 h. As shown in **Fig. 4.3**, no further increase in MCP yield was observed after catalyst removal, with the yield remaining at 36.2 %. This result clearly indicates that the catalytic activity originates from the solid catalyst rather than dissolved species. Notably, the non-calcined *cp*–La–Al–(OH) catalyst exhibited unexpectedly high catalytic activity, suggesting that unique structural or chemical features formed during the co-precipitation process may play a pivotal role, revealing a previously overlooked pathway for catalyst design.

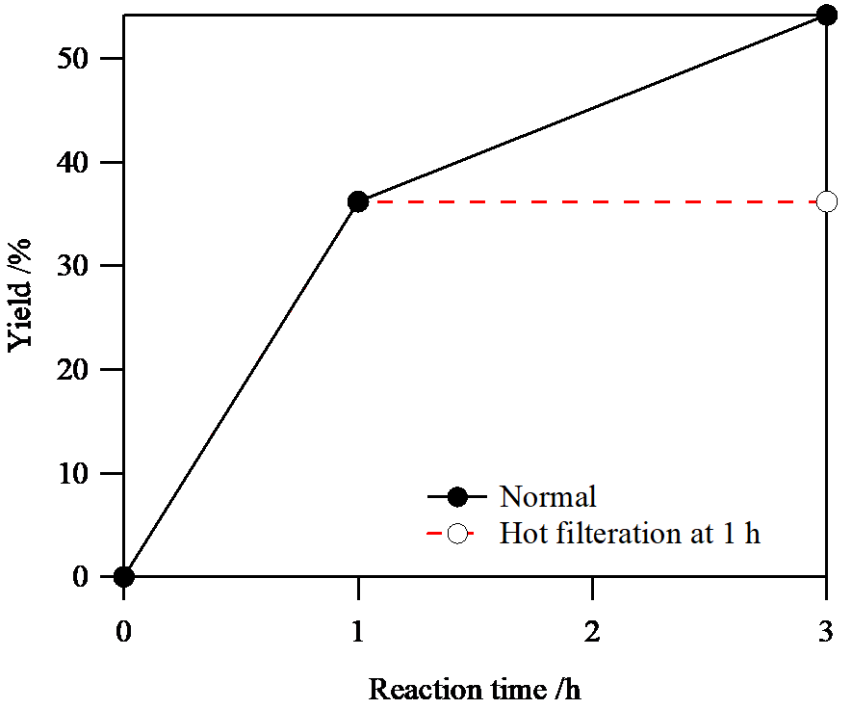

Figure 4.3 Hot filtration experiment with non-calcined *cp*-La-Al-(OH) with La:Al of 1:50. *Reaction conditions:* HD (3.0 mmol), catalyst (50 mg), 1,4-dioxane (5.0 mL), 3 h, 140°C, and 500 rpm.

Fig. 4.4 and **Fig. 4.5** shows the XRD patterns of non-calcined *cp*-La–Al-(OH) samples prepared with different La:Al ratios. When the La content is relatively high (La:Al ≤ 1:10), the dominant phase in the precipitates is $La(OH)(NO_3)_2$, whose characteristic diffraction peaks appear at $2\theta = 20.9°$, 24.2°,

30.4°, and 39.0°, corresponding to the (002), (021), (112), and (222) planes, respectively. As the Al content increases (from La:Al = 1:20 onward), the XRD patterns undergo a significant change, and the main crystalline phase shifts to AlOOH. Its characteristic reflections are observed at 2θ = 14.7°, 28.3°, 38.6°, and 49.6°, corresponding to the (110), (111), (020), and (130) planes. Notably, the phase transition threshold occurs at approximately La:Al = 1:10 (around 33 wt% La), which is consistent with the findings reported by Yamamoto et al. [8]. In contrast, the XRD patterns of the non-calcined *imp*-La/AlOOH samples (1–5 wt%) shown in **Fig. 4.6** reveal that the AlOOH phase remains unchanged regardless of La loading.

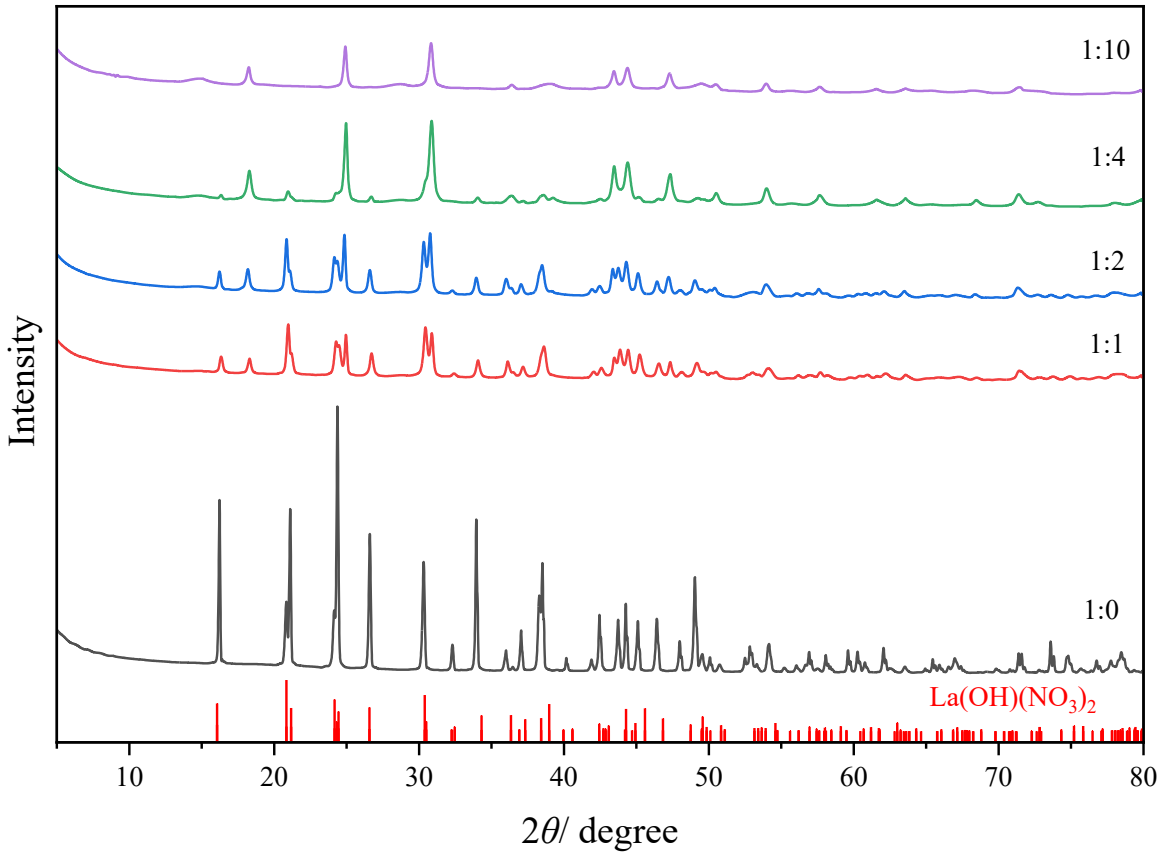

Figure 4.4 XRD patterns of non-calcined *cp*-La-Al-(OH) catalysts with different La:Al ratios. (1)

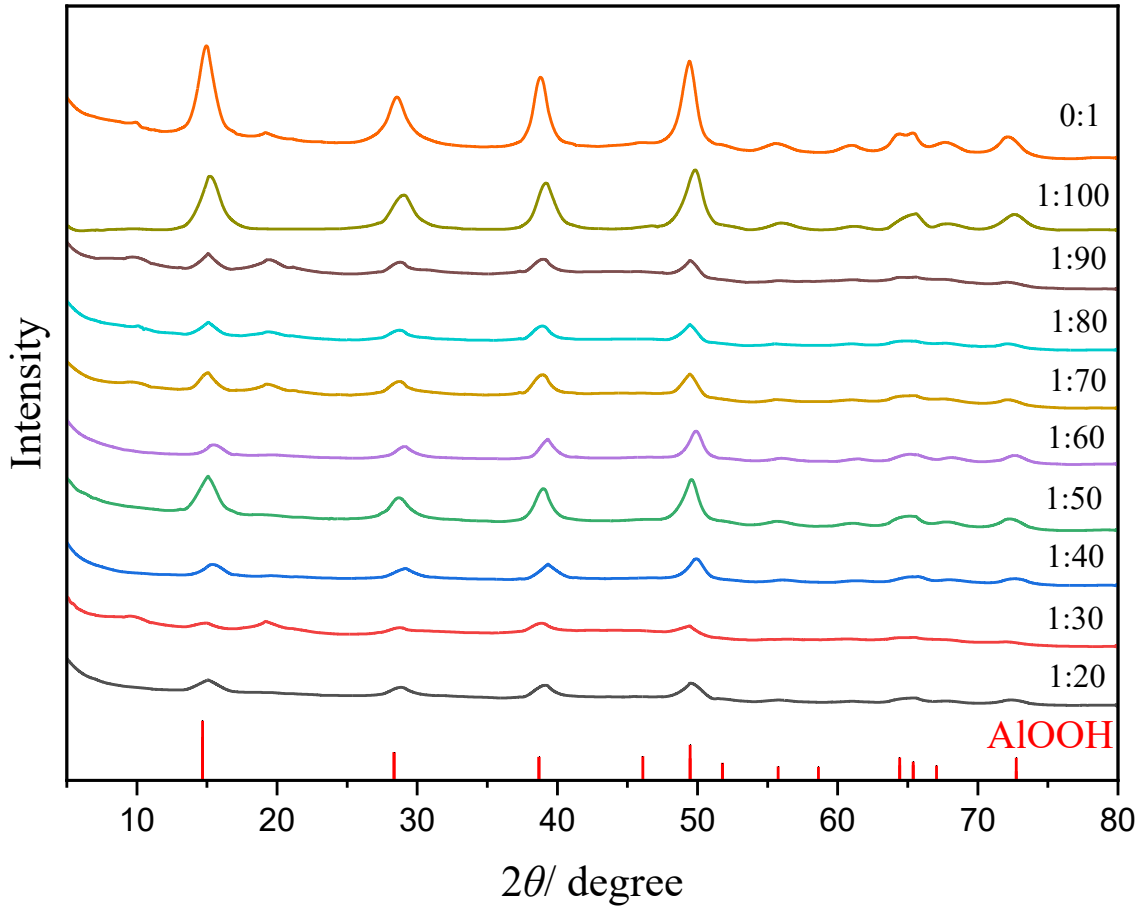

Figure 4.5 XRD patterns of non-calcined *cp*-La-Al-(OH) catalysts with different La:Al ratios. (2)

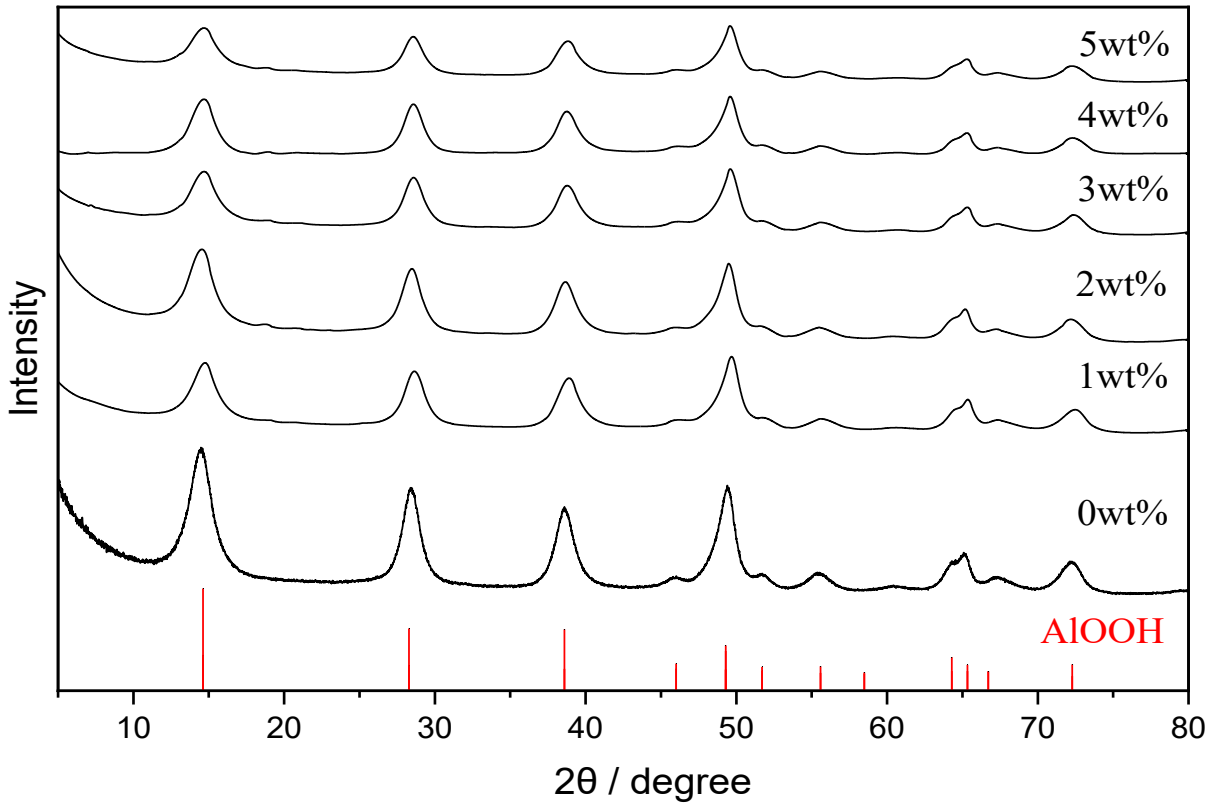

Figure 4.6 XRD patterns of non-calcined *imp*-La/AlOOH catalysts with various La loadings (0-5 wt%).

Fig. 4.7 and **Fig. 4.8** illustrate the pronounced structural differences between the samples prepared by the co-precipitation and impregnation methods as observed in the N_2 adsorption–desorption measurements. The non-calcined *cp*-La–Al-(OH) exhibits poorly defined mesoporosity together with pronounced macroporous features, whereas the non-calcined *imp*-La/AlOOH shows a typical Type IV isotherm characteristic of well-developed mesoporous structures. However, the high catalytic activity of *cp*-La–Al-(OH) (MCP yield 55%) indicates that mesoporosity is not the key factor governing activity in this system. In contrast, in our previous study, the calcined 5 wt% *imp*-La/AlOOH (500 °C) displayed high activity (MCP yield 60%) and showed a representative Type IV mesoporous isotherm pattern [1,2]. Additionally, the 0:1 (Al-only) *cp*-La–Al-(OH) sample and commercial AlOOH exhibited, respectively, a weakly defined mesoporous/macroporous profile and a typical mesoporous isotherm, as shown in **Fig. 4.9** and **Fig. 4.10**. Overall, no clear correlation was observed between physical textural properties and catalytic activity. Therefore, the high activity of

non-calcined *cp*-La–Al-(OH) is more likely attributed to the specific dispersion state or chemical environment of La species formed during synthesis rather than to pore structure.

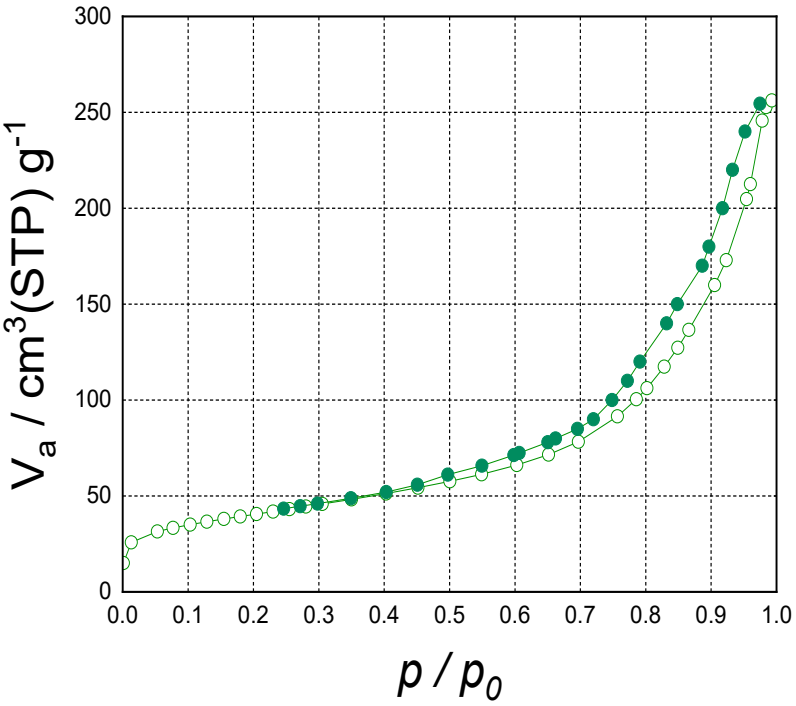

Figure 4.7 N_2 adsorption–desorption isotherms of non-calcined *cp*-La-Al-(OH) as La:Al = 1:50

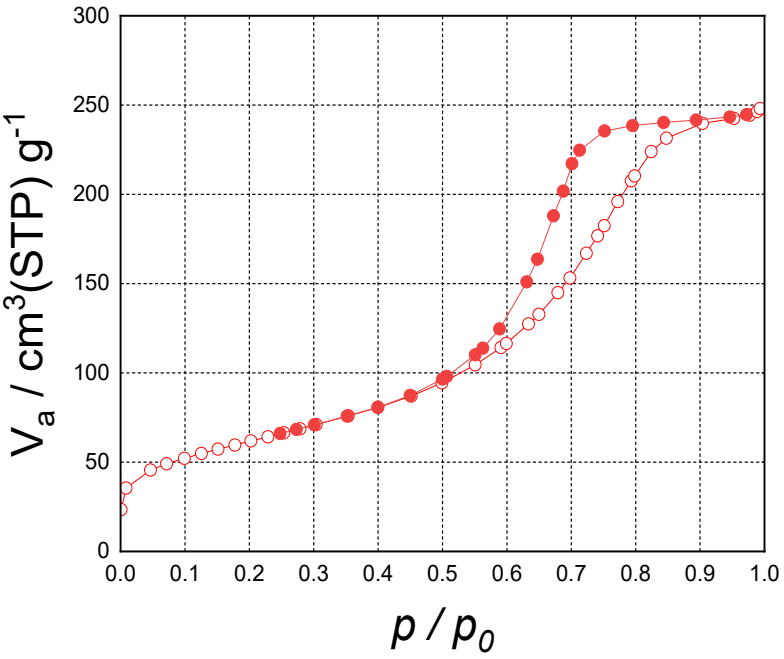

Figure 4.8 N_2 adsorption–desorption isotherms of non-calcined *imp*-La/AlOOH as 5 wt% La

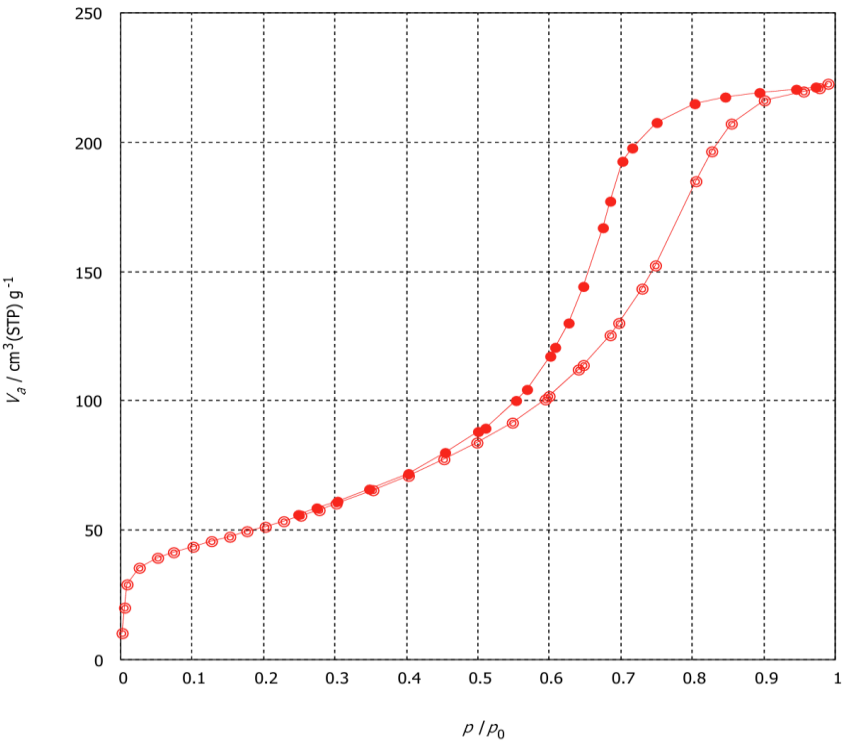

Figure 4.10 N_2 adsorption–desorption isotherms of non-calcined pristine AlOOH (commercial).

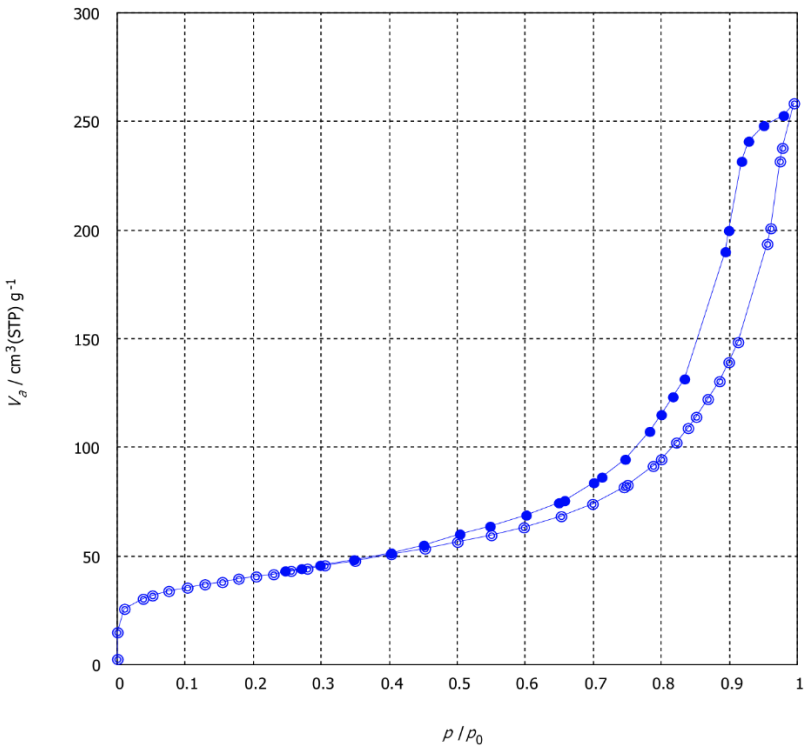

Figure 4.11 N_2 adsorption–desorption isotherms of non-calcined *cp*-La-Al-(OH) with La:Al = 0:1

Fig. 4.12 and **Table 4.3** show the poisoning test results of non-calcined cp-La–Al-(OH) samples with different La:Al ratios in the presence of benzoic acid (BA). Because the basicity of non-calcined samples cannot be quantitatively evaluated by CO_2-TPD [1,2], BA poisoning was used as an alternative method. In our previous study, the calcined *imp*-La/AlOOH (500 °C) exhibited a drastic drop in MCP yield from 60% to 6.9% upon the addition of 5 mg BA. In contrast, the non-calcined *cp*-La–Al-(OH) samples retained substantial catalytic activity under the same BA dosage; for instance, the La:Al = 1:50 sample still achieved a 21.7% MCP yield. This finding indicates that non-calcined *cp*-La–Al-(OH) possesses stronger or more resilient basic sites, enabling the catalyst to maintain activity under BA poisoning conditions. At the same time, however, a contradiction becomes apparent: although these samples exhibit stronger basicity, their maximum yield (54%) remains lower than that of the calcined *imp*-La/AlOOH (60%). This discrepancy suggests that, beyond basicity alone, acidic sites may also play an important role in the transformation of HD to MCP. Consistent with this

interpretation, numerous studies have reported that catalysts featuring bifunctional acid–base sites can effectively promote aldol condensation processes [9–14].

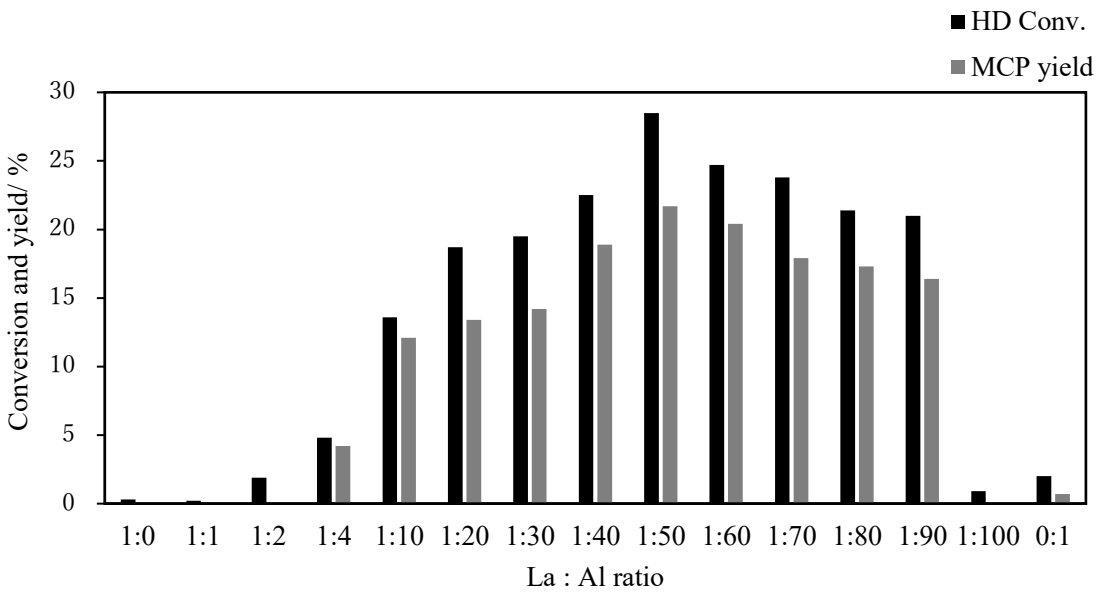

Figure 4.12 Poisoning test result with BA over non-calcined *cp*-La-Al-(OH) catalysts with different La:Al ratios.

Table 4.3 Poisoning test with BA over non-calcined *cp*-La-Al-(OH) with various La:Al ratios.

Molecular ratio of La: Al*	Conversion /%	Yield /%	Selectivity /%
1:0	0.3	0	0
1:1	0.2	0	0
1:2	1.9	0	0
1:4	4.8	4.2	87.9
1:10	13.6	12.1	89.1
1:20	18.7	13.4	71.7
1:30	19.5	14.2	72.4
1:40	22.5	18.9	84.0
1:50	28.5	21.7	76.1
1:60	24.7	20.4	82.4
1:70	23.8	17.9	75.2
1:80	21.4	17.3	80.8
1:90	21.0	16.4	78.0
1:100	0.9	0	0
0:1	2.0	0.7	35.9

Reaction conditions: HD (1.0 mmol), catalyst (50 mg), 1,4-dioxane (5.0 mL), 3 h, 140 °C, 500 rpm, and benzoic acid (5 mg). *La + Al = 0.0125 mmol (*const.*)

To investigate the differences in acidic sites between the non-calcined *cp*-La-Al-(OH) and the calcined *imp*-La/AlOOH catalysts, selective acid-site poisoning experiments were conducted using 2,6-dimethylpyridine (2,6-DMP) and 3,5-dimethylpyridine (3,5-DMP). It is known that 2,6-DMP selectively poisons Brønsted acid sites (BAS), whereas 3,5-DMP can poison both BAS and Lewis acid sites (LAS) [15,16]. As shown in **Fig. 4.13** and **Table 4.4**, the catalytic activity of the non-calcined *cp*-La-Al-(OH) remained essentially unchanged in the presence of either probe molecule (71–73 %), indicating that its surface contains very few acidic sites or that such sites are not accessible for adsorption. In contrast, **Fig. 4.14** and **Table 4.5** show that the calcined *imp*-La/AlOOH catalyst exhibited a slight decrease in activity upon the addition of 3,5-DMP, while 2,6-DMP had no measurable effect. This behavior suggests that its surface is predominantly composed of LAS with

almost no BAS. Taken together, these findings indicate that the excellent performance of the calcined *imp*-La/AlOOH catalyst originates from the presence of an appropriate amount of LAS, whereas the non-calcined *cp*-La-Al-(OH) catalyst relies mainly on basic sites for its activity.

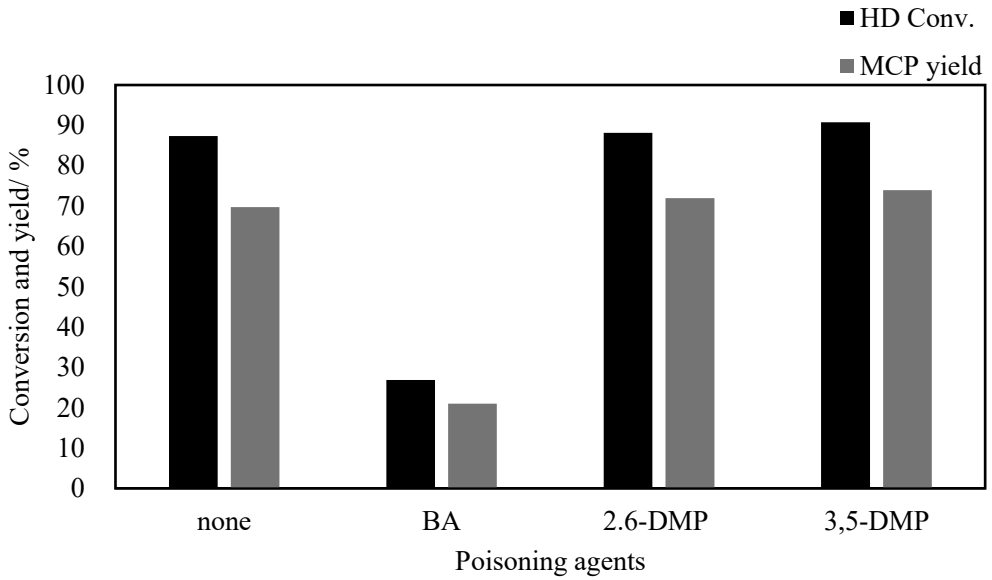

Figure 4.13 Effect of different poisoning agents on the catalytic activity of the non-calcined *cp*-La-Al-(OH) (La:Al = 1:50) catalysts

Table 4.4 Poisoning test with BA, 2,6-DMP, or 3,5-DMP over La–Al catalysts.

Catalyst	Poisoning agent	Conv. /%	Yield /%	Sel. /%
cp-La-Al-(OH)	none	87.3	69.8	79.9
(La:Al = 1:50, non-calcined)	BA	26.9	21.0	78.0
	2,6-DMP	88.2	71.9	81.6
	3,5-DMP	90.8	74.0	81.5

Reaction conditions: HD (1.0 mmol), catalyst (50 mg), 1,4-dioxane (5 mL), 3 h, 140 °C, 500 rpm, and BA (5 mg), 2,6-DMP (10 mg), or 3,5-DMP (10 mg).

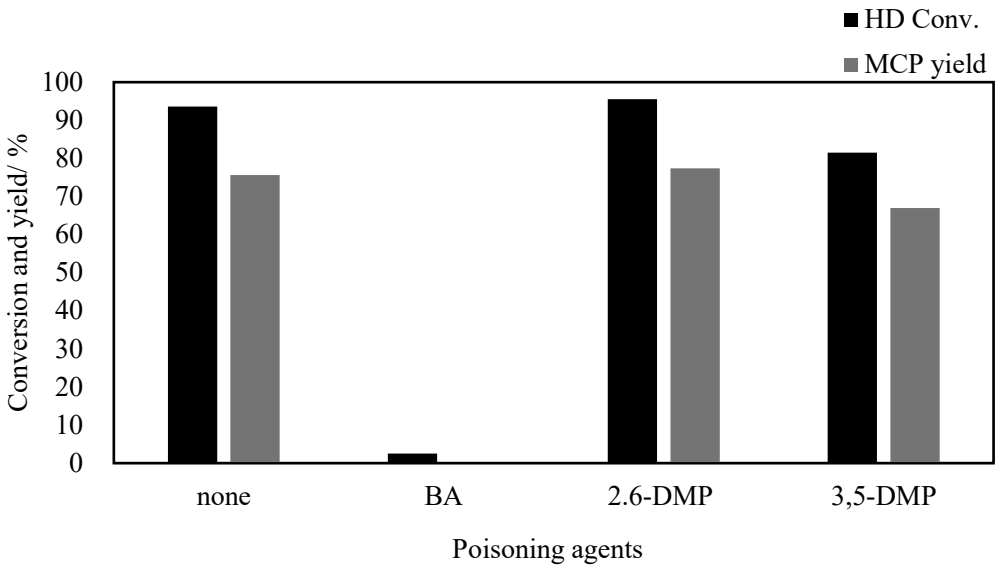

Figure 4.14 Effect of different poisoning agents on the catalytic activity of the calcined *imp*-La/AlOOH (5 wt% La, 500 °C) catalysts

Table 4.5 Poisoning test with BA, 2,6-DMP, or 3,5-DMP over La–Al catalysts.

Catalyst	Poisoning agent	Conv. /%	Yield /%	Sel. /%
Calcined *imp*-La/AlOOH	none	93.6	75.6	80.7
(5 wt% La, calcined at 500 °C)	BA	2.5	0	0
	2,6-DMP	95.5	77.4	81.1
	3,5-DMP	81.5	67.0	82.2

Reaction conditions: HD (1.0 mmol), catalyst (50 mg), 1,4-dioxane (5 mL), 3 h, 140 °C, 500 rpm, and BA (5 mg), 2,6-DMP (10 mg), or 3,5-DMP (10 mg).

Taken together, the findings indicate that the transformation of HD to MCP proceeds through an acid–base cooperative mechanism, in which basic sites promote deprotonation to generate the enolate intermediate, while acidic sites assist the subsequent cyclization and dehydration steps. The balance and accessibility of acidic and basic sites in each catalyst ultimately determine the observed activity and selectivity.

The effect of calcination on the activity of the *cp*-La-Al-(OH) catalysts was further examined. The non-calcined sample with the highest activity (La:Al = 1:50) was calcined in the range of 300 to 900 °C and subsequently evaluated. As shown in **Fig. 4.15** and **Table 4.6**, all calcined samples

exhibited lower activity than the non-calcined material, with the yield decreasing from 54 % to 32–42 %. This clearly indicates that calcination destroys the key basic sites responsible for the high activity of the non-calcined catalyst. The XRD patterns of the calcined samples (**Fig. 4.16**) reveal that the crystalline phase transforms into γ-Al_2O_3 or δ-Al_2O_3, similar to the impregnated samples. However, the N_2 adsorption–desorption isotherms (**Fig. 4.17**) show no significant changes in pore structure after calcination, suggesting that the pore architecture is primarily determined by the preparation method rather than by thermal treatment. Acid–base characterization further confirmed that calcination leads to a substantial loss of basicity, and no evident acidic sites were detected. When 5mg of benzoic acid was introduced, the catalytic activity nearly disappeared (from 76 % to < 2 %) as shown in **Fig 4.18** and **Tabel 4.7**. These results indicate that specific basic sites present in the non-calcined *cp*-La-Al-(OH), which are easily damaged by high temperatures, are essential for the high catalytic performance of this material.

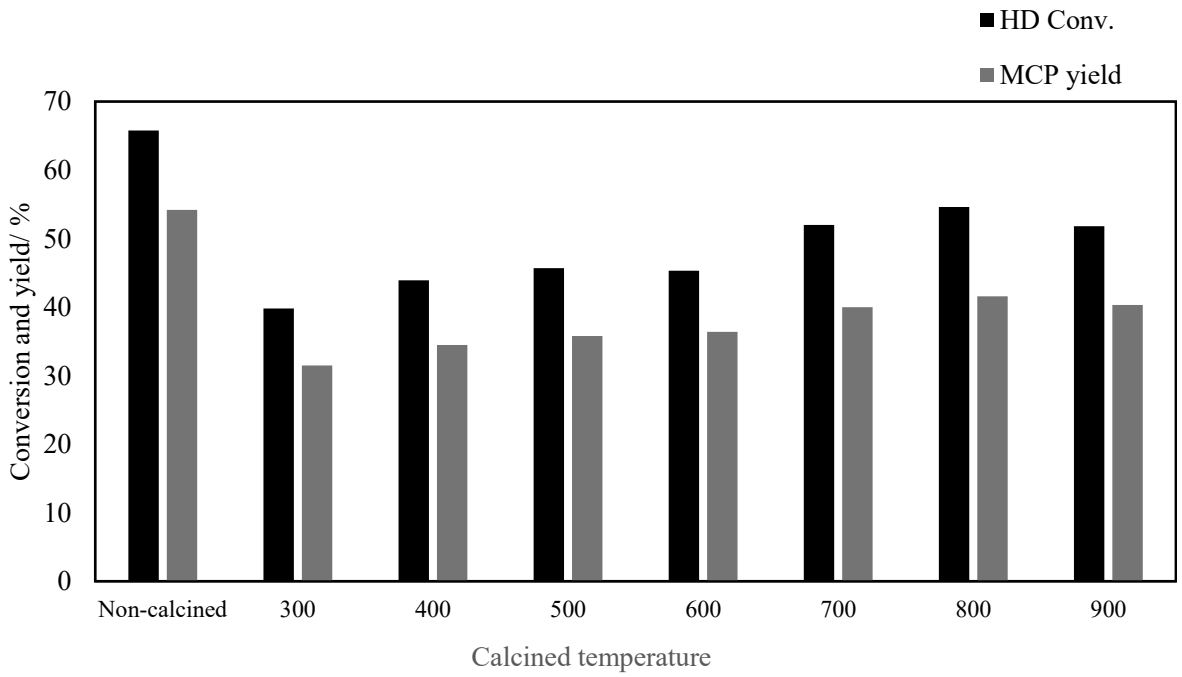

Figure 4.15 Reactivity over *cp*-La-Al-(OH) (La:Al = 1:50) calcined at various temperatures

Table 4.6 Reactivity over *cp*-La-Al-(OH) (La:Al = 1:50) calcined at various temperatures with S_{BET} values.

Calcination temp. /°C	Conv. /%	Yield /%	Sel. /%	Specific surface area /m^2 g^{-1}
Non-calcined	65.8	54.2	82.4	141.9
300	39.8	31.5	79.0	192.7
400	43.9	34.5	78.5	206.1
500	45.7	35.8	78.3	189.3
600	45.3	36.4	80.4	185.4
700	52.0	40.0	77.0	161.1
800	54.6	41.6	76.2	156.6
900	51.8	40.3	77.8	107.9

Reaction conditions: HD (3.0 mmol), catalyst (50 mg), 1,4-dioxane (5.0 mL), 3 h, 140 °C, and 500 rpm.

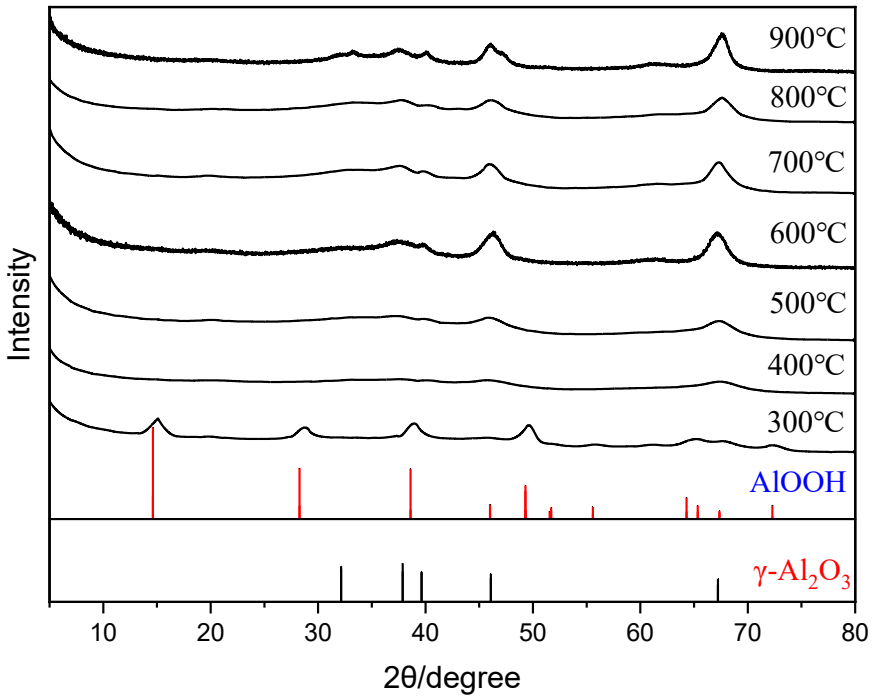

Figure 4.16 XRD patterns of *cp*-La-Al-(OH) (La:Al ratio = 1:50) calcined at various calcination temperatures of 300-900°C.

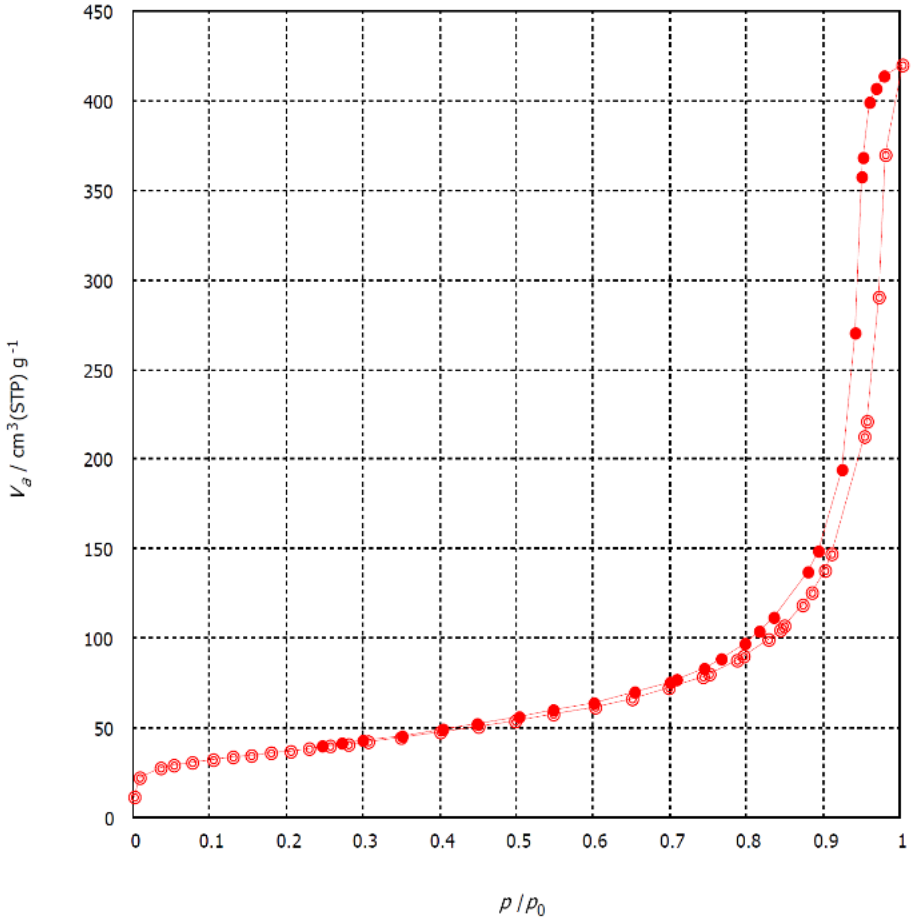

Figure 4.17 N_2 adsorption–desorption isotherm of *cp*-La-Al-(OH) (La:Al = 1:50) calcined at 900°C.

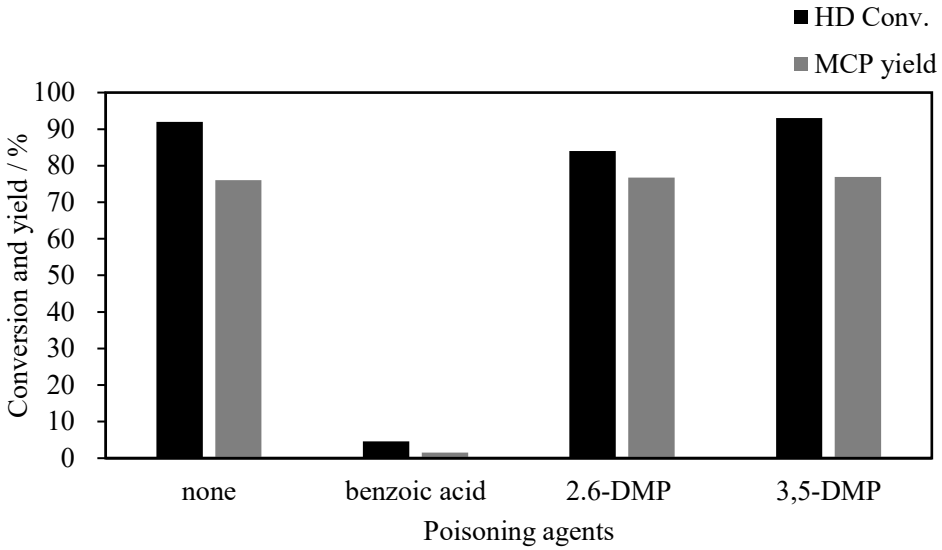

Figure 4.18 Effect of different poisoning agents on the catalytic activity of the *cp*-La-Al-(OH) (La:Al = 1:50, calcined at 900ºC).

Table 4.7 Poisoning test with BA, 2,6-DMP, or 3,5-DMP on the catalytic activity of the *cp*-La-Al-(OH) (La:Al = 1:50) calcined at 900ºC.

Poisoning agent (amount)	Conv. /%	Yield /%	Sel. /%
None	92.0	76.0	82.6
Benzoic acid (5 mg)	4.6	1.6	34.1
2,6-DMP (10 mg)	84.0	76.8	91.4
3,5-DMP (10 mg)	93.0	77.0	82.7

Reaction conditions: HD (1.0 mmol), catalyst (50 mg), 1,4-dioxane (5.0 mL), 3 h, 140 °C, 500 rpm, and poisoning agent (5 or 10 mg).

For the purification and product isolation of MCP, I think it's possible to follow a tandem resin-based procedure adapted from the environmentally benign isolation protocol reported by Bagnell et al [17]. This approach avoids conventional liquid–liquid extraction and instead relies on selective adsorption on solid resins: residual HD is preferentially removed using a bisulfite-form anion-exchange resin, followed by capture and recovery of MCP on a hydrophobic macroporous resin. Specifically, after completion of the reaction, the solid catalyst was removed by syringe filtration (e.g., 0.20 μm PTFE). The filtrate was then subjected to bisulfite-resin treatment to remove most of the

residual HD, and the resulting solution was loaded onto a hydrophobic polymeric resin column to enrich and recover MCP. This operation is essentially a physical adsorption–desorption process and can be regarded as an application of solid-phase extraction (SPE) or adsorption chromatography. The separation is enabled by the moderate hydrophobicity of MCP, which allows the neutral organic molecule to be temporarily retained on a nonpolar macroporous resin through weak interactions (e.g., van der Waals forces), whereas the reaction solvent (1,4-dioxane) and weakly retained impurities preferentially pass through the bed. A polystyrene-based nonpolar macroporous adsorbent resin (e.g., Amberlite XAD series or Lewatit VP OC 1066) was wet-packed into a glass column, pre-wetted/activated with methanol or ethanol, and then equilibrated by flushing with 1,4-dioxane. After sample loading at a controlled flow rate, the column was washed with 1,4-dioxane (or a water/1,4-dioxane mixture, depending on the optimized conditions) to remove residual solvent and weakly retained impurities while keeping MCP adsorbed. Finally, MCP was desorbed and eluted using a stronger organic eluent (e.g., ethanol, methanol, or acetone); the MCP-rich fraction was collected, and the solvent was removed by rotary evaporation to afford purified MCP. Overall, the tandem use of a chemical adsorption resin for HD removal and a hydrophobic adsorption resin for MCP capture enabled efficient purification without conventional liquid–liquid extraction or complex distillation.

4.4 Conclusion

This study focused on the development and characterization of lanthanum-modified alumina catalysts prepared by a urea homogeneous co-precipitation method and compared their catalytic performance with catalysts synthesized by an impregnation method. In the intramolecular aldol condensation of HD, the *cp*-La–Al–(OH) catalyst exhibited high catalytic activity (54% MCP yield) even without calcination, whereas the *imp*-La/AlOOH catalyst required calcination at 500°C to achieve comparable performance (60% yield). Structural and surface analyses revealed that the co-precipitation method

generated abundant and unique basic surface sites that were largely diminished after calcination, while the calcined *imp*-La/AlOOH catalyst developed pronounced Lewis acid sites in addition to basic sites. Poisoning experiments demonstrated that the reaction proceeds via a base-driven mechanism over the non-calcined *cp*-La–Al–(OH) catalyst, whereas the calcined *imp*-La/AlOOH catalyst follows an acid–base cooperative mechanism. Flow hot-filtration experiments further confirmed that the catalytic activity originates from the solid catalyst rather than from leached or dissolved species, validating the intrinsic heterogeneity of the *cp*-derived catalyst. Taken together, these results highlight the decisive roles of preparation method and thermal history in determining the formation and distribution of active surface sites and underscore the potential of non-calcined *cp*-La–Al–(OH) catalysts as promising solid base systems in aldol condensation reactions where preservation of surface basicity is crucial.

References

[1] Z. J. Ling, Master's Thesis, Japan Advanced Institute of Science and Technology (JAIST), 2023.

[2] S. Nishimura, Z. Ling, *ChemistrySelect*, 2025, *10*(6), e202404244.

[3] A. A. Ati, Z. Othaman, A. Samavati and F. Y. Doust, *J. Mol. Struct*., 2014, 1058, 136–141.

[4] H. Tang, C. Cheng, G. Yu, H. Liu and W. Chen, *Mater. Chem. Phys.*, 2015, 159, 167–172.

[5] S. Nishimura, T. Shishido, K. Ebitani, K. Teramura and T. Tanaka, *Appl. Catal. A: Gen*., 2010, 387, 185-194.

[6] J. A. Widegren, R. G. Finke, J. *Mol. Catal. A Chem.*, 2003, 198, 317–341.

[7] R. A. Sheldon, *Chem. Soc. Rev.*, 2012, 41, 1437–1451.

[8] T. Yamamoto, T. Hatsui, T. Matsuyama, T. Tanaka, and T. Funabiki, *Chem. Mater,* 2003, 15, 25, 4830–4840.

[9] D. Sun, S. Moriya, Y. Yamada and S. Sato, *Appl. Catal. A: Gen.*, 2016, 524, 8–16.

[10] C. Cobzaru, S. Oprea, E. Dumitriu and V. Hulea, *Appl. Catal. A: Gen*., 2008, 351, 253–258.

[11] A. Lilić, S. Bennici, J. F. Devaux, J. L. Dubois and A. Auroux, *ChemSusChem*, 2017, 10, 1916–1930.

[12] A. Lilić, T. Wei, S. Bennici, J. F. Devaux, J. L. Dubois and A. Auroux, *ChemSusChem*, 2017, 10, 3459–3472.

[13] Q. Bao, T. Bu, J. Yan, C. Zhang, C. Ning, Y. Zhang, M. Hao, W. Zhang and Z. Wang. *Catal. Lett*., 2017, 147, 1540–1550.

[14] Q. Bao, Y. Hu, X. Liu, G. Wu, P. Sun, J. Ge and M. Xu, *Energy Fuel*., 2022, 36, 978–990.

[15] S. Sato, M. Tokumitsu, T. Sodesawa and F. Nozaki, *Bull. Chem. Soc. Jpn*., 1991, 64, 1005–1007.

[16] L. Yu, E. Kurniawan, T. Ozawa, H. Kobayashi, Y. Yamada and S. Sato, *Mol. Catal*., 2023, 537, 112939.

[17] L. Bagnell, M. Bliese, T. Cablewski, C. R. Strauss and J. Tsanaktsidis, *Aust. J. Chem.*, 1997, 50, 921–926,

Chapter 5 General Conclusion

The catalytic conversion of biomass-derived oxygenates into value-added chemicals requires solid catalysts that are not only active and selective, but also structurally robust and tunable in their surface acid–base functions. In this dissertation, the intramolecular aldol condensation of 2,5-hexanedione (HD) to 3-methyl-2-cyclopentenone (MCP) was employed as a typical reaction to elucidate how lanthanum modification and catalyst synthesis route govern the creation, evolution, and cooperation of catalytically relevant surface sites in boehmite-derived alumina materials. By systematically comparing lanthanum-modified catalysts prepared via impregnation (*imp*-La/AlOOH) and urea homogeneous co-precipitation (*cp*-La–Al–(OH)), both with and without thermal treatment, this work establishes a coherent structure–site–function relationship that explains why catalysts of similar bulk crystalline phases can nonetheless exhibit fundamentally different catalytic behaviors and mechanisms.

A central outcome of this study is the clear demonstration that the synthesis pathway determines whether the La–Al material behaves primarily as a solid base or as an acid–base cooperative catalyst, and that thermal treatment can either activate or degrade the relevant surface site ensembles depending on how La is incorporated. When La is introduced by impregnation onto boehmite, the resulting *imp*-La/AlOOH catalyst exhibits negligible activity prior to calcination, indicating that the as-prepared surface does not provide the necessary accessible/basic ensemble to initiate efficient enolate formation and cyclization. However, after calcination, the catalytic function is markedly enhanced: the optimized *imp*-La/AlOOH catalyst calcined at 500 °C achieves a high MCP yield (60%) with substantial HD conversion (84%), highlighting that thermal reorganization of La–Al interactions is essential for creating the active architecture in the impregnation route. In contrast, when La and Al are co-precipitated, *cp*-La–Al–(OH) exhibits strong activity even without calcination (MCP yield 55% and HD conversion 65%), demonstrating that co-precipitation intrinsically generates catalytically

competent basic surface sites in the hydroxide/boehmite-derived framework without requiring thermal activation. Importantly, calcination of *cp*-La–Al–(OH) decreases performance, indicating that the most effective sites in the co-precipitated catalyst are at least partially heat-labile and can be weakened or removed during dehydration/phase evolution.

From a structural viewpoint, a notable and practically important finding is that bulk crystallinity alone cannot explain activity trends. XRD analysis shows that both non-calcined *cp*-La–Al–(OH) and non-calcined *imp*-La/AlOOH are dominated by boehmite (AlOOH), while calcination yields γ-Al_2O_3 as the dominant crystalline phase for both catalyst families. Nevertheless, their catalytic behaviors diverge strongly, meaning that the decisive factors are associated with surface chemistry, La distribution, hydroxyl environments, and the local acid–base topology rather than the bulk phase identity. Similarly, N_2 adsorption–desorption indicates that while pore characteristics differ between the two non-calcined materials (more macroporous features for *cp*-La–Al–(OH) and clearer mesoporosity for *imp*-La/AlOOH), these textural features are not the sole determinants of activity; instead, they act as enabling features that influence accessibility and diffusion, whereas the governing factor remains the nature and stability of the active acid–base sites created through synthesis and heat treatment.

Mechanistically, this dissertation provides evidence that the reaction pathway can shift depending on whether the catalyst surface is dominated by basic sites or contains a cooperative acid–base ensemble. Selective poisoning experiments establish that the non-calcined *cp*-La–Al–(OH) catalyst operates primarily through a base-catalyzed route, consistent with the presence of hydroxyl-rich basic sites generated by co-precipitation and preserved in the absence of calcination. In contrast, the calcined *imp*-La/AlOOH catalyst proceeds via an acid–base cooperative mechanism, where calcination promotes the emergence of Lewis acid sites in addition to basic sites, enabling a bifunctional sequence in which carbonyl activation and enolate formation/dehydration are jointly facilitated.

A further methodological and interpretive contribution of this work is the explicit recognition that non-calcined catalysts can contain residual species such as synthesis-derived ions, hydroxylated phases, or weakly bound components that may complicate acid–base interpretation unless heterogeneity is carefully validated. In response to this concern, the dissertation emphasizes the necessity of confirming that observed activity arises from the solid catalyst rather than dissolved/leached species, motivating the use of hot-filtration protocols as a key control experiment when working with non-calcined hydroxide-derived solids. This approach strengthens the reliability of the mechanistic conclusions where the boundary between truly heterogeneous catalysis and solution-mediated contributions must be rigorously tested. Taken together, the results in Chapters 3 and 4 lead to an overarching principle: the catalytic behavior of La–Al solids is governed by how acid–base sites are generated, reorganized, or preserved during synthesis and thermal treatment, rather than by nominal composition or bulk phase alone. In practical terms, the co-precipitation route offers an attractive strategy to obtain highly active solid-base catalysts without calcination, provided that the targeted basic sites can be stabilized against thermal or chemical degradation. Meanwhile, the impregnation route offers a pathway to create robust acid–base cooperative catalysts through controlled calcination, enabling high activity when the restructured La–Al surface can simultaneously provide accessible basic centers and Lewis-acid functionality. This synthesis–site–mechanism framework provides actionable guidance for catalyst design: if the target transformation benefits predominantly from strong/basic enolate-forming sites, co-precipitated hydroxyl-rich materials may be optimal; if the transformation requires balanced bifunctionality and improved thermal robustness, calcination-driven reconfiguration of impregnated La–Al materials may be preferred.

Finally, the implications of this dissertation extend beyond the transformation of HD to MCP. Many biomass upgrading reactions including intermolecular aldol condensation, Knoevenagel condensation, and related C–C bond-forming transformations are similarly governed by the balance, proximity, and stability of acid and base sites. The core lesson from this work is that synthesis is not merely a

preparative step but a mechanistic determinant: it sets the spatial distribution of dopants, the hydroxyl/oxide environment, and the emergent acid–base topology that ultimately defines catalytic function. In this sense, the comparative analysis performed here contributes a generalizable design concept for oxide and lanthanum-modified catalysts: by choosing a synthesis route that either (i) preserves hydroxyl-rich basicity or (ii) intentionally builds acid–base cooperativity through thermal reorganization, one can rationally steer both catalytic mechanism and performance toward the needs of a target reaction class. Although this dissertation focuses on La, the same synthesis-driven principle may also guide future exploration of other lanthanide modifiers.

The scope of this dissertation extends beyond the specific transformation of HD to MCP typical system and provides a transferable framework for understanding how synthesis pathways encode surface acid–base topology in oxide catalysts. By integrating materials synthesis, structure characterization, and mechanistic interrogation, this work demonstrates that only composition or bulk phase alone is insufficient to predict catalytic function; instead, catalytic performance and even the dominant reaction pathway are determined by the generation, spatial distribution, and thermal stability of surface site ensembles created through a given preparation route. Within this scope, the concepts established here are most directly applicable to acid–base-driven transformations in biomass upgrading such as C–C bond-forming reactions (aldol condensation or Knoevenagel condensation reaction) and related condensation/dehydration sequences where activity and selectivity depend sensitively on the balance and proximity of basic and Lewis acidic sites. Importantly, the comparative conclusions also define boundaries of applicability. Hydroxyl-rich, co-precipitated solids favor base-dominant pathways under mild conditions but may be vulnerable to site loss upon dehydration or harsh thermal environments, whereas calcination-reconfigured, impregnated La–Al materials offer a general route to more thermally robust acid–base cooperativity but may be less suited to transformations requiring strictly hydroxyl-derived strong basicity. Recognizing these boundaries enables rational selection of synthesis route and thermal history based on the mechanistic

requirements of a target reaction class. From the perspective of Transdisciplinary Sciences, this dissertation illustrates how catalyst design can be treated as a cross-cutting problem that links synthesis chemistry (dopant incorporation and hydroxyl/oxide environments), surface science (site ensembles and their evolution), reaction engineering (robustness under practical operating conditions), and downstream separations (product isolation strategies compatible with heterogeneous systems). Accordingly, the synthesis–site–mechanism framework developed here is not merely a catalyst-specific conclusion, but a transdisciplinary design concept for constructing efficient and scalable heterogeneous processes for the sustainable upgrading of biomass-derived oxygenates.

List of Published Paper

[1] S. Nishimura, Z. Ling, *ChemistrySelect.,* 2025, *10*(6), e202404244.

[2] Z. Ling, S. Nishimura, *React. Chem. Eng.*, 2025, *10*, 2895-2091.

List of Conference

[1] Z. Ling, S. Nishimura, Effect of La-modified alumina catalyst on intramolecular aldol condensation reaction of 2,5-hexanedione, 53rd Petroleum Petrochemical Symposium of the Japan Petroleum Institute, Oct 26–27, 2023, Osaka Science & Technology Center, Osaka, Japan (oral presentation, 2D06, 15 min).

[2] Z. Ling, S. Nishimura, Textural characteristics in La-modified alumina catalyst prepared by impregnation and co-precipitation method on the intramolecular aldol condensation of 2,5-hexanedione, 55th Joint Autumn Meeting of the Chubu Branches of Chemical Societies, Nov 2–3, 2024, Nagoya Institute of Technology, Nagoya, Japan (oral presentation, 2C203).

[3] Z. Ling, S. Nishimura, Genesis of Lanthanum-modified Boehmite-derivatives for the Intramolecular Aldol Condensation of 2,5-Hexanedione, 2025 Hokuriku District Symposium & Research Presentation Meeting, Nov 21, 2025, Ishikawa High-Tech Exchange Center, Nomi, Ishikawa, Japan (poster presentation, 4P34).